2008

# ELASTIC-PLASTIC INDENTATION DEFORMATION IN HOMOGENEOUS AND LAYERED MATERIALS: FINITE ELEMENT ANALYSIS

SIVA NAGA VENKATA RAVI KIRAN KURAPATI
*University of Kentucky*

**Click here to let us know how access to this document benefits you.**

ABSTRACT OF THE THESIS

ELASTIC-PLASTIC INDENTATION DEFORMATION IN HOMOGENEOUS AND
LAYERED MATERIALS: FINITE ELEMENT ANALYSIS

The complex phenomenon of indentation deformation is studied using finite element analysis for both homogeneous and layered materials. For the homogeneous materials, the elastic-plastic deformation at large indentation depth is studied. The variation of the load-displacement curves as well as the variation of the energy ratio with the applied indentation depth for different strain hardening indices is presented. The power law relation between the indentation load and depth for shallow indentation becomes invalid for deep indentation. The ratio of plastic energy to total mechanical work is a linear function of the ratio of residual indentation depth and maximum indentation depth. For the layered materials (film-substrate systems), the elastic deformation under an indenter is studied. Various material parameters are investigated, including film thickness and modulus. A generalized power law equation is presented for characterizing the indentation load-displacement responses of film-substrate structures.

KEYWORDS:   Indentation; Spherical indenter; Homogeneous Material; Layered Material; Finite Element Method.

SIVA N V R K KURAPATI

DATE: 01/16/2008

ELASTIC-PLASTIC INDENTATION DEFORMATION IN HOMOGENEOUS AND
LAYERED MATERIALS: FINITE ELEMENT ANALYSIS


By


SIVA NAGA VENKATA RAVI KIRAN KURAPATI


<u>Dr. Yuebin Charles Lu</u>

Co-Director of Thesis

<u>Dr. Fuqian Yang</u>

Co-Director of Thesis

<u>Dr. Scott L Stephens</u>

Director of Graduate Studies

Date: 01/16/2009

RULES FOR THE USE OF THESES

Unpublished theses submitted for the Master's degree and deposited in the University of Kentucky Library are as a rule open for inspection, but are to be used only with due regard to the rights of the authors. Bibliographical references may be noted, but quotations or summaries of parts may be published only with the permission of the author, and with the usual scholarly acknowledgments.

Extensive copying or publication of the thesis in whole or in part also requires the consent of the Dean of the Graduate School of the University of Kentucky.

A library that borrows this thesis for use by its patrons is expected to secure the signature of each user.

Name                                                    Date

_____

_____

_____

_____

_____

_____

_____

_____

THESIS

SIVA NAGA VENKATA RAVI KIRAN KURAPATI

THE GRADUATE SCHOOL

UNIVERSITY OF KENTUCKY

2009

ELASTIC-PLASTIC INDENTATION DEFORMATION IN HOMOGENEOUS AND
LAYERED MATERIALS: FINITE ELEMENT ANALYSIS

_____

THESIS

_____

A thesis submitted in partial fulfillment of the
requirements for the degree of Master of Science in Mechanical Engineering
in the College of Engineering
at the University of Kentucky

By

SIVA NAGA VENKATA RAVI KIRAN KURAPATI

Lexington, Kentucky

Co-Directors: Dr. Yuebin Charles Lu, Assistant Professor of Mechanical Engineering
and Dr. Fuqian Yang, Assistant Professor of Materials Engineering

Lexington, Kentucky

2009

Dedicated to my parents and family

# ACKNOWLEDGEMENTS

I am very grateful to my parents, my younger brother and my relatives for their immense love, moral and financial support. I wouldn't have been here without their help. With due respect and love I would like to dedicate this thesis to my parents.

I wish to thank my research advisor and committee chair, Dr. Yuebin Charles Lu, for his intellectual support and enthusiasm on the whole process of this research project and thesis writing, which made this thesis possible. I thank Dr. Fuqian Yang for his valuable guidance throughout my research work and serving on my thesis committee as co-chair. I genuinely appreciate for his continuous encouragement.

I am thankful to Dr. Tingwen Wu and Dr. Haluk Karaca for being as my committee members, for their precious suggestions and persistent support. I am also thankful to Colleagues and friends in the research group who offered many discussions that were helpful for this work.

I am grateful to my parents for their support and encouragement. They are my indispensable impetus to move forward.

# Table of Contents

# List of Tables

# List of Figures

## 1.0 Introduction

### 1.1 Background

By virtue of the senses provided by the nature, all living things have always been sensing and distinguishing the hard and soft nature of the objects that they come across in their day to day life right from the day of existence. But it was not until recently that humans learn the importance of this unique sensing quality, which can be effectively used in their quest to make things which fulfill their requirements. The difference between the hard and soft surface can be defined by the hardness nature of the surface, but quantitative evaluation of the hardness was not made possible until Johan August Brinell (1849-1925) who developed the hardness test, also known as the "indentation" test, a non-destructive means to categorize the steels in the Fagersta Ironworks as a chief engineer at Jernkontoret. Since then, other standard hardness tests have been developed and are routinely used, including the Vickers, Knoop, and Rockwell tests. Usually the hardness is determined by indenting a surface using a harder surface (a steel ball in Brinell method, a square-based pyramid with an angle of 136° between opposite faces in Vickers method, a pyramidal diamond in Knoop method, and a diamond cone in Rockwell method) to form a permanent impression with plastic deformation, and is defined by a number called as hardness number obtained by the ratio of the applied load to the projected area of the residual surface. A illustration of hardness test using a sphere is shown in Figure 1.1-1.
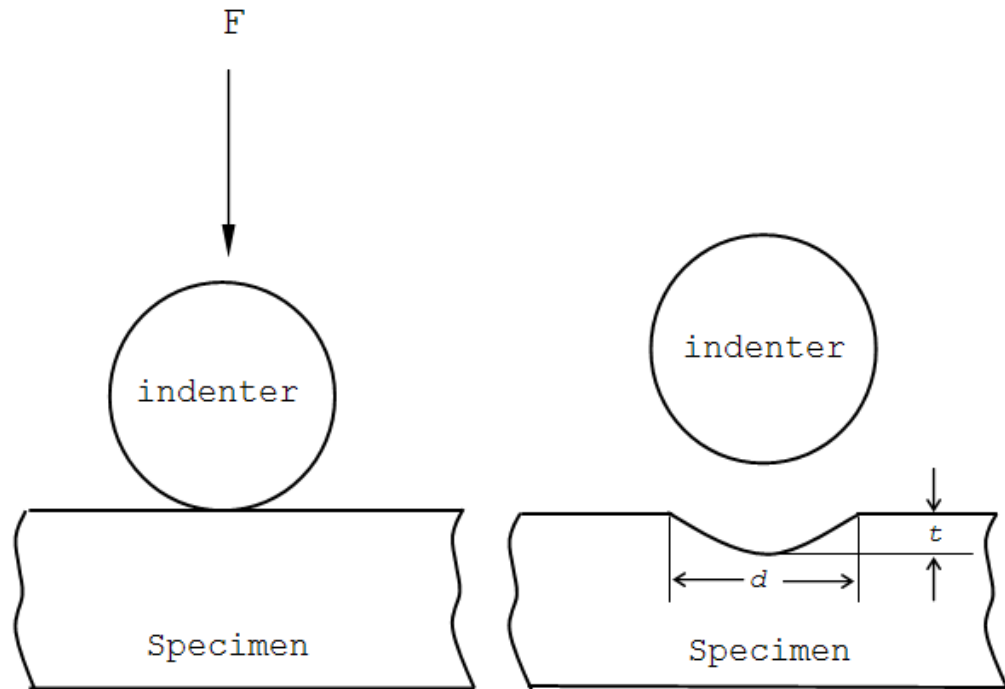
Figure 1.1-1    The hardness test as illustrated by a sphere. (a) A loaded indenter

is placed in contact with the specimen; (b) The hardness number depends on the

indentation that remains when the indenter is removed. The indentation can be

estimated either by the impression area or the impression depth - O'Neill 1967 [9].


In the past two decades, a more sophisticated form of indentation test has been

developed, namely "microindentation" or "nanoindentation" test. The renewed

interest in developing this small-scale indentation has been driven mostly by the

modern interests in designing micro-/nano- materials and structures and in studying

the micro-/nano- mechanics and deformation. The small-scale instruments are made

possible by the improvements in piezoelectric positioning instrumentation which

allow for the atomically precise displacement control.
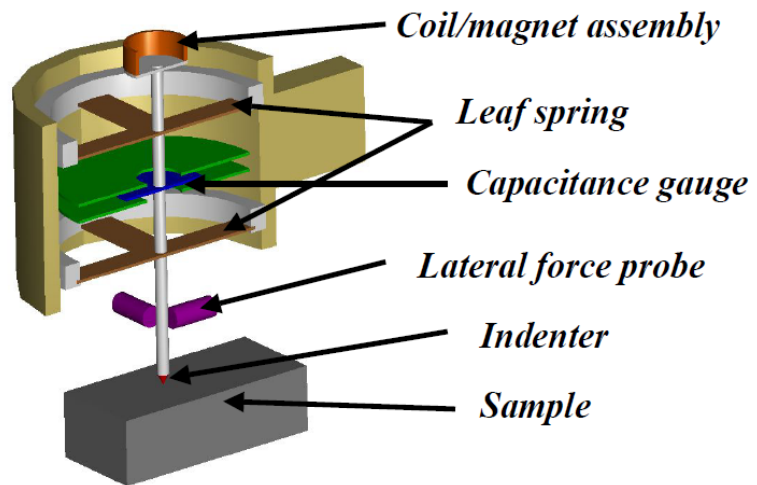
Figure 1.1-2     A Commercial Nanoindentation Apparatus for Nano-Scale

Mechanical Measurements   (MTS Nano Indenter User's Manuel, [81]).

3

The new "microindentation" or "nanoindentation" test offers significant advantages over a traditional hardness test. In this test, an indenter tip is pushed into the surface of the material under precise load or displacement control (the load and displacement resolutions are in the magnitude of mille-Newton ($\mu$N) and nanometer (nm), respectively). The extremely small forces and displacements are recorded continuously throughout the loading-unloading cycle. By analyzing the load-displacement curve, one can obtain many material properties which extend beyond the obtainable from the standard hardness test.

The elastic deformation under a microindenter or nanoindenter can be well described by the classical contact theories developed by Hertz [1] and Sneddon [4]. Based on these theories, the elastic properties of the materials are calculated. However, the plastic deformation under the indenter is much more complex. Since the constitutive equations are nonlinear and a number of material parameters must be included to describe material behavior (e.g., yield strength and work hardening exponent), analytical solutions are not easily obtained. The available theoretical treatments are limited because of the simplifying assumptions required to make such analysis tractable. As a result, much of our understanding of the importance of plasticity in the indenter contact problems has been derived through experimentation and finite element modeling (FEM). With the advancements of computational methods and computer hardware, the FEM has proven to be effective tool in conducting a pre assessment of the procedure that is being considered.

## 1.2 Objectives of the Thesis

In this thesis, we conducted the finite element analysis on the indentation of homogeneous and layered materials. The overall objective is to study the elastic-plastic deformation occurred under the indenter in both homogeneous and layered material systems. For homogeneous materials, existing work as reported in literatures mostly deal with shallower indentation (the normalized indentation depth $\delta/R<0.05$ where $\delta$ is the indenter penetration and R is the indenter radius). The present analysis focuses on relatively "deeper" indentation, where the normalized indentation depth reaches a unity ($\delta/R\approx1$). The load-displacement response and mechanical energy at that level of indentation are explored. For the indentation of layered materials (film-substrate systems), the classical Hertz contact theorem becomes invalid. The present analysis aims to explore the load-displacement responses of layered materials with various film/substrate properties, and then to find a empirical equation to characterize these responses.

## 1.3  Organization of the Thesis

The second chapter (Chapter 2) details the literature in the areas of the deep indentation of homogenous and layered materials. There is a large volume of literature dealt with micro-/nano-indentation. The review is focused on the

numerical aspects of nanoindentation analysis (using finite element method). Chapter 3 gives a brief overview of the finite element method (FEM) used in the present work in relation to the indentation models as well as a brief review of the software package ABAQUS used to obtain the present results. Chapter 4 details the work concerning the elastic-plastic indentation of homogeneous materials. Chapter 5 details the work concerning the elastic indentation of layered materials. Chapter 6 summarizes the overall results and gives in brief the possible future work.

## 2.0 Review of Literatures

## 2.1 Elastic-Plastic Indentation of Homogeneous Materials

Various methods have been developed to solve the indentation deformation of elastic materials, including the use of stress-potential functions and integral transforms [1-4, 7, 50, 72]. Those analytical solutions provide the rational for characterizing the elastic properties of materials from micro- or nano-indentation. Finite element modeling has been applied to indentation measurements to help understand the indentation process and improve the accuracy of the analytical methods.

Bhattacharya and Nix [20, 23] used the finite element method to study the indentation experiment. A simulation on conical indentation was performed. The indentation load-depth curves were obtained, from which the elastic modulus was calculated. The results justified the use of the stiffness method commonly used in analyzing nanoindentation data. Pharr and Bolshakov [51] conducted similar analysis on Berkovich indentation. Using finite element simulation, they analyzed the deformation process during unloading and proposed the concept of "effective indenter shape". The concept provides a physical justification to the mathematical equation used to describe the nano-indentation unloading curve.

Larsson et al [44] performed finite element simulation of Berkovich indentation. The indentation load-depth curves were obtained and then compared to experimental measurements. The contact area between material and indenter was computed based on the displacement contours. Shih et al. [25] evaluated the effect of the indenter tip on the relation between contact area and depth of indent. The blunt tip geometry of the so-called nano-indenter is modeled by a spherical cap of various radii. It was found that the relation between area and penetration depth of the indenter is comparable with experimental results only if the radius of the tip is above 1.0 μm. A similar study was conducted later by Cheng and Cheng [54] using finite element method and the effect of indenter tip roundness on indentation measurement was comprehensively studied.

The elastoplastic deformation during indentation is much more complex; and there is no analytical solution describing the indentation deformation. Numerical analysis has become a major technique to study the indentation deformation of elastoplastic materials [25, 33, 38, 40, 48-50, 87].

Shu and Fleck [48], Sinisa, Mesarovic and Fleck [62] conducted the finite element simulation on spherical indentation. The elastic-plastic deformation under the sphere was analyzed using the linear power law theory and Ramberg-Osgood law. The boundary of the plastic zone was analyzed as a function of elastic and plastic properties of the indented materials. The friction between the indenter and the

substrate was also investigated and found to have a strong effect on strain field beneath the indenter. The indenter size effect on indentation was also evaluated using the theory of the strain gradient plasticity.

Taljat et al. [49, 79] used the finite element method to study the material pile-up occurred around elastic-plastic indentation. A wide range of materials with different elastic moduli, yield strength, strain hardening exponents, and friction coefficients were examined. Results showed that the material pile-up increases as the indenter is driven into the material, even when the deformation reached full plastic stage. The amount of pile-up was affected by the friction between indenter and material and the heights of the pile-up were quite different before and after unloading the indenter.

Montmitonnet et al. [33] and Sadeghipour et al. [38] used the finite element method to study the friction and sliding/sticking phenomena between indenter and specimen. The formation of ring cracks developed in these materials was also discussed.

Most of the studies mentioned above have been focused on relative shallower indentation. There is little study on deeper indentation of elastic-plastic materials.

Previously, the deep indentation of elastic-plastic materials was conducted with a flat-ended indenter, as seen in Appendix A.

## 2.2 Elastic-Plastic Indentation of Layered Materials (Thin Film-Substrate Systems)

In the indentation of homogeneous materials (as discussed in previous section), the material is assumed to have an infinite thickness. When the thickness of the specimen becomes finite (as in the case of film-substrate systems), the substrate will strongly affect the indentation measurement and this effect should be considered when calculating the film properties. Numerous investigators have used both experimental [17, 24, 47, 52, 57] and theoretical [16, 18, 22, 26, 50] methods to study the problem of extracting 'true' film properties from nano-indentation of film/substrate systems. Finite element technique has also been employed to simulate the elastic and plastic response of the layered materials.

King [16] has studied the elastic properties of the films adhered on rigid substrates. It was found that the substrate played a dominating role in increasing or decreasing the hardness of a film. Doerner et al [14] examined the plastic properties of the films (Al and W) on silicone substrate (Si). The effect of thickness on the strength of Al and W thin films on Si was studied. For Al the film strength was found to

increase with decreasing film thickness whereas for tungsten the strength decreases with decreasing film thickness. The effective composite Young's modulus, $E_{\text{eff}}$, in a layered solid can be described as a function of plane strain Young's modulus,

$\frac{1}{E^*} = \frac{(1-v^2)}{E}$ , of the relevant materials: $\frac{1}{E^*_{eff}} = \frac{1}{E^*_f}\left(1 - e^{-\beta\left(\frac{t}{h}\right)}\right) + \frac{1}{E^*_s}e^{-\beta\left(\frac{t}{h}\right)}$ where

$\beta$ is an unknown parameter, $t$ the film thickness, $E$ Young's modulus, and $v$ Poisson's ratio. Subscripts $f$ and $s$ refer to the film and substrate properties, respectively.

Djabella and Arnell [31] used finite element method to investigate the contact stresses due to Hertzian indentation of coating/substrate systems consisting of a high modulus surface coating on a relatively low modulus substrate. The stresses which cause the coating failure in-plane compressive tensile and interfacial shear stresses depend on the coating thickness and the modulus ratio in a complicated fashion i.e., the stress is compressive and tensile for different thickness of the layer. Also using FEM, Cai [33] studied the influence of different parameters involved in calculation of the material properties in indentation and the most influential parameters, the geometry and the blunting of the indenter tip, cause a decrease or an increase of the calculated hardness at very low indentation depths. It is also reported that the calculations depend on the substrate properties.

Page and Hainsworth [36] studied the coated systems and found that the critical ratio of thickness is a function of the yield strength ratio of the coating to the substrate and the indenter tip radius. The effect of thickness on the stress magnitude is demonstrated by normal stress $\sigma_{zz}$ and the principal stress on a Zirconia-stainless steel couple. It was reported, to reduce the substrate effect the indentation penetration should be less than 15% of the layer thickness [47]. The roundness or truncation of the indenter tip is crucial for the measurement of thin films using nanoindentation, based on the finite element analysis conducted by Tang and Arnell [54].

Mesarovic and Fleck [62] conducted comprehensive finite element studies on layered systems and found that the substrate hardness effect over the film hardness for a soft film over the hard substrate was negligible but the effect was considerable for the hard film over the soft substrate. The results from Chollacoop et al [73] had showed that to eliminate the substrate effect the indentation displacement should be only 5% of the thickness instead of 10% the rule of thumb.

Using an axi-symmetric conical indenter and FEM, Panich and Sun [80] studied the influence of yield strength ratio on critical indentation depth. For the range of 0.2-0.8 of yield strength ratio the critical depth increased with the decreasing ratio and below 0.2 an abrupt increase was reported. A model is generated to study the loading and unloading curves for either the coating or the substrate for a wide range of depths. The mechanical properties obtained using this model is sensitive to the

indentation depth. It was reported that at large indentation depths, the properties are asymptotic to values of the substrate [83]. Numerical simulation of bulk materials pure copper, pure titanium, pure iron and copper film are obtained using ABAQUS. It was found that the results depended greatly on mesh size, indenter tip radius and the hardening law used [84].

So far, most published work has been using the finite element method to simulate the deformation process. Fewer have focused on the quantitative aspects of the indentation of layered materials, i.e., the load-displacement responses. The classical Hertz contact theory that is used to characterize the load-displacement curves of homogeneous materials is invalid for the indentation of layered materials. An empirical solution for describing the load-displacement responses of layered materials is still lacking.

## 3.0  Finite Element Modeling

## 3.1  Introduction

In the present work, the finite element method was used to study the elastic-plastic deformation in homogeneous and layered materials. A spherical indenter was used. The advantage of using spherical indenter, as compared to other indenters, lies in the fact that the indentation strain increases with the penetration depth so that the deformation transitions from purely elastic at small indentation to elastic-plastic at large indentation. Finite element analysis (FEA) software package ABAQUS version 6.7 [92] was used in the indentation simulation which is a commercial product. In this chapter, a brief overview about the FEA software and analysis procedure is presented.

## 3.2 ABAQUS Software Package

ABAQUS is developed by Hibbitt, Karlsson & Sorensen, Inc [92]. It is a complete package of powerful engineering simulation programs, based on the finite element method. This simulation software is capable of performing simple linear analysis to the most complex nonlinear simulations.

ABAQUS-Standard and ABAQUS-Explicit are two main analysis modules available in ABAQUS. ABAQUS-Standard is an all purpose analysis module that can solve a variety of problems covering linear and nonlinear problems maintaining the accuracy and the reliability of the results. ABAQUS-Explicit is a special-purpose analysis module that uses dynamic finite element formulation, which is applied to deal with the problems of transient and dynamic in nature. The indentation procedure is assumed to be quasi-static problem, in which no time effect is considered. Hence ABAQUS-Standard is used in this work. ABAQUS process of solving usually consists of three distinct stages: preprocessing, simulation and post processing.

ABAQUS-CAE is the total ABAQUS working interface that includes all the options to generate ABAQUS models, to submit and monitor jobs for analysis and also a means to review the results. In the present work, ABAQUS-CAE is used for the preprocessor of different stages of the model creation starting from the creation of Part, Property, and Assembly, defining the Step, Interaction, Load, Mesh, and generating the Job from the respective module and postprocessor to extract the results using Visualization module.

### 3.3 Nonlinear Analysis in ABAQUS

Non-linearity in simulating the indentation problem is primarily due to two sources one of which is material nonlinearity and the other is geometric nonlinearity.

Stress strain follows Hooke's law giving a linear relationship at low strain values which is true for most of the metals but at higher strains the material yields, at which point the relationship becomes nonlinear and irreversible, can be described as material nonlinearity. The process of indentation generates large deformation in the specimens below and around the indenter. The magnitude of displacement affects the response of the structure can be stated as the geometry nonlinearity.

Newton-Raphson method is used in ABAQUS to obtain solutions for nonlinear problems. By applying the specified loads gradually and incrementally the solution is found reaching towards the final solution. ABAQUS breaks the analysis into a number of load increments and finds the approximate equilibrium configuration at the end of each load increment. Hence it often takes ABAQUS several iterations to find an acceptable solution for a defined loading condition. The sum of all of the incremental responses is the approximate solution for the nonlinear analysis.

The load history for a simulation may have one or more steps. The steps consists the information related to the type of the analysis to be performed like static, thermal etc., and the different loading conditions for each specific type of analysis and the different output requests as required by the user depending on the type of the problem. Since ABAQUS carries out the analysis in small increments, an increment is part of a step. Hence in a nonlinear analysis the total load applied in a step is broken into smaller increments so that the nonlinear solution can be analyzed

making it linear between very small increments. However the user suggests the size of the first increment and ABAQUS program automatically chooses the size of the subsequent increments. At the end of each increment the structure is in approximate equilibrium and results are available for writing to the restart, data or results files. ABAQUS uses several iterations in an attempt to find equilibrium solution. In a nonlinear analysis a step takes place over a finite period of 'time', although this 'time' has no physical meaning unless otherwise inertial effects or rate dependent behavior are important.

## 3.4 Material Characteristics

### 3.1.1   Linear Elastic Model

Elastic deformation is observed in all the materials, when the deformation is small. For isotropic linear elastic materials, the deformation is proportional to the applied load. For a uniaxial tension state the stress-strain relationship can be expressed as

$$\sigma = E\varepsilon \qquad \text{---------------3.4.1}$$

where $\varepsilon$ is the uni-axial strain, $\sigma$ is the uni-axial stress, and E, is the elastic modulus, the proportional coefficient  also known as Young's modulus.

In three dimensional state, the stress-strain relationship of a linear elastic material can be expressed as

$$\sigma_{ij} = \frac{E}{1+v}\varepsilon_{ij} + \frac{Ev}{(1+v)(1-2v)}\delta_{ij}\varepsilon_{kk} \qquad \text{---------------3.4.2}$$

where $\sigma_{ij}$ and $\varepsilon_{ij}$ are the stress components and strain components respectively. $\upsilon$ is the Poisson's ratio which is a measure of transverse strain against axial strain when a uniaxial stress is applied.

### 3.1.2   Power Law Work Hardening Models

Once the external force applied on a material cross its elastic limit, the material will undergo plastic deformation. A power law work hardening model is accepted by most engineering materials such as metals and alloys approximately which is a material constitutive relation, the modified uniaxial stress-strain ($\sigma$-$\varepsilon$) curve of a stress free material can be expressed as

$$\begin{cases} \sigma = E\varepsilon \ for \ \varepsilon \leq \frac{\sigma_y}{E} \\ \sigma = K\varepsilon^n \ for \ \varepsilon \geq \frac{\sigma_y}{E} \end{cases} \qquad \text{---------------3.4.3}$$

where E is elastic modulus, $\sigma_y$ is yield stress, n is the work hardening exponent and K= $\sigma_y(\frac{E}{\sigma_y})^n$ is the work hardening rate. When n is zero, the above (Equation 3.4-3) reduces to an elastic-perfectly plastic material. To completely characterize the elasto-plastic properties of a power-law material, four independent parameters, i.e., elastic modulus E, yield stress $\sigma_y$, work-hardening exponent n, and Poisson's ratio

υ, are needed. One of the major objectives of this thesis, is to relate these parameters (E, $\sigma_y$, n, υ) with the indentation responses. Since indentation induces very complicated stress and strain field beneath the indenter, FEM results obtained are useful in guiding future experiments.

To define the plastic properties of a material in ABAQUS the power law hardening material model is used, a true stress strain data spreadsheet at first is generated from the Equation 3.4-3. Then using the below equation, plastic strain ($\varepsilon_p$) is calculated.

$$\varepsilon_p = \varepsilon - \frac{\sigma_y}{E} \qquad \text{----------------}$$

$$3.4.4$$

One thing to point out is the unit system in the FEM simulation. Since the ABAQUS does not specify a unit system, the users could use a unit system arbitrarily, as long as they are in consistency in one problem. In this problem, we are considering Newton (N) for the force(load) and millimeter (mm) as the unit for the penetration(displacement). So the input mechanical properties value should be converted to be consistent with the units. For example, for 6061 T6 aluminum alloys, E=69 GPa, $\sigma_Y$=255 MPa. In ABAQUS, for aluminum the value of Young's modulus input as E=69000 N/(mm)$^2$ and $\sigma_y$=255N/(mm)$^2$ and for silicon the respective values are E=150000 N/(mm)$^2$ and $\sigma_y$=4410N/(mm)$^2$.

### 3.5 Modeling of Indentation Deformation

Due to the symmetries of both geometry and loading condition, the present indentation problem can be reduced to an axi-symmetric (2-dimensional) model. Since the indenter is much stiffer than the solids, the indenter is considered to be perfectly rigid and is modeled as analytical rigid surface. It is cost-effective since the only variables associated with a rigid surface are the translations and rotations on a single node, known as the rigid body reference node. In our case, reference point is assigned on the indenter tip, which manipulates the rigid body translation of the indenter. In addition, ABAQUS does not need to calculate the stiffness or stresses within the rigid body. The rigid surface is always the master surface in a contact pair.
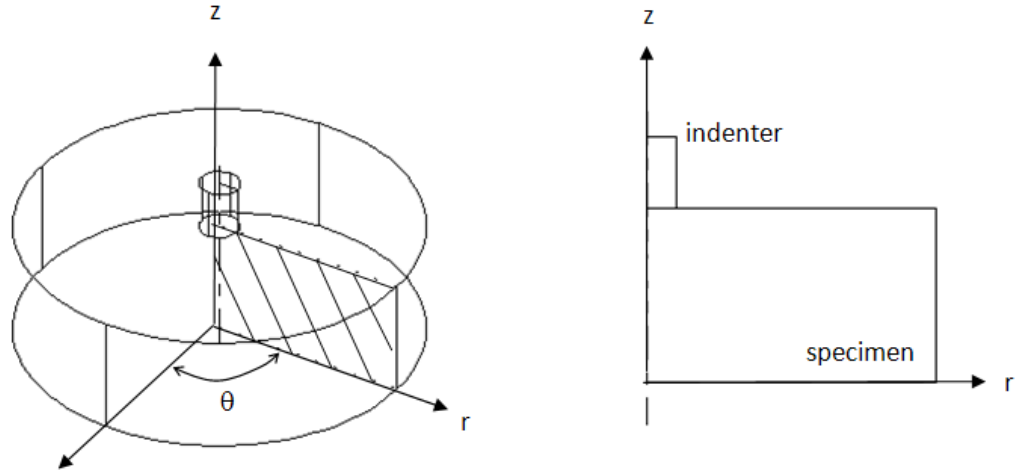
Figure 3.5-1 – Schematic Diagrams Show that a 3-D Indentation Problem Can Be

Solved Using A 2-D Axisymmetric Model.

(Left) 3-dimensional indentation, (right) 2-dimensional axisymmetric model.

Four-node axi-symmetric linear quadrilateral elements are employed in the analysis. The Reduced integration option available is used to save calculation time. The element type used in ABAQUS is 'CAX4R', in which the letter or number indicates the type of element which is of continuum type, axi-symmetric in nature has 4-nodes bilinear and reduced integration with hourglass control respectively. ABAQUS user manual [92] indicates, while selecting elements for contact analysis, it is better to use first-order elements for those parts of a model which will form a slave surface. Second order elements can cause problems in contact simulations because of the way these elements calculate consistent nodal loads for a constant pressure.

### 3.6 Types of Load Application

In ABAQUS there are two methods to simulate the process of indentation into a half space material: load control and displacement control.

A concentrated force is applied to an analytically rigid indenter in the load controlled mode. In order to avoid the non linearity in the finite element analysis the total load is applied in incremental steps as the applied load is large. The entire load increments are divided such that the total time for the step is 1. Linear interpolation is employed for each increment in the step, to calculate real load F. For the applied concentrated force the rigid indenter penetrates into the half space material. Hence calculating the displacement of a node of the material right below the indenter gives the indenter penetration depth. Measuring these two quantities the force applied and the indenter penetration can be used to generate the load displacement data.

In the case of the displacement controlled analysis displacement is specified as input, which is equal to the indentation depth. As in the above case of force controlled, here the indentation depth ($\delta$) is calculated by linear proportion to the incremental time. For the applied displacement the reaction load (F) on the indenter is the summation of force over the contact zone along the penetration direction. Hence the F-$\delta$ curve is obtained.

Two simulations based on these two methods respectively are performed to observe the influence. The material is selected as aluminum, which has the material mechanical properties as below:

E=69 GPa, ν=0.33

The spherical indenter which has diameter of 100mm is used in the simulation. The load-displacement curves (F-δ) are extracted respectively from both simulations and results are shown in (Figure 3.6-1). The comparison shows the two curves overlapped each other very well, which indicates the results are essentially the same no matter which method of applying load is used. In the subsequent simulations, the 'control displacement' method is employed unless otherwise specified.
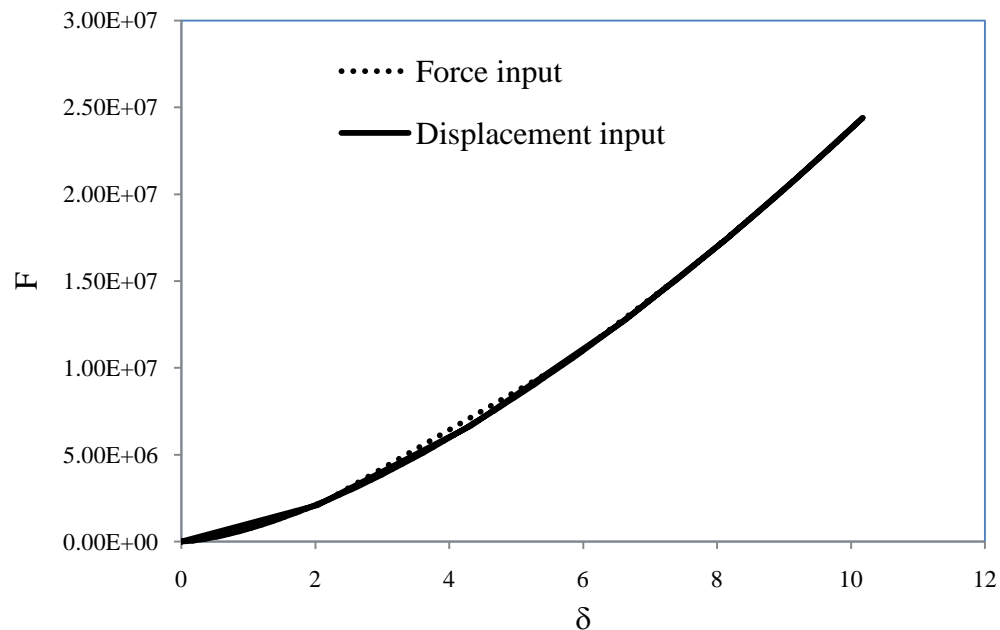


Figure 3.6-1 Load-Depth Curve Comparisons for Different Loading Methods

### 3.7 Contact Interaction

Since Indentation is an example of typical contact problem, it is very important to define the contact formulation in ABAQUS. In general the interaction between contacting surfaces consists of two components: one normal to the surfaces and one tangential to the surfaces. The normal component may be referred as contact pressure and the tangential component generates the relative motion (sliding) of the surfaces involving friction. ABAQUS uses Coulomb friction model to define the interaction of contacting surfaces. The model characterizes the friction behavior between the surfaces using a coefficient of friction $\mu$. The product $\mu P$, where P is the contact pressure between the two surfaces, gives the limiting frictional shear stress. The contact surfaces will not slip (sliding relative to each other) until the shear stress across their interface equals the limiting frictional shear stress, $\mu P$.

In our work it is assumed that the friction effect is negligible and $\mu=0$ is defined in all the models assuming there is no slip between the surfaces in contact. The interaction between the indenter and the specimen is modeled as contact pair without any friction. According to ABAQUS user manual [92], the indenter surface is defined as the 'master' surface since the indenter is rigid body. The top of the specimen is the 'slave' surface.

**4.0 Elastic-Plastic Indentation of Homogeneous Materials**

**4.1 Introduction**

In this chapter, the finite element method is used to analyze the indentation of elasto-plastic materials by a rigid, spherical indenter. The elastoplastic materials are modeled by a power-law constitutive relationship between stress and strain. In contrast to the work reported in literature, the focus is on deep indentation and on the effect of the strain hardening index on the indentation deformation. Discussions are also given on the effect of the strain hardening index on the energy ratio of the dissipated plastic energy to the total mechanical work. In the simulation, we assume: 1) the material is isotropic and homogeneous, 2) the system is isothermal, and 3) the material is not subjected to body force.

**4.2 Spherical Indentation as a Boundary Value Problem**

Without any body force, the mechanical equilibrium conditions are valid during indentation,

$$\frac{\partial \sigma_{ij}}{\partial x_j} = 0$$

---------------4.2.1
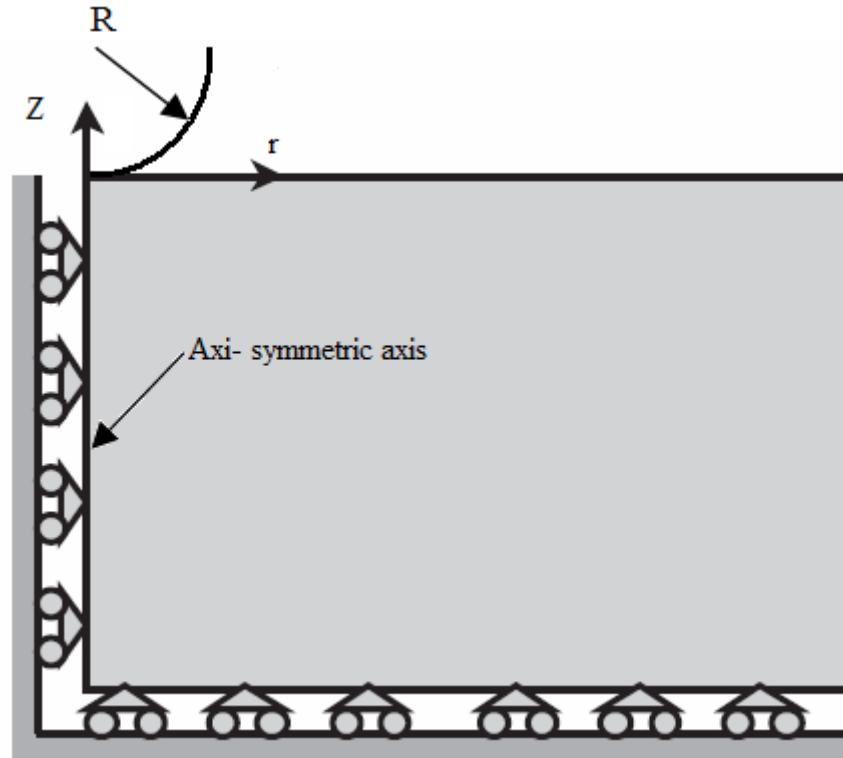


Figure 4.2-1    Schematic of the Axisymmetric Indentation of a Semi-Infinite

Elastoplastic Material with a Spherical Indenter

where $\sigma_{ij}$ $(i, j = 1, 2, 3)$ are the components of the stress tensor and $x_i$ are the

components of the position vector of a material point.

As shown in (Figure 4.2-1), a rigid, spherical indenter is pressed onto the surface of a semi-infinite elasto-plastic material. The contact boundary conditions in a cylindrical coordinate $(r, \theta, z)$ are

$$\sigma_{rz}(r,0) = 0 \quad \text{for } r < a \qquad \text{----------------4.2.2}$$

$$u_z(r,0) = f(r) - \delta \quad \text{for } r < a \qquad \text{----------------4.2.3}$$

where $\sigma_{rz}$ and $\sigma_{zz}$ are respectively the shear and normal components of the stress tensor, $u_z$ is the displacement component along the loading direction, $f(r)$ is the surface profile of the indenter tip, $\delta$ is the displacement of the indenter, and $a$ is the radius of the contact area to be determined in the simulation.

Equation 4.2-2 and Equation 4.2-3 represents the condition of frictionless contact between the indenter and the material. Outside the contact area, the surface is at stress-free state, i.e.

$$\sigma_{rz}(r,0) = \sigma_{zz}(r,0) = 0 \quad \text{for } r > a \qquad \text{----------------4.2.4}$$

The far field condition requires, $\sigma_{rz}(r,z) \to 0$, $\sigma_{zz}(r,z) \to 0$, $u_r(r,z) \to 0$, and $u_z(r,z) \to 0$ as $r \to \infty$ or $z \to -\infty$. The indentation load applied to the indenter can be calculated as

$$F = -2\pi \int_0^a \sigma_{zz}(r,0)\,rdr \qquad \text{---------------4.2.5}$$

### 4.3 Finite Element Model of Homogeneous Material

The overall size of the finite element model is taken large enough to ensure the characteristic of a half space. The ratio of the radius of the rigid, spherical indenter to the length of the geometrical model is 1:12 along the loading and radial directions to allow for considerable decrease in deformation before reaching constrained boundaries. As shown in (Figure 4.3-1) finer mesh is created around the indenter and the element size is increased making the mesh denser away from the indenter towards the boundary of the model.

Using the homogenous model the effect of strain hardening index 'n' in Equation 3.4-3 is analyzed by varying the material properties generated using Equation 3.4-3. Figure 4.3-2 shows the variation of the material properties for different strain hardening indices which are used.
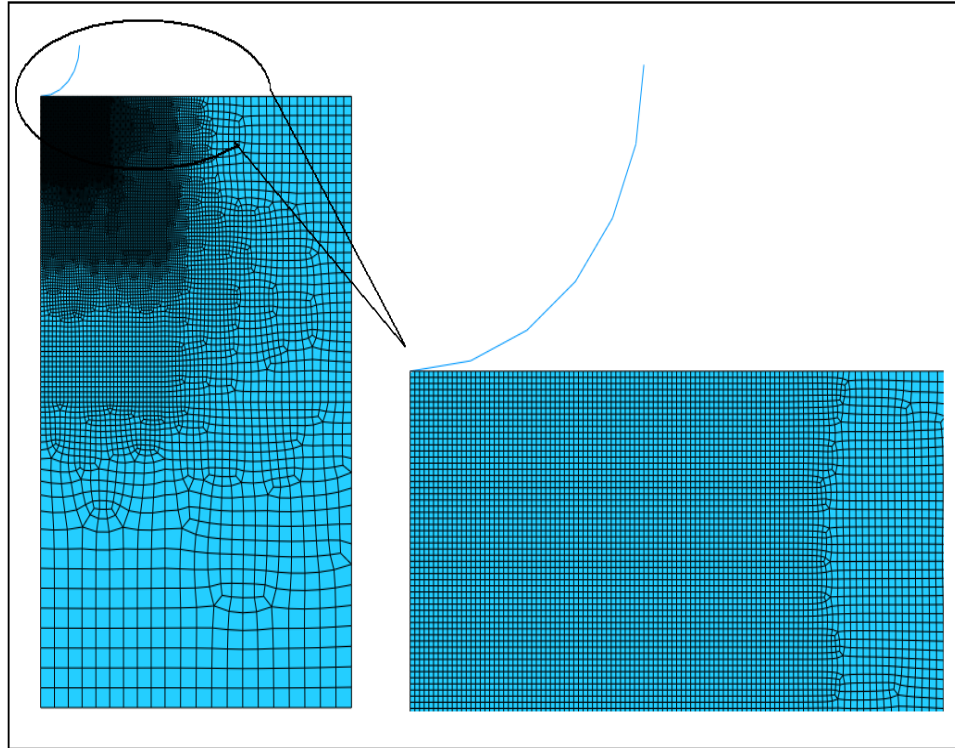
Figure 4.3-1    Finite Element Model of the Homogeneous Model
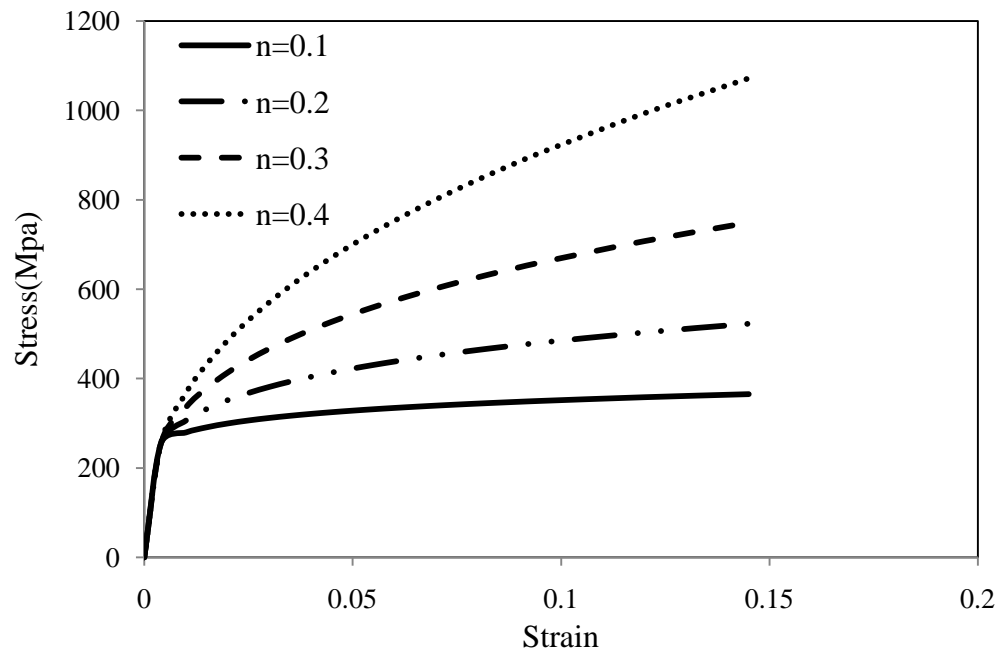


Figure 4.3-2        Stress Strain Curves for Different Strain Hardening Indices

## 4.4 Results and Discussion

### 4.4.1 Validation of the Spherical Indentation

A general theoretical framework can be proposed in terms of the original formulation derived by Hertz [1]. In the context of F-δ measurements on a flat surface (with infinite radius of curvature), which is indented by an elastic sphere, Hertz showed that:

$$F = C\delta^{\frac{3}{2}}$$

----------------4.4.1

$$C = \frac{2\sqrt{2}}{3} E_{eff} D^{\frac{1}{2}}$$

----------------4.4.2

where D is the diameter of the sphere and E_eff is the reduced Young's modulus of the specimen indenter system defined by Equation 4.4-3.

$$\frac{1}{E_{eff}} = \frac{1-v^2}{E} + \frac{1-v_i^2}{E_i}$$

----------------4.4.3

Where $E$ and $v$ are the elastic parameters for the material, $E_i$ and $v_i$ are the elastic parameters related to indenter.

Assuming spherical indenter to be perfectly rigid the above equation for the force reduces to

$$F = \frac{2\sqrt{2}}{3} \frac{E\sqrt{D}}{1-v^2} \delta^{\frac{3}{2}}$$         ----------------4.4.4

### 4.4.1.1 Elastic finite element model

In the elastic finite element model, the frictionless interface is assumed to compare results with the Hertz analytical solution. Only elastic properties are required to be input in ABAQUS. Here E=69 MPa and v=0.33 are used.

Since the analytical elastic solution is based on the assumption of small deformation, a relatively shallow indentation is simulated to compare with it. The maximum indentation depth δ=50 mm, using diameter D=100 mm indenter. Also the indenter here is assumed to be perfectly rigid.
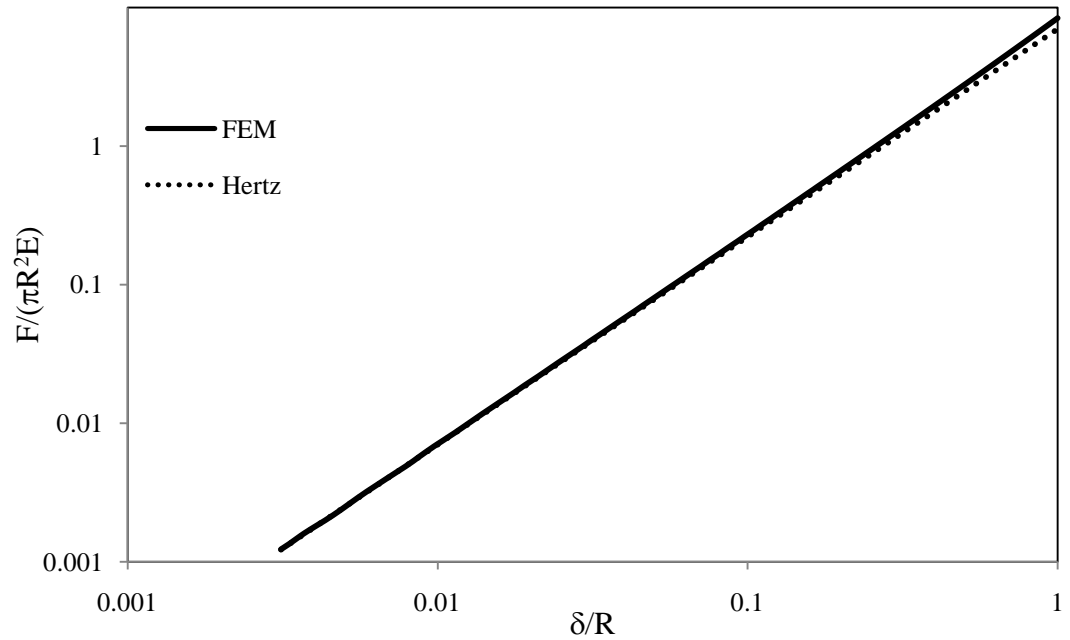
Figure 4.4-1     Comparison of Reaction Force from FEM Model and Hertz Model

for Spherical Indenter


It can be noticed from (Figure 4.4-1) that the agreement of load-depth curve fits better in the small load than the large load. The latter part error on the comparison curve could result from the large deformation underneath the indenter caused by large load, which is not compatible with the small deformation assumption of elastic theory. In view of the favorable comparisons with Hertz analytical results, it may be concluded that the finite element mesh and modeling assumptions are appropriate for simulating the indentation of a half-space by a rigid sphere.

### 4.4.2 Load-Displacement Response

The finite element simulation has been performed by using the condition of frictionless contact between the indenter and the material. The indentation results are normalized by using the parameters of $F/\pi ER^2$ and $\delta/R$ for the indentation load and the indentation depth, respectively. Figure 4.4-2 shows the indentation loading-unloading curves for the strain hardening indexes of 0, 0.1, 0.2, 0.3, and 0.4. Clearly, higher indentation load is required to make the same indentation depth for the materials of large strain hardening index than that for the materials of small strain hardening index. The strain hardening has no significant effect on the slope of the unloading curves at the onset of the unloading, as expected. This suggests that the unloading behavior is controlled by the elastic properties of materials if there is no change in the microstructure and defects of materials. It is worth mentioning that there exist numerous dislocations and dislocation networks in metals, which could alter the unloading behavior of metals due to plastic recovery. However, this work only focuses on the indentation deformation from continuum plasticity.

Figure 4.4-3 shows the effect of the strain hardening index on the ratio of the dimensionless force, $F/\pi ER^2$, to the dimensionless indentation depth, $\delta/R$. In general, the ratio increases with the increase in the strain hardening index for the same indentation depth due to the strain hardening behavior. However,

approximately linear relation between the strain hardening index and the ratio is observed for $\delta / R < 0.05$ and $\delta / R \geq 0.2$. The ratio reaches the maximum value at $\delta / R \approx 0.1$, dependent of the strain hardening index. Such a behavior reveals the effect of the indenter size on the indentation deformation. The indentation deformation is a complicated function of the strain hardening index and the indentation load, even though the indentation depth increases with the increase in the indentation load.
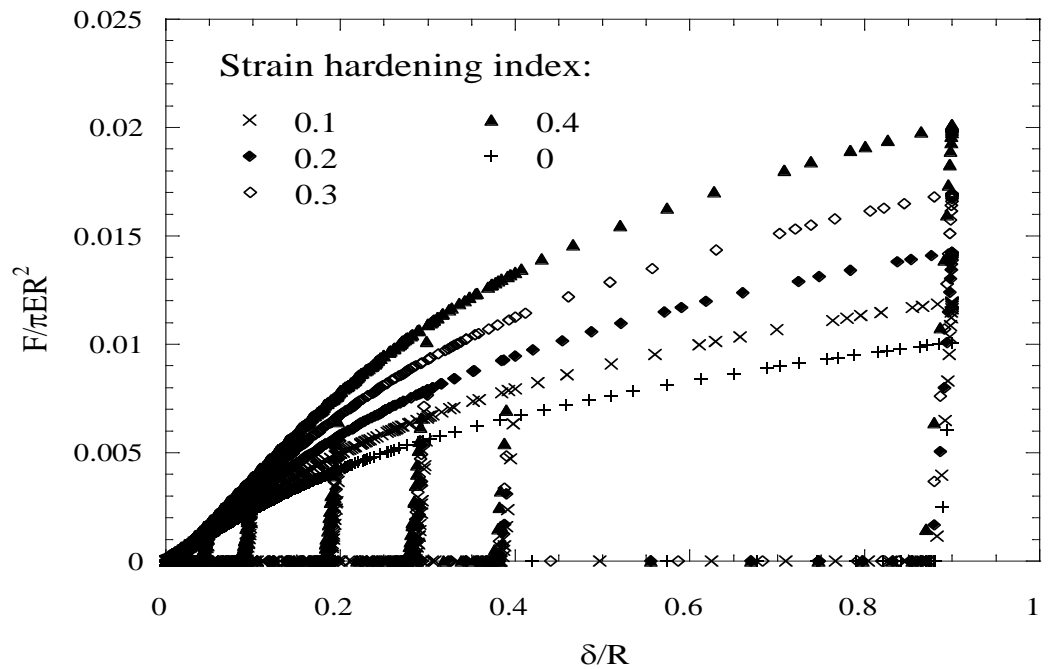


Figure 4.4-2    Typical Indentation Loading-Unloading Curves for Various Strain Hardening Indexes
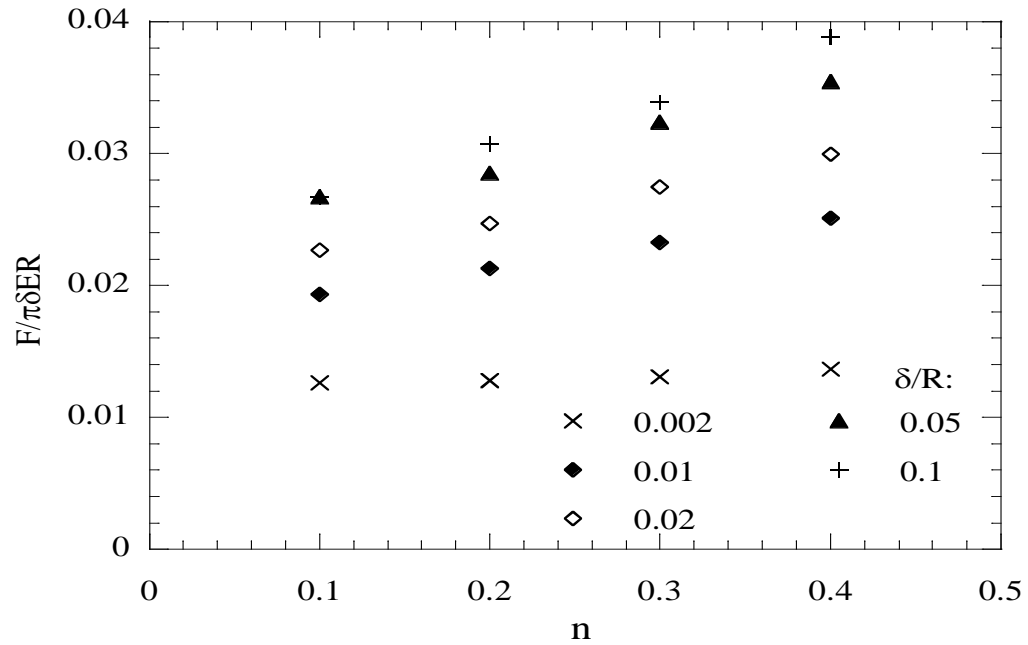
(a)
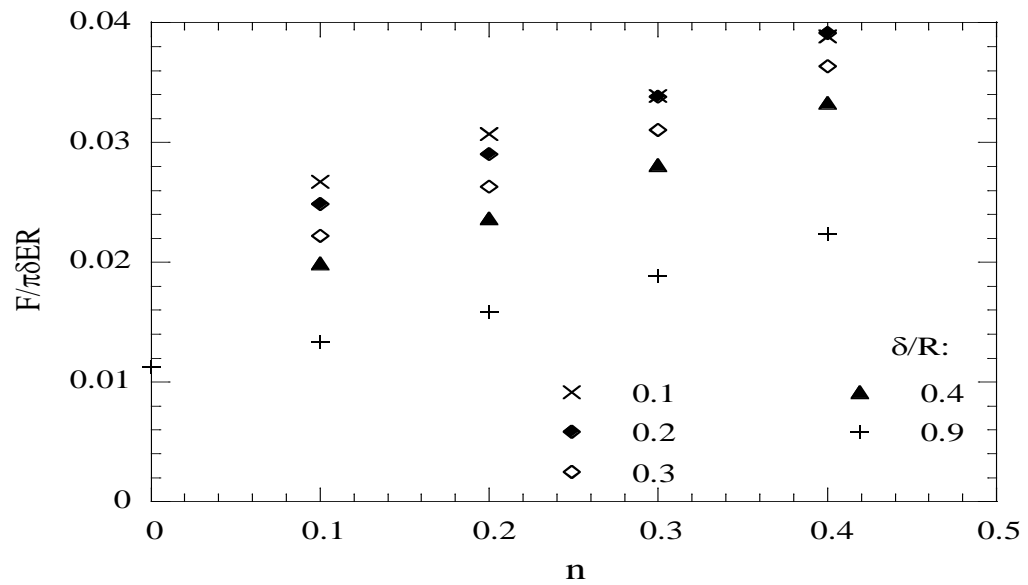


(b)

Figure 4.4-3  Dependence of the Ratio of the Dimensionless Load ($F/\pi ER^2$) to the

Dimensionless Depth ($\delta/R$) on the Strain Hardening Index;

(a) The Results for $\delta/R \leq 0.1$, & (b) The Results for $\delta/R \geq 0.1$

35
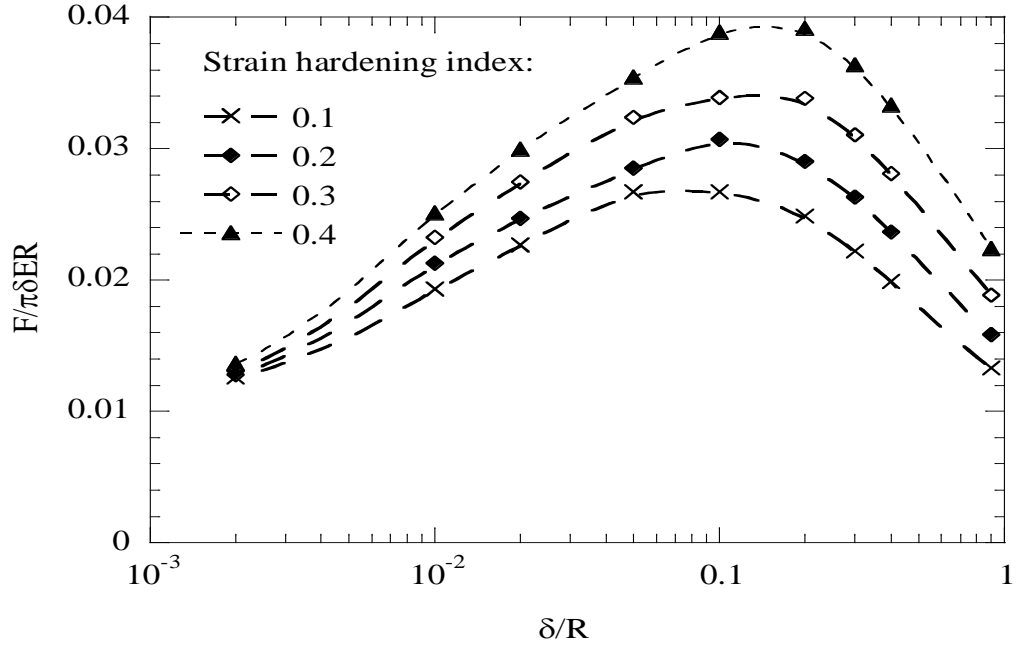
Figure 4.4-4      Dependence of the Ratio of the Dimensionless Load ($F / \pi ER^2$) to

the Dimensionless Depth ($\delta / R$) on the Indentation Depth for Different Strain

Hardening Indexes

In general, the indentation load is a power function of the indentation depth with the

power in the range of 1.2 to 2 for shallow indentation. Figure 4.4-4 shows the

dependence of the ratio on the indentation depth for different strain hardening

indexes. The ratio increases first with increasing the indentation depth, reaches the

maximum value, and then decreases with the indentation depth. The results suggest

that the relation between the indentation depth and the indentation load cannot be

simply described by a power function. Actually, such a power law relation can only

hold for shallow indentation of $\delta / R \leq 0.05$ for $0.1 \leq n \leq 0.4$, as shown in Figure

4.4-4. Caution needs to be taken in analyzing experimental results for indentations by rigid, spherical indenters.

### 4.4.3  Elastic Energy

From the computed indentation loading-unloading curve, one can calculate the total mechanical work done to the material as

$$W = \int_0^{\delta_{max}} F d\delta \qquad \text{----------------4.4.5}$$

where $\delta_{max}$ is the maximum indentation depth. The mechanical work can be calculated from the area under the indentation loading curve. One can calculate the elastic recovery energy released during the unloading process, $E_{elastic}$, as

$$E_{elastic} = \int_{\delta_r}^{\delta_{max}} F_{un} d\delta \qquad \text{----------------4.4.6}$$

where $\delta_r$ is the residual indentation depth. The elastic recovery energy can be evaluated from the area under the unloading curve. Thus the plastic energy dissipated in an indentation loading-unloading cycle, $E_{plastic}$, as represented by the area enclosed by the indentation loading-unloading curve and the depth axis, is given as

$$E_{plastic} = W - E_{elastic} \qquad \text{----------------4.4.7}$$

37

Table 4.4-1 summarizes the different parameters of the indentation as function of strain hardening index. The stiffness decreases with increasing the strain hardening index. Residual depth is shown a reducing trend with the increasing 'n' for a given friction factor and for a given 'n' the residual depth decreased with increase in friction factor. Increase in reaction force was observed as 44% for n-0.1 from that of 0. The plastic energy and total energy increased constantly with 'n'.

It has been proposed [71] for sharp indenters that there exists a linear relationship between the energy ratio, $E_{plastic}/W$, and the indentation depth ratio, $\delta_r/\delta_{max}$, for $\delta_r/\delta_{max} > 0.4$. Figure 4.4-5 shows the dependence of the energy ratio on the indentation-depth ratio for the indentation depth up to $0.9R$. Clearly, the energy ratio is a linear function of the indentation-depth ratio in accordance with the results for indentation by sharp indenters [71]. Using curve-fitting for a linear function, one can obtain the extrapolated value of the energy ratio as $\delta_r/\delta_{max} \to 0$. The extrapolated value of the energy ratio is 0.093 in contrast to the value of -0.27 given by Cheng et al. [71] for sharp instrumented indentations. Such a difference is likely due to the shape effect of the indenter tip, which creates different stress field underneath the indenter and different plastic deformation zone. Severer plastic deformation is made by sharp indenters than those by spherical indenters.

Table 4.4-1  Different properties of the indentation.

| n | Contact stiffness | Contact radius | Max. depth | Residual Depth | E (total) | E (plastic) | Reaction force | Yield stress location from indenter |
|---|---|---|---|---|---|---|---|---|
| 0 | 7786807 | 49.25 | 45 | 43.97 | 1.58E+08 | 1.56E+08 | 5.47E+06 | |
| 0.1 | 7540706 | 49.28 | 45 | 43.67 | 1.88E+08 | 1.85E+08 | 6.48E+06 | 156 |
| 0.2 | 7429638 | 49.35 | 45 | 43.49 | 2.23E+08 | 2.19E+08 | 7.73E+06 | 166 |
| 0.3 | 7404118 | 49.45 | 45 | 43.30 | 2.64E+08 | 2.58E+08 | 9.19E+06 | 177 |
| 0.4 | 7398427 | 49.54 | 45 | 42.73 | 3.12E+08 | 3.03E+08 | 1.09E+07 | 184 |
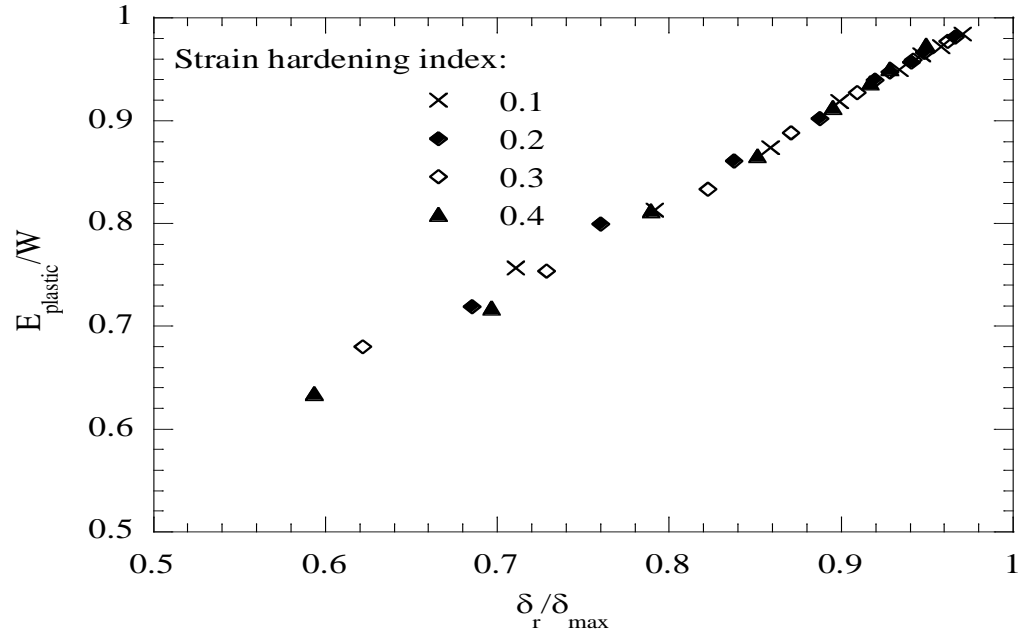
Figure 4.4-5    Dependence of the Energy Ratio, $E_{plastic} / W$ , on the Depth Ratio,

$\delta_r / \delta_{max}$ for Various Strain Hardening Indexes

### 4.4.4   Surface Profile

One of important parameters affecting the analysis of the indentation deformation is the size of the pile-up, $\delta_{pile-up}$ (Figure 4.4-6).  Pile-up occurs during the indentation of elasto-plastic materials. Bolshkov and Pharr [79] examined the significance of materials pile-up for conical indenters and found that if pile-up is neglected, the calculated material properties can be underestimated by as much as 60%.
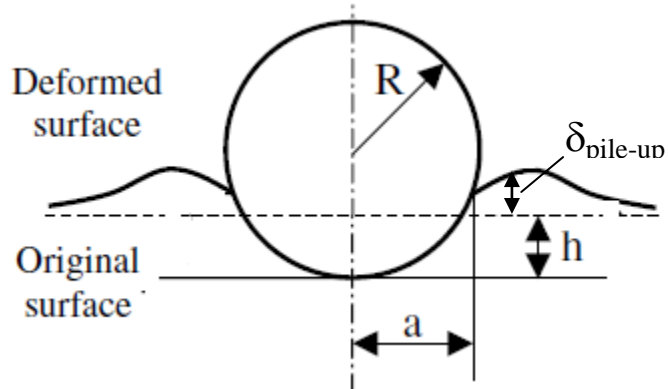
Figure 4.4-6    Sketch of Pile-Up Occurred During Indentation of an Elastic-

Plastic Material.

The material pile-up occurred during deep indentation by a spherical indenter was examined using the finite element simulation. The surface profiles during indentation were constructed, as seen in Figure 4.4-7, based upon the nodal displacements. From these plots, the amount of pile up was calculated.
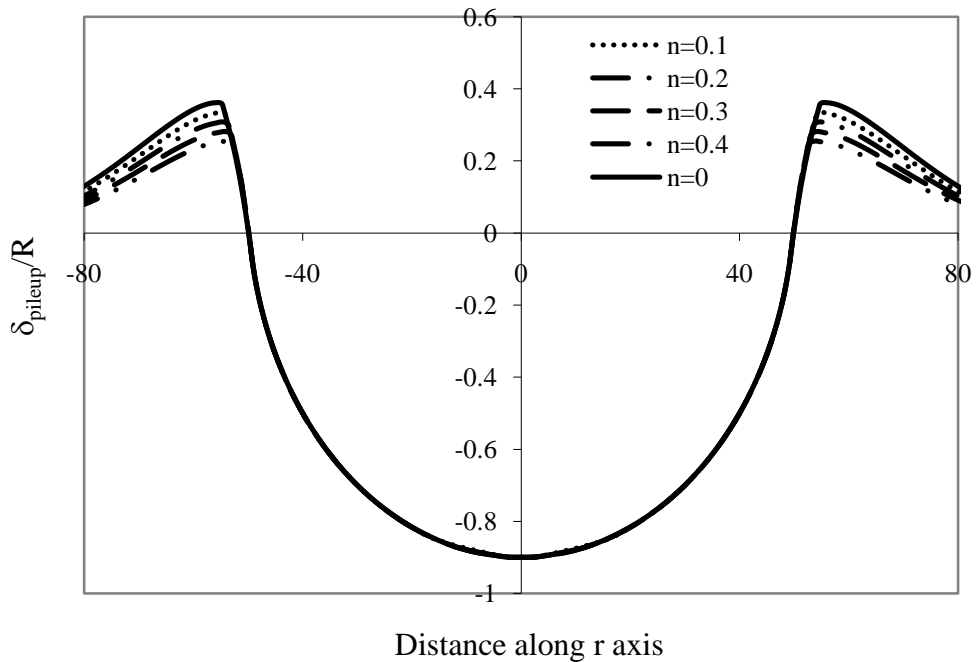


Figure 4.4-7  Surface Profiles of a Specimen under a Spherical Indenter.
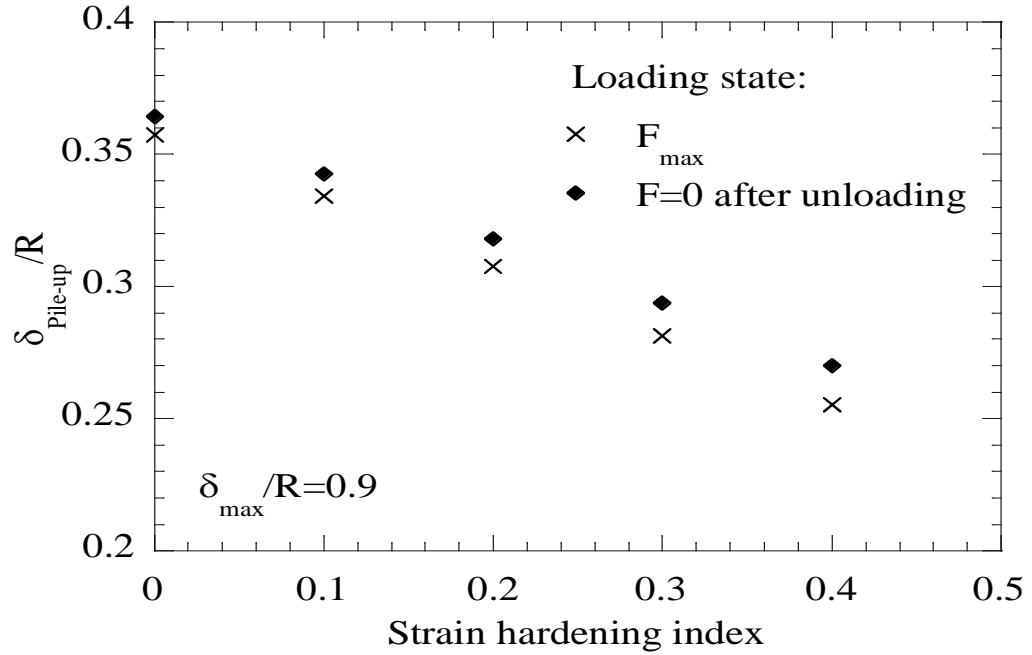
Figure 4.4-8  Dependence of the Pile-Up on the Strain Hardening Index.

Figure 4.4-8 shows the dependence of the pile-up on the strain hardening index with the maximum indentation depth of 0.9 R. The pile-up linearly decreases with the increase in the strain hardening index. The material has larger pile-up at the unloading state than that subjected to the peak indentation load. During the unloading, elastic recovery occurs which allows material to move to the self-equilibrium state.

## 4.5 Summary

The finite element analysis has been used to simulate the deep indentation of strain-hardening, elastoplastic materials by a rigid, spherical indenter. The displacement of the indenter has been pushed up to 90% of the radius of the spherical indenter onto the materials. A linear relation is observed between the strain hardening index and the ratio of the peak indentation load to the maximum indentation depth. The power law relation between the indentation load and the indentation depth is only valid for shallow indentation of the maximum indentation depth up to 5% of the indenter radius. For deep indentation, the power law relation breaks, and caution needs to be taken in analyzing experimental results for deep indentations by spherical indenters. Similar to sharp instrumented indentation for the ratio of the residual indentation depth to the maximum indentation depth larger than 0.57, the ratio of the plastic energy to the total mechanical work is a linear function of the ratio of the residual indentation depth to the maximum indentation depth for the indentations by spherical indenters, independent of the strain hardening index. However, the extrapolated value of the energy ratio is different from that for the sharp instrumented indentation.

## 5.0 Elastic Indentation of Layered Materials

## 5.1 Introduction

Layered materials (film-substrate systems) have been increasingly used in applications such as microelectronics, optoelectronics and protective coatings on engineering structures. The low-load/low-depth indentation, or nano-indentation, has recently been used to characterize the mechanical properties of films and multi layers. When a thin film is deposited on a substrate, the deformation and stress field in the resultant layered materials becomes much more complex. The classical Hertz contact theorem is no longer valid in characterizing the load-depth response for the indentation of a layered material. Considerable efforts have been devoted to analyzing the indentation on film-substrate systems, including experimental testing and analytical modeling. In the present study, the finite element analysis was carried out on the film-substrate systems (layered materials) under a spherical indenter. The emphasis was placed on the quantitative aspects of the indentation: the load-depth response.

There are two types of film-substrate systems: soft film-hard substrate systems and hard film-soft substrate systems. Both types of system were modeled in the present study. In all studies, the substrate was assumed to be the same, i.e., having the fixed

elastic modulus ($E_2$) and Poisson's ratio ($v_2$). The films were assigned to different property $E_1$ as normalized with the properties of the substrate, however $v_2$ itself used as the Poisson's ratio.

## 5.2    Spherical Indentation as a Boundary Value Problem
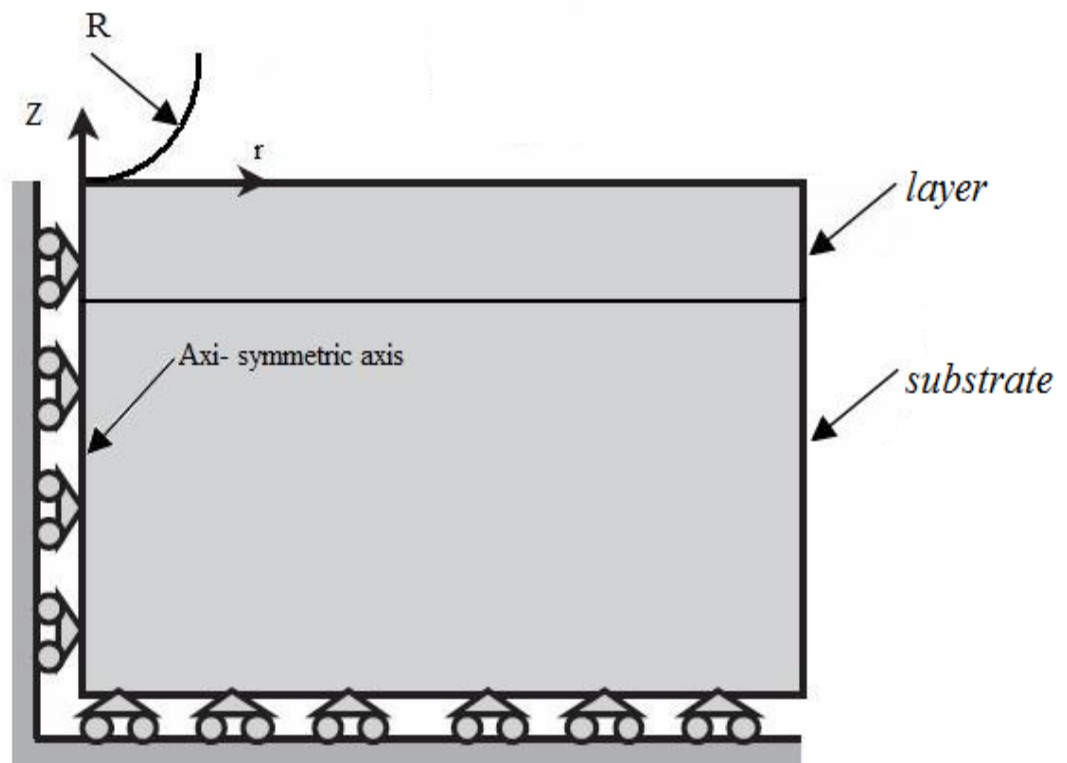


Figure 5.2-1 Schematic of the Axi-Symmetric Indentation of a Semi-Infinite Thin Film-substrate Material with a Spherical Indenter.

Without any body force, the mechanical equilibrium conditions are assumed valid during indentation,

$$\frac{\partial \sigma_{ij}^{(1)}}{\partial x_j} = \frac{\partial \sigma_{ij}^{(2)}}{\partial x_j} = 0 \qquad \text{----------------5.2.1}$$

where $\sigma_{ij}^{(k)}$ ($i, j = 1, 2, 3$) are the components of the stress tensor, for superscript k=1,2 for film and substrate respectively, $\partial x_j$ are the components of the position vector of a material point.

As shown in (Figure 5.2-1), a rigid, spherical indenter is pressed onto the surface of a semi-infinite elasto-plastic thin film-substrate material. The contact boundary conditions in a cylindrical coordinate $(r, \theta, z)$ are

$$\sigma_{rz}^{(1)}(r, 0) = 0 \quad \text{for r < a} \qquad \text{----------------5.2.2}$$

$$u_z^{(1)}(r, 0) = \text{f(r)} - \delta \quad \text{for r < a} \qquad \text{----------------5.2.3}$$

where $\sigma_{rz}^{(1)}$ and $\sigma_{zz}^{(1)}$ are respectively the shear and normal components of the stress tensor for the film, $u_z^{(1)}$ is the displacement component along the loading direction, $f(r)$ is the surface profile of the indenter tip, $\delta$ is the displacement of the indenter, and $a$ is the radius of the contact area to be determined in the simulation. Equation 5.2-2 and Equation 5.2-3 represents the condition of frictionless contact between the

indenter and the material. Outside the contact area, the surface is at stress-free state, i.e.

$$\sigma_{rz}^1(r,0) = \sigma_{zz}^1(r,0) = 0 \text{ for } r > a \qquad \text{----------------5.2.4}$$

The far field condition requires, $\sigma_{rz}^{(k)}(r,z) \rightarrow 0$, $\sigma_{zz}^{(k)}(r,z) \rightarrow 0$, $u_r^{(k)}(r,z) \rightarrow 0$, and $u_z^{(k)}(r,z) \rightarrow 0$ as $r \rightarrow \infty$ and $z \rightarrow -\infty$.

At the interface, it requires the continuity of the displacement and stresses, i.e.

$$u_r^{(1)} = u_r^{(2)} \text{ and } u_z^{(1)} = u_z^{(2)}$$

$$\sigma_{rz}^{(1)} = \sigma_{rz}^{(2)} \text{ and } \sigma_{zz}^{(1)} = \sigma_{zz}^{(2)}$$

where superscripts (1) and (2) represent the film and substrate respectively.

The indentation load applied to the indenter can be calculated as

$$F = -2\pi \int_0^a \sigma_{zz}(r,0) r dr \qquad \text{----------------5.2.5}$$

**5.3 Finite Element Model of Film-Substrate Systems**

As shown in Figure 5.3-1, a thin film-substrate model is generated with thin film and substrate making up the entire model to simulate the layered condition in the process of indentation using finite element method. Spherical indenter is used to simulate the layer model.

47
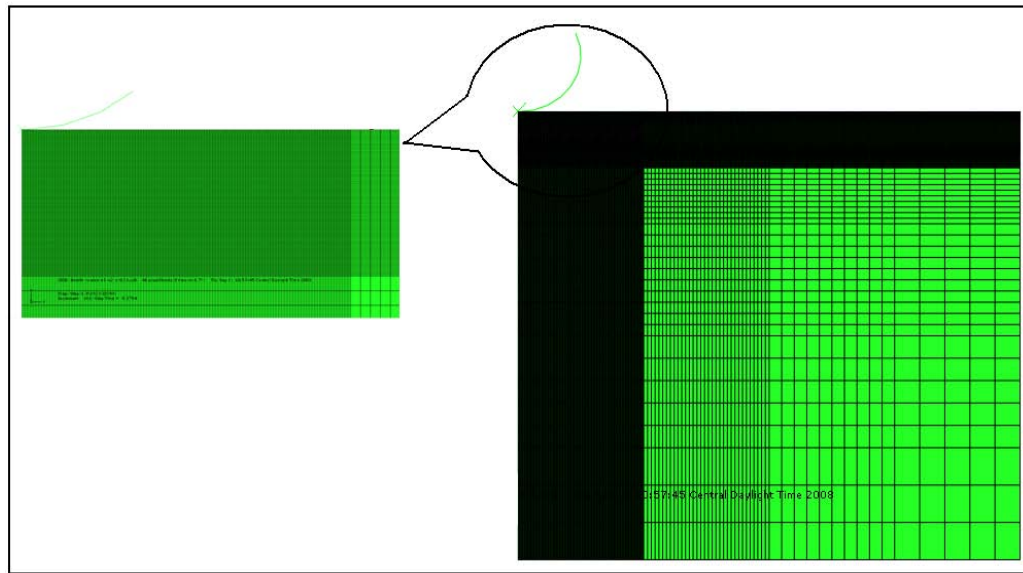
Figure 5.3-1    Finite Element Model of a Double Layer Model.

Both soft and hard films were analyzed using the layered model with varying material properties. The surfaces between interior parts of the sample, as the interface between the deposited layer and the substrate is defined as being perfectly bonded, that is no delamination or slippage can occur. To study the effect of the layer thickness, different models are generated with varying thickness of the layers. The coating thickness is varied as listed out in

Table **5.3-1**. Starting with minimum thickness of 10 of the layer equal to 20% of the indenter radius, with a step increase of 10 also equal to 20% of the indenter radius, the models are analyzed for a maximum coating thickness of 50 which is equal to the radius of the indenter in relation to the model size of 400X400.

48

Table 5.3-1 Film Thickness Used in Finite Element Analysis.

| Thickness of film (h) | Normalized Thickness of the film (h/R) |
|---|---|
| 10 | 0.2 |
| 20 | 0.4 |
| 30 | 0.6 |
| 40 | 0.8 |
| 50 | 1 |

The effect of the film modulus was also investigated. In the present analysis, the substrate material was fixed (Al-6061) and its properties are shown in Table 5.3-2.

The properties of the film ($E_1$) were varied by normalizing with the modulus of substrate ($E_2$), as shown in Table 5.3-3.

Table 5.3-2 Material Properties of the Substrate Used in Finite Element Analysis.

| Material | E (N/mm$^2$) | Poisson ratio |
|---|---|---|
| AA 6061-T6 | 69000 | 0.33 |

Table 5.3-3 Ratio of Young's Modulus for Film and Substrate

| $E_1/E_2$ |
|---|
| 0.01 |
| 0.025 |
| 0.05 |
| 0.075 |
| 0.1 |
| 0.25 |
| 0.5 |
| 0.75 |
| 1 |
| 10 |
| 25 |

| 50 |
|---|
| 75 |
| 100 |

To verify the FE model, the film-substrate system was first analyzed by assuming that the film and the substrate have the same properties. The problem therefore becomes an indentation of homogeneous material. The resultant load-displacement curve of this film-substrate system is seen in Figure 5.3-2. Also included is the Hertz's solution calculated using Equation 4.4-4. It is observed that the data generated from the FE model is in good agreement with the Hertz equation. Hence the FE model generated can be used for subsequent film-substrate analysis.
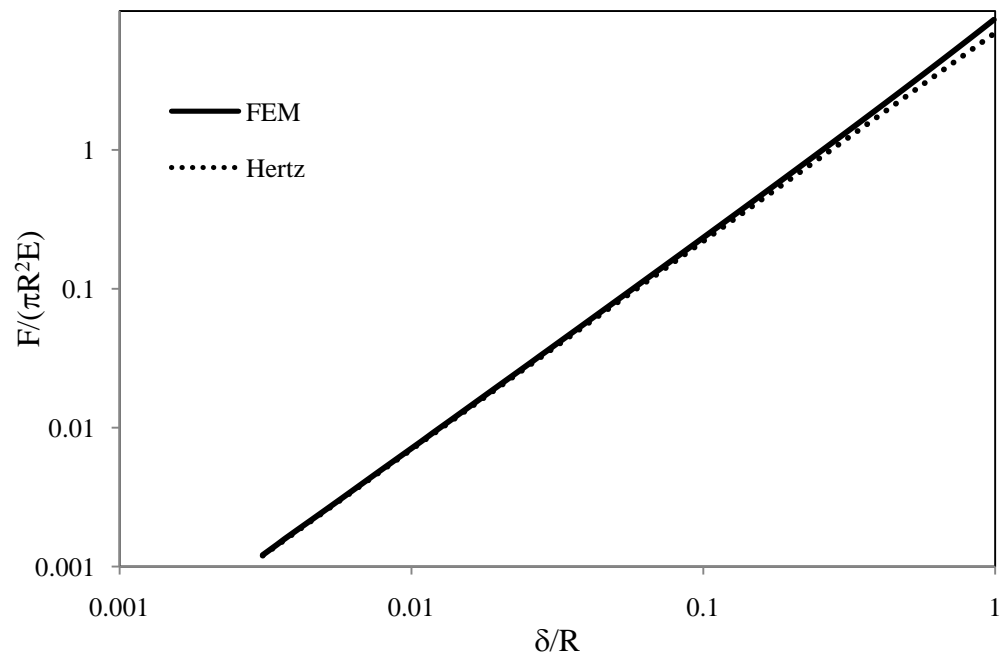


Figure 5.3-2    Comparison of the FEM Result with the Hertz Equation.

**5.4 Results and Discussion**

**5.4.1 Load-Displacement Response**

Figure 5.4-1 and Figure 5.4-2 show the typical load-displacement curves of a hard film- substrate system and a soft film- substrate system, respectively.  As expected, the load-displacement responses of the film-substrate systems are bounded between the homogeneous films and substrates.
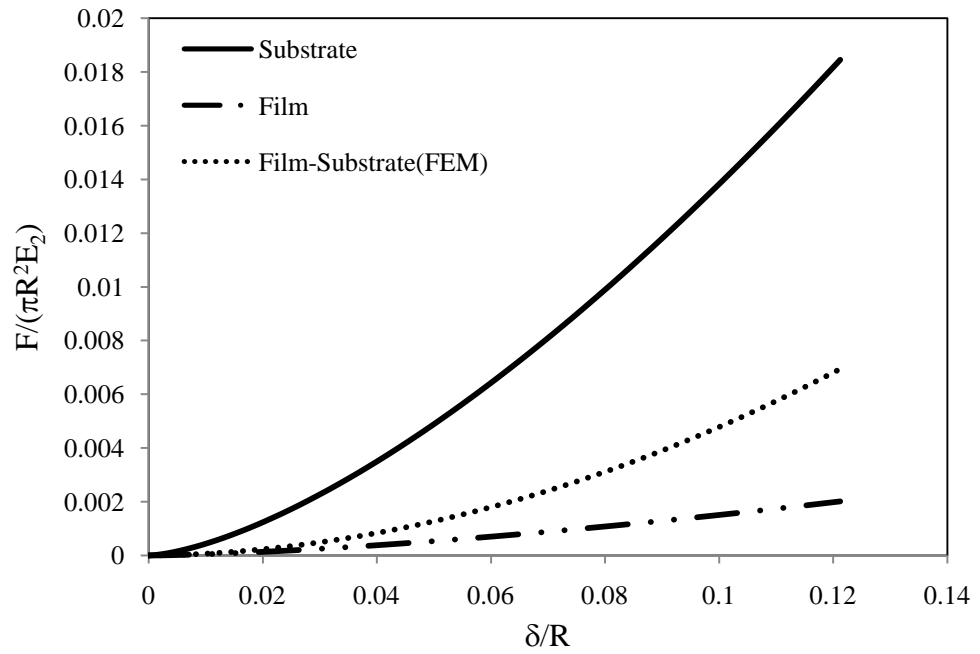


Figure 5.4-1 Load-displacement Curve for Soft Film-Hard Substrate

(h=10 & $E_1/E_2$-0.01, $\nu_1/\nu_2$-1)
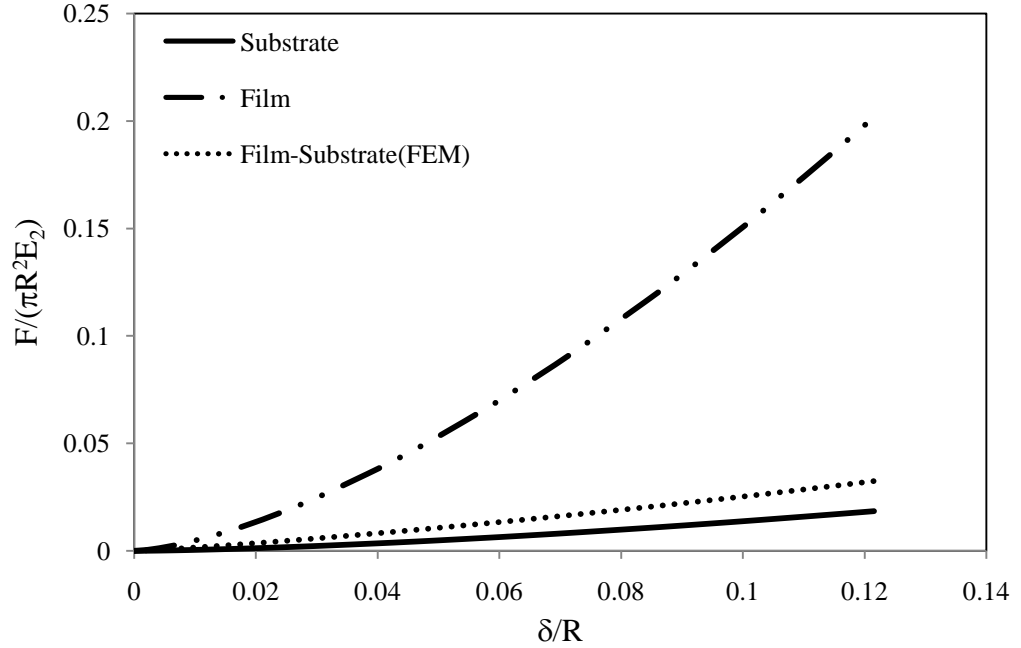
Figure 5.4-2 Load-displacement Curve for Hard Film-Soft Substrate

(h=10 & $E_1/E_2$-10, $\nu_1/\nu_2$-1)

Figure 5.4-3(a) and (b) shows the stress plots for a soft film over hard substrate and for a hard film over soft substrate for same penetration depth and same spherical indenter. From these two plots we can observe for the soft film over the hard substrate the maximum Mises stress is right underneath the indenter whereas for the other model which is hard film over the soft substrate the value is observed at the interface of thin film and substrate. Hence for the hard film over the soft substrate, the interface is prone to more failure risk than the other condition.
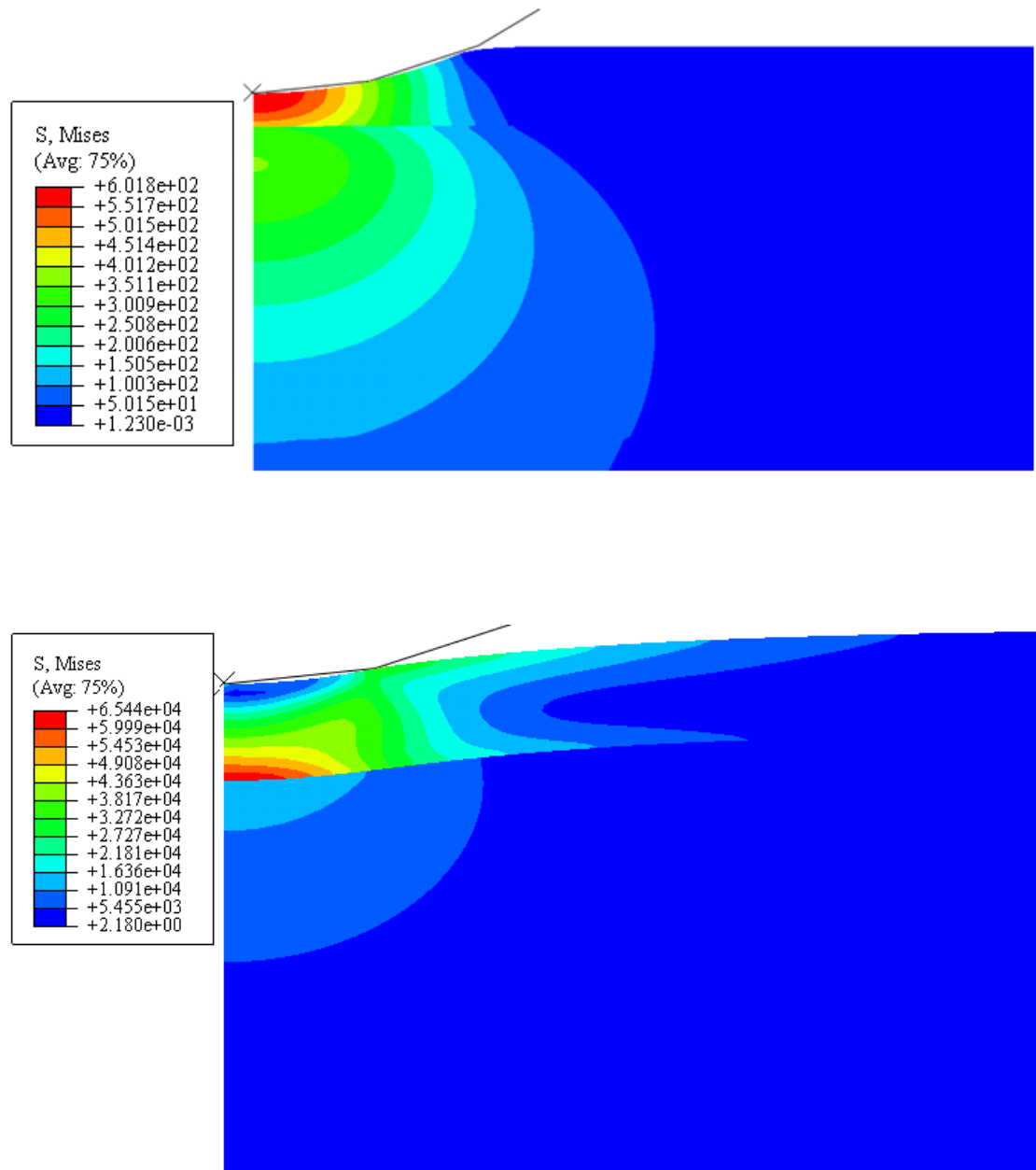
Figure 5.4-3 Stress Patterns for (a) Soft Film Over Hard Substrate and (b) Hard Film

over the Soft Substrate for the Same Applied Indentation Penetration.

### 5.4.4 Effect of Film Thickness

Figure 5.4-4 & Figure 5.4-5 show the indentation load-displacement curves in film-substrate structures with varying the film thickness. From these plots, we can observe that the maximum load reached and also the slope of the load-displacement curve changed with the thickness of the layer for the same applied penetration displacement. In the case of soft film-hard substrate system, the indentation load decreases with the increase of the film thickness; while in the case of hard film-soft substrate system, the indentation load increases with the increase of the film thickness.
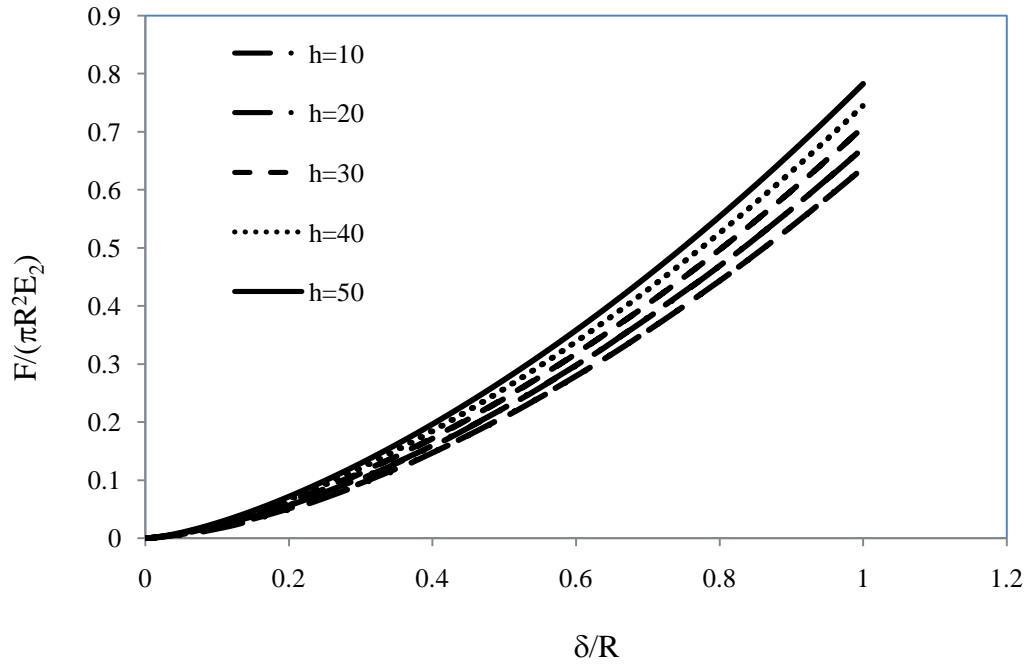


Figure 5.4-4     Variation of Load-displacement Data with Increase in the Layer

Thickness ($E_1/E_2$=2.2)
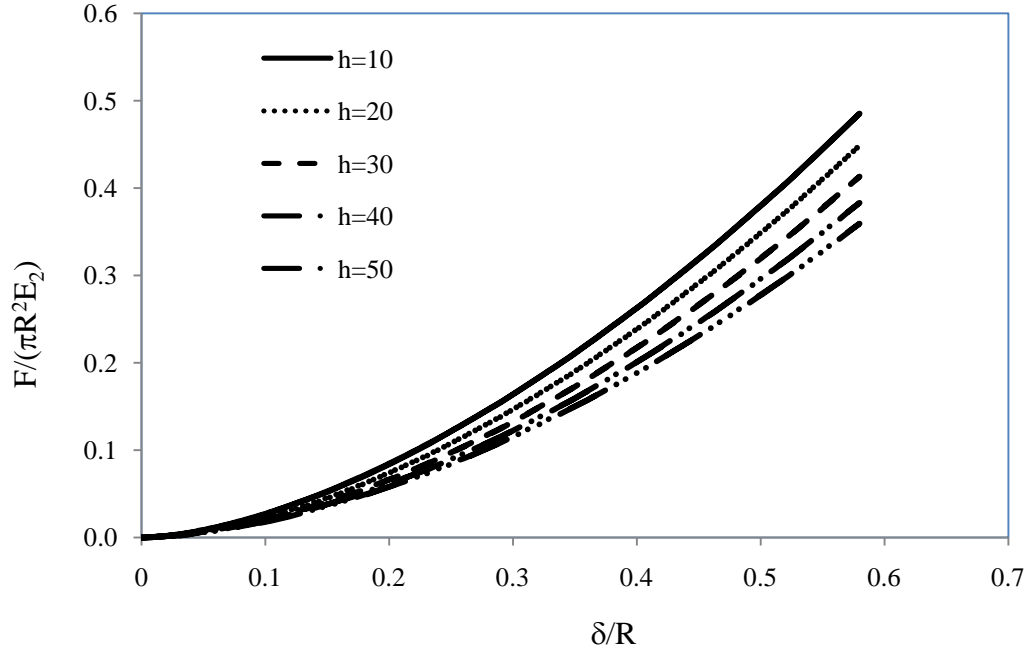
Figure 5.4-5     Variation of Load-displacement Data with increase in the Layer

Thickness ($E_1/E_2$=0.45)
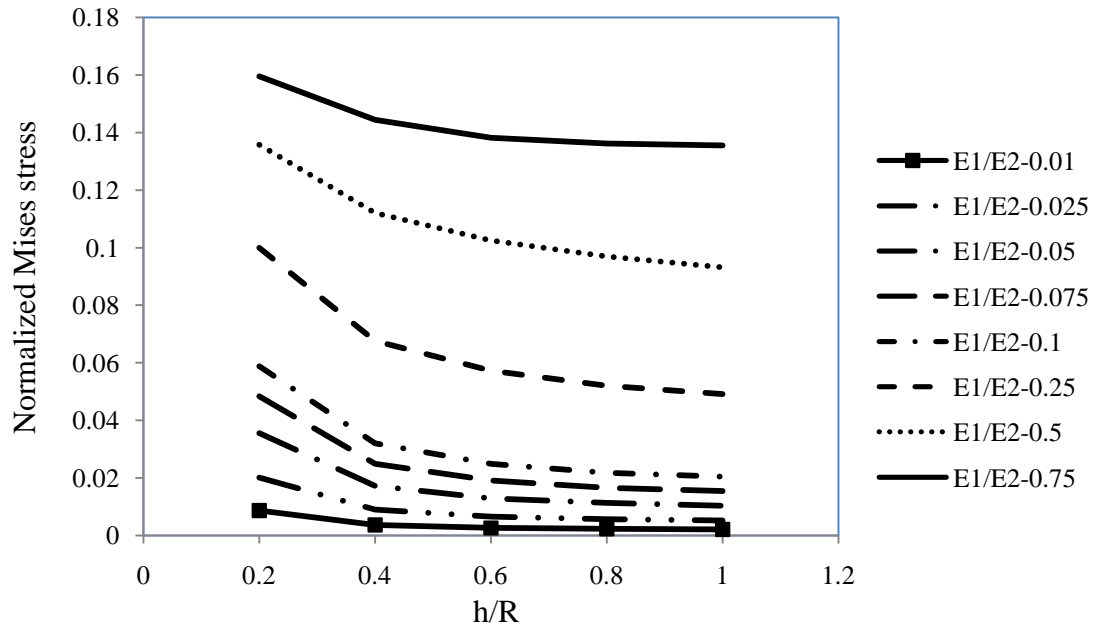


Figure 5.4-6     Variation of Maximum Mises Stress for Soft Thin Film over Hard

Substrate Model
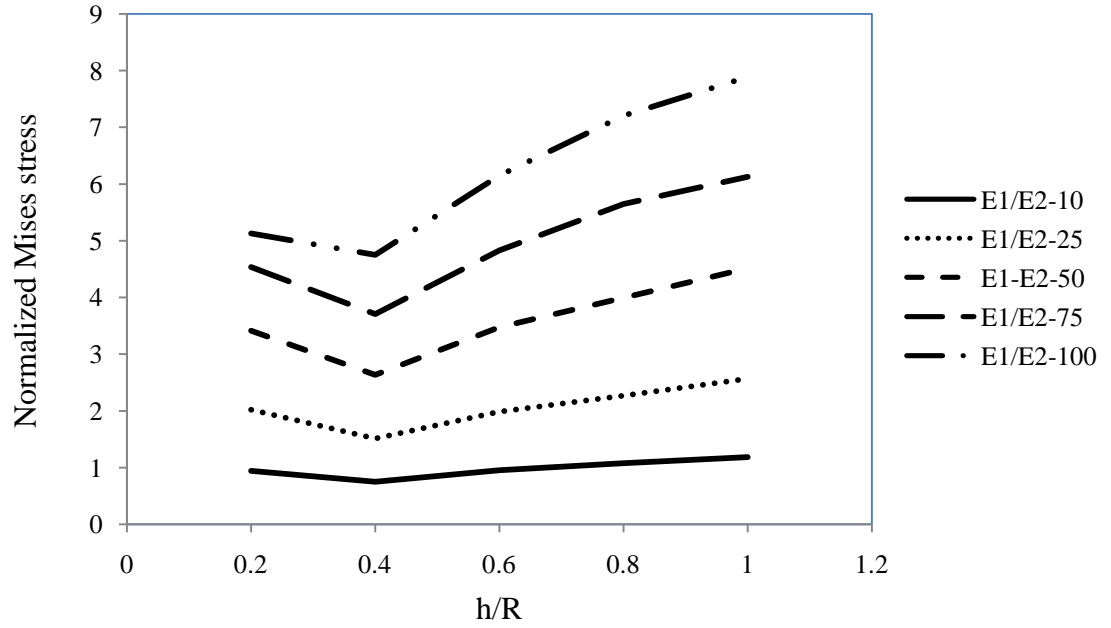
Figure 5.4-7 Variation of Maximum Mises Stress for Hard Thin Film over Soft

Substrate Model

Figure 5.4-6 show the effect of film thickness on von Mises stress soft thin film over

hard substrate and Figure 5.4-7 shows hard thin film over soft substrate. The

maximum stress is observed to reduce with increase in the value of h for $E_1/E_2<1$, but

for $E_1/E_2>1$ the maximum stress is observed to reduce first and then increase with the

increase in the layer thickness.

### 5.4.5 Effect of Film Elastic Modulus

Figure 5.4-8 (a) (b) & (c) shows the load-displacement responses of film-substrate

systems with different elastic modulus ratio mentioned in the Table 5.3-3 for h=10,

30 and 50 respectively . It is observed that the maximum load as well as the slope of

the load-displacement curve change with the Young's modulus ratio. The variation of

the maximum Mises stress underneath the indenter along the symmetric axis is given in Figure 5.4-9. From the figure, we can observe that the maximum stress increases with increasing the ratio of Young's modulus ($E_1/E_2$).
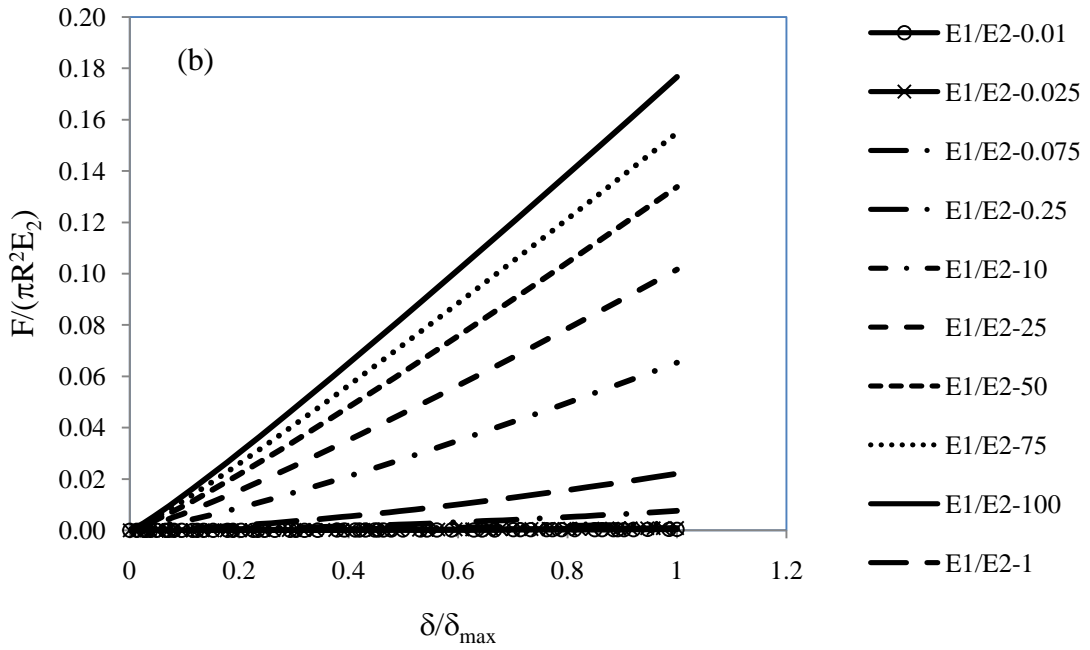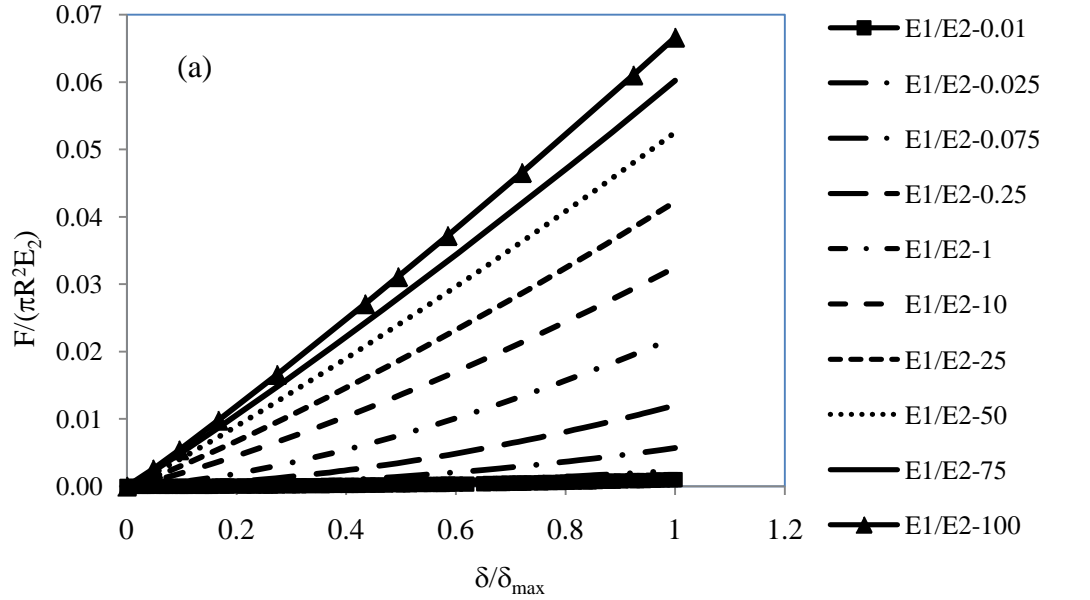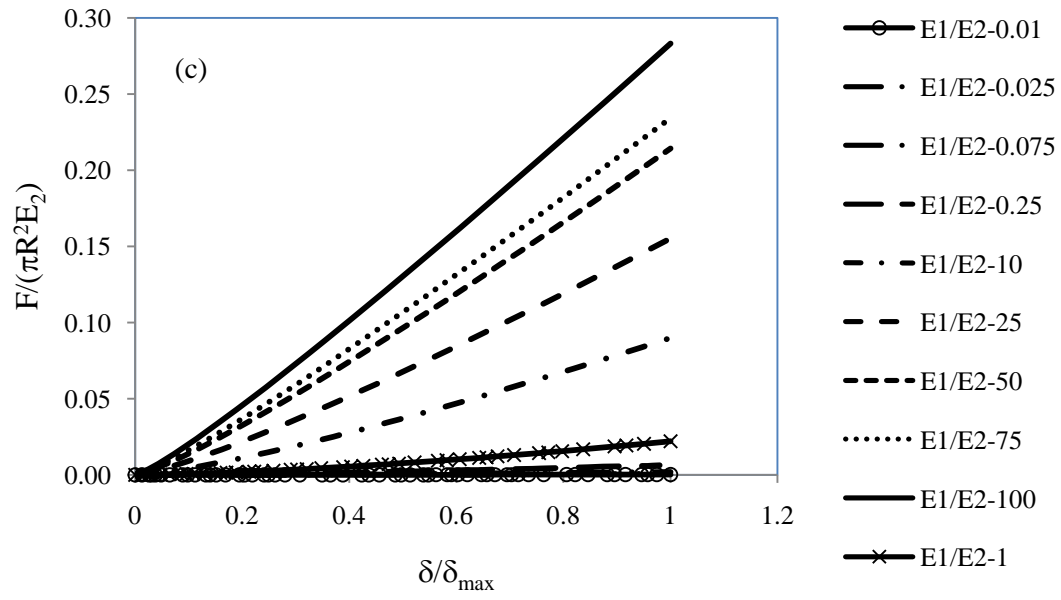
Figure 5.4-8    Variation of Load-displacement Data for Different Layer and

Substrate Combinations for a Given Thickness of the Layer

(a) h=10, (b) h=30, (c) h=50.
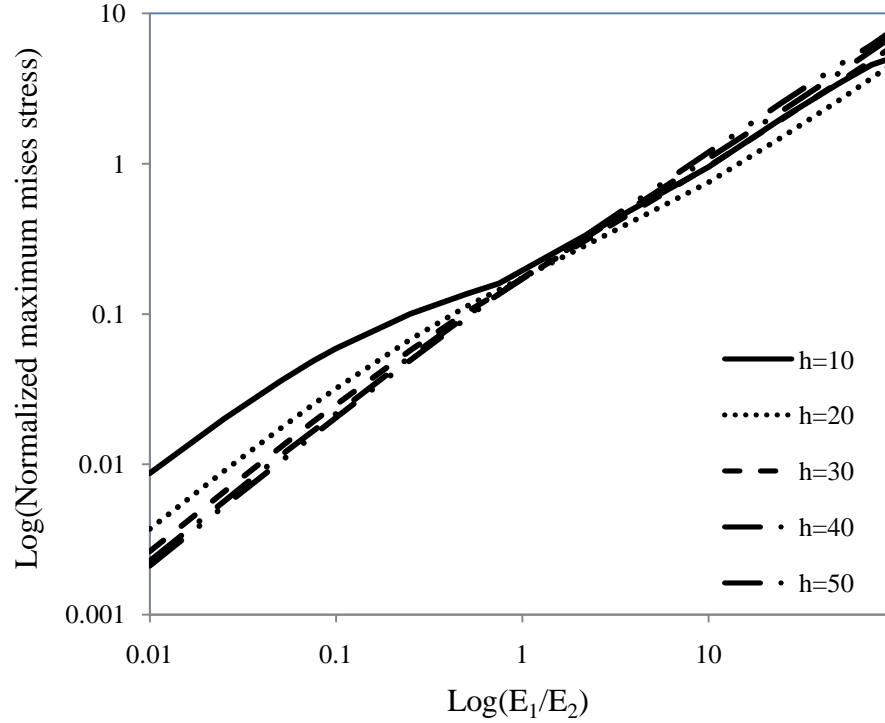
Figure 5.4-9Variation of Maximum Mises Stress for a Given Thin Film-substrate

Model with the Ratio of the Young's Modulus of Thin Film and Substrate

### 5.4.6   Load-displacement Relation: A Generalized Power Law Model

All the models generated with different layer thickness mentioned in the

Table **5.3-1** and different film modulus mentioned in Table 5.3-3 were analyzed for

the load-displacement data up to a penetration equal of 12% of the indenter radius.

It was found that the load-displacement curves in the layered materials vary with

the film thickness and modulus. By fitting the load-displacement data generated

using a wide range of film/substrate properties, a generalized power-law equation is obtained as follows

$$F = CE_2\delta^p \qquad\qquad \text{----------------5.4.1}$$

where F is the indentation load and $\delta$ the indentation penetration. C and p are material constants and defined by

$$C = 10 \wedge \{C_0 + C_1\left(\text{Log}\left(\frac{E_1}{E_2}\right)\right) + C_2\left(\text{Log }\left(\frac{E_1}{E_2}\right)\right)^2 + C_3\left(\text{Log }\left(\frac{E_1}{E_2}\right)\right)^3\}$$

$$C_0 = 0.9892 - 0.02725\left(\frac{h}{R}\right) + 0.068268\left(\frac{h}{R}\right)^2 - 0.03375\left(\frac{h}{R}\right)^3$$

$$C_1 = 0.2939 + 1.7397\left(\frac{h}{R}\right) - 1.9264\left(\frac{h}{R}\right)^2 + 0.77333\left(\frac{h}{R}\right)^3$$

$$C_2 = -0.11509 + 0.064477\left(\frac{h}{R}\right) + 0.00013037\left(\frac{h}{R}\right)^2 - 0.013021\left(\frac{h}{R}\right)^3$$

$$C_3 = 0.038188 - 0.15565\left(\frac{h}{R}\right) + 0.18009\left(\frac{h}{R}\right)^2 - 0.072568\left(\frac{h}{R}\right)^3$$

$$p = 10 \wedge \{p_0 + p_1\left(\text{Log}\left(\frac{E_1}{E_2}\right)\right) + p_2\left(\text{Log }\left(\frac{E_1}{E_2}\right)\right)^2 + p_3\left(\text{Log }\left(\frac{E_1}{E_2}\right)\right)^3 + p_4\left(\text{Log }\left(\frac{E_1}{E_2}\right)\right)^4\}$$

$$p_0 = 0.18478 - 0.010549\left(\frac{h}{R}\right) + 0.0081517\left(\frac{h}{R}\right)^2 - 0.0017708\left(\frac{h}{R}\right)^3$$

$$p_1 = -0.11958 + 0.15183\left(\frac{h}{R}\right) - 0.082706\left(\frac{h}{R}\right)^2 + 0.013552\left(\frac{h}{R}\right)^3$$

$$p_2 = -0.0000081967 - 0.081956\left(\frac{h}{R}\right) + 0.11148\left(\frac{h}{R}\right)^2 - 0.047344\left(\frac{h}{R}\right)^3$$

$$p_3 = 0.0089133 -0.0059241 \left(\frac{h}{R}\right) -0.010213 \left(\frac{h}{R}\right)^2 +0.0081615 \left(\frac{h}{R}\right)^3$$

$$p_4 = 0.0006394+ 0.0070813 \left(\frac{h}{R}\right) -0.010569 \left(\frac{h}{R}\right)^2 + 0.0045875 \left(\frac{h}{R}\right)^3$$

where   $E_1$-elastic modulus of the layer material

$E_2$- elastic modulus of the substrate material

h-layer thickness

R-radius of the indenter

The above equation indicates that for the indentation of any elastic film-substrate system, the resultant load-displacement response follows a general power-law relation that is defined by the normalized film modulus ($E_1/E_2$) and the normalized film thickness (h/R).  The validity of this generalized power-law equation has been validated with the testing data generated from the FEM.

Figure 5.4-10 show the comparison of the load-displacement curves from FEM and from Equation 5.4-1 for the case of film thickness ratio h/R=0.5 and Young's modulus ratio ($E_1/E_2$-5). In the plot, the load-displacement curves of the film and substrate as homogeneous materials were also included. The plot is presented in the log-log scale to have good comparison. From the plots, we can observe that the load-displacement curves generated from FEM can be well fitted by the generalized

power law equation (Equation 5.4-1), up to the indentation penetration of 12% of the indenter radius.
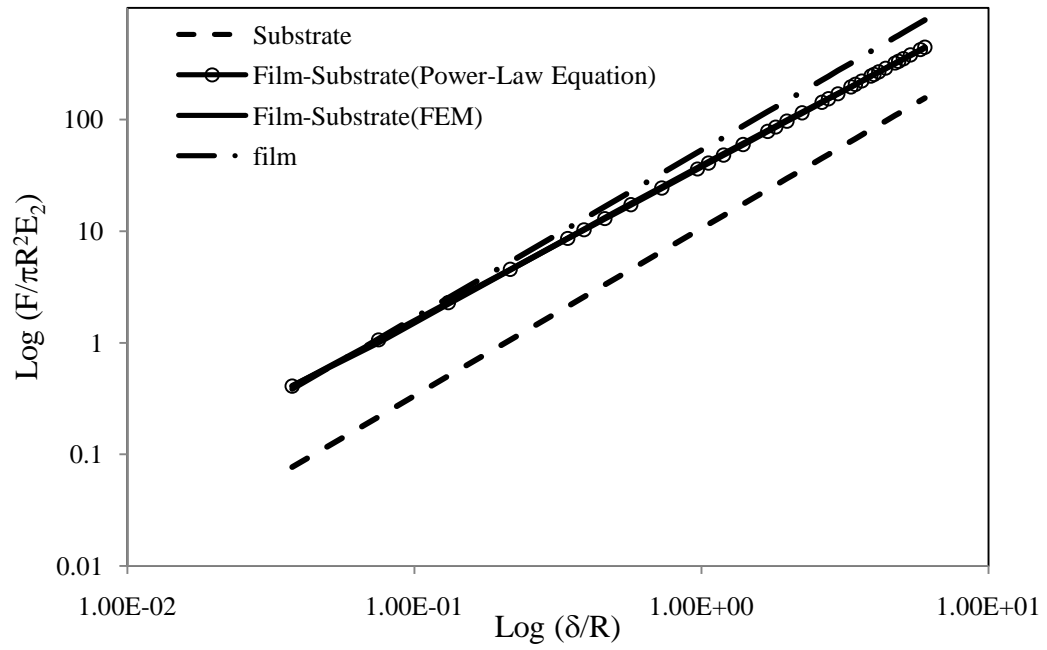


Figure 5.4-10 Load-displacement Curves from FEM and from Equation Generated

$(h/R=0.5$ & $E_1/E_2-5)$.

## 5.5 Summary

The finite element analysis has been used to simulate the indentation of layered materials (film-substrate systems) by a rigid, spherical indenter. The configurations of the layered materials include both soft film-hard substrate structures ($E_1/E_2 < 1$) and hard film-soft substrate structures ($E_1/E_2 > 1$). The indentation response was found to be dependent upon the film thickness ($h/R$). For soft film-hard substrate materials, the maximum Mises stress decreases with increasing film thickness; while for hard film-soft substrate materials, the maximum Mises stress decreases first and then increase with increasing film thickness. In all cases, the maximum Mises in the film increases with the increase of film modulus ($E_1/E_2$). The indentation load-displacement curves of layered materials in wide range of configurations have been generated from the present finite element simulation (FEM). An empirical power law equation has been proposed for characterizing the indentation load-displacement responses of layered materials. Good correlations between the FEM and the power law equation have been obtained. The equation takes into account of film properties (thickness, $h/R$, and modulus, $E_1/E_2$) and thus is applicable to a generic film/substrate system.

**6.0 Conclusions and Future Work**

**6.1 Conclusions**

Micro-/nano-indentation is widely used to measure the mechanical properties of materials and structures in small volumes. Although the elastic contact deformation between a rigid indenter and a homogeneous medium is now well understood, the elastic-plastic contact deformation occurred at larger indentation depth has not been well studied, nor the contact deformation occurred in layered systems. In this thesis, the comprehensive finite element simulations are performed to study the elastic-plastic indentation of homogeneous materials and the elastic indentation of layered materials.

(1) Elastic-plastic indentation of homogeneous materials

The finite element analysis is used to simulate the deep indentation of elastic-plastic materials under a spherical indenter. The depth of the indentation has been pushed up to 100% of the indenter radius ($\delta/R \approx 1$). The following remarks can be drawn from the investigations:

- The power-law relation between indentation load and indentation depth is valid only at shallow indentation, $\delta/R \approx 0.05$.

- The power-law relation between indentation load and indentation depth breaks at deep indentation, $\delta/R > 0.2$. Thus, caution needs to be taken in analyzing experimental results involving deep indentation.

- The ratio of the plastic energy to the total mechanical work is a linear function of the ratio of the residual indentation depth to the maximum indentation depth for the indentations by spherical indenters, independent of the strain hardening index.

- The extrapolated value of the energy ratio for a spherical indenter is different from that for the sharp instrumented indentation.

- The material pile-up occurred during large indentation decreases linearly with the increase of the strain hardening index.

(2) Elastic indentation of layered materials

The finite element analysis is used to simulate the elastic indentation of layered materials (film-substrate structures) under a spherical indenter. Materials in a wide range of configurations are studied, including film thickness ($h/R$) and film modulus ($E_1/E_2$). The following remarks can be drawn from the investigations:

- The load-displacement response of a film-substrate system is bounded between the film and substrate in homogeneous form.

- The indentation response of a film-substrate system depends upon the film thickness (h/R). For soft film-hard substrate materials, the maximum Mises stress decreases with increasing film thickness; while for hard film-soft substrate materials, the maximum Mises stress decreases first and then increase with increasing film thickness.

- The indentation response of a film-substrate system depends upon the film modulus ($E_1/E_2$). The maximum Mises in the film increases with the increase of film modulus ($E_1/E_2$).

- A universal power law equation has been proposed to characterize the indentation load-displacement responses of layered materials. The equation takes into account of film properties (thickness, h/R, and modulus, $E_1/E_2$) and thus is universally applicable to an elastic film/substrate system.

## 6.2 Future Works

Finite element simulation has become a powerful tool to study the micro-/nano-indentation processes and thus to help develop improvements in the analytical methods used to extract mechanical properties from experimental data. In this

thesis, the finite element simulations are used to study the elastic-plastic indentation of homogeneous materials and elastic indentation of layered materials. To support the current studies, some experimental investigations can be performed to validate the numerical findings and proposed empirical model. For the indentation of layered materials, the work can be extended to the elastic-plastic film-substrate systems. In addition, the existing numerical model can be extended to study some urgent issues that are facing the nanomechanics community, such as the indentation deformation of visco-elatsic materials and visco-elastic-plastic materials. Engineering materials such as polymers have properties that are dependent upon time/frequency. The current empirical equation for extracting mechanical properties from nanoindenation data is only applicable to the elastic materials. Finite element simulation on the indentation of visco-elastic and visco-elastic-plastic materials will help develop reliable analytical solutions for extracting mechanical properties of materials that are time-dependent.

**Appendix - A**

**Finite element analysis of cylindrical indentation**

**for determining plastic properties of materials in small volumes**

**Y. Charles Lu,[1, 2] \* Siva N V R K Kurapati,[2] Fuqian Yang[3]**

[1]Department of Mechanical Engineering

University of Kentucky

Paducah, KY 42071 USA

[2]Department of Mechanical Engineering

[3]Department of Chemical and Materials Engineering

University of Kentucky

Lexington, KY 40506 USA

\* Corresponding author.  Tel.: 1 270 534 3115; fax: 1 270 534 6292.

Email address: chlu@engr.uky.edu (Y.C. Lu)

**Abstract**

The cylindrical indentation is analyzed, using finite element method, for determining the plastic properties of elastic-plastic materials and the effect of strain hardening. The results are compared to those obtained from spherical indentation, the commonly used technique for measuring plastic properties of materials in small volumes. The analysis shows that the deformation under a cylindrical indenter quickly reaches a fully plastic state and that the size (diameter) of the plastic zone remains constant during further indentation. The indentation load is proportional to the indentation depth at large indentation depth, from which the indentation pressure $P_m$ at the onset of yielding can be readily extrapolated. The analysis of cylindrical indentation suggests that it does not need such parameters as impression radius (a) and contact stiffness (S) for determining the plastic behavior of materials. Thus the cylindrical indentation can suppress the uncertainties in measuring material properties.

## 1. Introduction

Micro- and nano-indentation have been widely used for measuring the mechanical properties of materials and structures in small dimensions. Most of works have focused on measuring the elastic properties of materials using sharp indenters such as conical and Berkovich indenters. There has been continuous interest in measuring the plastic properties of materials such as yield strength using spherical indenters [1-6]. The advantage of using spherical indenters (in comparing to sharp indenters) is that the indentation strain can be associated with the tension strain through Tabor's relation. By analyzing the stress (or strain) distribution underneath the indentation, the onset of plastic yielding of a material can be identified and the corresponding indentation pressure ($P_m$) be calculated, which is proportional to the yield strength of the material [1, 6, 7].

The indentation of elastic-plastic materials with cylindrical indenters has been reported [8, 9, 10]. The main advantage of using cylindrical indenter is that the contact area between the indenter and the specimen remains constant during the indentation test. As a result, the deformation underneath the indenter can change distinctly from purely elastic at initial contact to fully plastic in the later stage. Wright et al [8] performed the cylindrical indentation tests on polycarbonate using macroscopic indenters (3.5<diameter<14mm). The measured indentation load increased linearly with the indentation depth initially, with a sudden, relatively sharp decrease in slope, followed by a second linear portion at deep indentation.

The linear response of the indentation load at the deep indentation indicates that the material underneath the indenter deformed fully plastically. By back-extrapolating the load-depth curve at large indentation depth to zero displacement, the mean axial load was determined which was used subsequently for computing the mean indentation pressure $P_m$. Lu and Shinozaki [9] have recently extended this technique to smaller indenters (10<diameter<100μm) to measure the plastic properties of polymeric solids.

The present work is to compare the cylindrical indentation to the spherical one in measuring the plastic property (yield strength) of materials of small volumes. The finite element simulation is used to investigate the indentation load-depth responses of the cylindrical and spherical indentations and to explore the deformation behavior under these two types of indenters. The methods for estimating the yield strength from the indentations are described.

In the simulation, the compression molded high impact polystyrene (HIPS) and cast aluminum (Al) are used as testing materials to compare the indentation behavior by the cylindrical and spherical indenters. These materials are chosen since their deformation behaviors have been extensively studied in the literature [1, 11-15], and the constitutive behaviors of these two materials can be accurately modeled by the linear elastic and power-law plasticity [5, 6, 9] available in most commercial finite element codes.

## 2. Theory

### 2.1 Spherical indentation

The use of spherical indenters to measure plastic properties of materials of small volumes or dimensions has been well studied [1, 2], and generally followed the approach developed by Oliver and Pharr [16, 17]. The indentation pressure (P) by a spherical indenter is calculated as the ratio of the normal load ($L_a$) to the impression area ($A=\pi a^2$)

$$P = \frac{L_a}{\pi a^2} \qquad (1)$$

where a is the impression radius, given by

$$a = \sqrt{2h_c R - h_c^2} \qquad (2)$$

where R is the radius of the spherical indenter and $h_c$ the actual contact depth. The contact depth $h_c$ is calculated from the Oliver-Pharr model [16, 17]

$$h_c = h - \eta \frac{L_a}{S} \qquad (3)$$

where h is the total indentation depth into the specimen, and η is a geometric constant (η=0.75 for spherical indenter). S is the elastic contact stiffness that can be determined from the slope of the initial indentation unloading curve [16, 17]. In general, an area function needs to be established between the impression area and the indentation depth through the calibration process.

Substitution of Eqs. (2) and (3) into (1) gives the indentation pressure as

$$P = \frac{L_a}{\pi[(2h - 0.75\frac{L_a}{S})R - (h - 0.75\frac{L_a}{S})^2]} \qquad (4)$$

It is observed that the indentation pressure (P) depends upon three quantities: (1) the normal indentation load ($L_a$), (2) the indentation depth (h), and (3) the contact stiffness (S). In a typical indentation test, the indenter is moved onto and then withdrawn from the specimen and the indentation load and displacement are recorded. From the loading-unloading curve, the three quantities ($L_a$, h, S) can be obtained. Then, the corresponding indentation pressure P can be computed using Eq. (4). By performing a multi-step loading-unloading test, the indentation pressure at different indentation depths can be determined. From engineering point of view, a mean indentation pressure ($P_m$), also known as hardness, is more useful, which is determined as the indentation pressure corresponding to the initial yielding [2, 6].

## 2.2 Cylindrical indentation

The elastic-plastic indentation using a cylindrical indenter has been studied by Wright, Huang and Fleck [8] and Lu and Shinozaki [9]. When a cylindrical indenter of a in radius is pressed onto a specimen, the total load ($L_{total}$) acting on the indenter is:

$$L_{total} = L_a + L_f \qquad (5)$$

where $L_a$ is the axial load acting on the indenter end face and $L_f$ the frictional load acting on the indenter side wall.

The mean indentation pressure (P) acting on the indenter end is simply expressed as

$$P_m = \frac{L_a}{\pi a^2} \qquad (6)$$

The frictional load ($L_f$) on the indenter side wall is defined by $L_f = 2\pi a h_c \tau$, where $\tau$ is the frictional shear stress. Assume that the frictional stress is constant on the indenter wall, then the frictional load ($L_f$) should increase linearly with indentation depth, since the lateral surface area in contact with the material ($2\pi a \cdot h_c$) increases almost linearly.

The mean indentation pressure ($P_m$) defined in Eqs. (4) and (6) is found to be proportional to the yield strength of the material obtained from conventional

uniaxial test: $P_m = C \cdot \sigma_y$, where C is a constraint factor and $\sigma_y$ the yield strength corresponding to a plastic strain of 0.2% [7]. The magnitude of the constraint factor has been found to depend upon the material properties, particularly on the ratio of the modulus to the yield stress, $E/\sigma_y$ [1, 6]. For most metals, $E/\sigma_y > 100$, the constraint factor is approximately equal to 3 ($C \approx 3$) [1, 6]. For polymers, the ratio of $E/\sigma_y < 10$, and the constraint factor is less than 3 (C<3) [9].

## 3. Finite element modeling

The deformation of purely elastic indentation has been well understood for indenters of various geometries, and the stress fields around indentation can generally be described accurately in closed form equations for the indentation of semi-infinite elastic materials [18, 19]. The indentation deformation of elastic-plastic or plastic materials is more complex. In this study, the large-depth indentations by a spherical indenter and a cylindrical indenter of flat end were simulated using the finite element method (Figure 1). The commercial nonlinear finite element (FE) code ABAQUS was used [20]. 4-node axisymmetric elements were used in the FE simulation to deal the potential large distortions of the elements present during the deep indentation. The indenter was assumed as rigid and thus modeled by rigid surfaces. Most analyses were conduced by using an indenter of a radius of 50 μm unless stated otherwise. The base of the specimen was completely constrained while the nodes along the center line are constrained in the horizontal direction. A vertical displacement was applied to the rigid surface through a

reference node and the reactant force was calculated. The plasticity was modeled by the von Mises ($J_2$) flow criterion [20].

Two linear elastic, power-law plastic materials were used in the simulation: one was the compression molded high-impact polystyrene (HIPS) – a low modulus material and the other the cast aluminum (Al) – a high modulus material.   The one-dimensional constitutive relation for the linear elastic, power law plastic material was described as

$$\sigma = \begin{cases} E\varepsilon & \text{for } \sigma \le \sigma_0 \\ \sigma_0 (\dfrac{\varepsilon}{\varepsilon_0})^n & \text{for } \sigma > \sigma_0 \end{cases} \tag{7}$$

where "$\sigma$" and "$\varepsilon$" were the uniaxial stress and strain; "$\sigma_0$" and "$\varepsilon_0$" the proportionality limit of the corresponding stress and strain;   "E" the Young's modulus; and "n" the strain hardening index describing the post-yield material behavior as a power law relation. The properties of the two materials are listed in Table 1.

# 4 Results and discussion

## 4.1 Indentation load-depth responses

The load-depth responses for the indentations of high-impact polystyrene (HIPS) and aluminum (Al) by a spherical indenter are shown in Figures 2a and 2b. At small indentation, the material beneath the indenter experiences elastic deforms, while the indentation load-depth curves exhibit nonlinear response (inserted figure in Figure 2a), since the contact area between the spherical indenter (or any sharp indenter) and the specimen increases nonlinearly. This elastic deformation at small indentation can be described by the classical Hertz solution: $L = \frac{2\sqrt{2}}{3} \frac{E\sqrt{2a}}{1-v^2} h^{3/2}$ [18]. It is seen that the results from the finite element simulation are in good accord with the Hertz's contact theory, which indicates that the present FEM model is appropriate for the spherical indentation.

As the indentation depth further increases, the material underneath the indenter starts to deform plastically. The resultant load increases continuously due to the increase in the contact area. The change rate of the indentation load with the indentation depth decrease progressively at large indentation, particularly for a material that possesses a larger value of $E/\sigma_y$ (aluminum).

77

Figures 3a and 3b show the indentation load-depth curves for the indentations of high-impact polystyrene (HIPS) and aluminum (Al) by a cylindrical, flat-tipped indenter. Each curve exhibits a distinguished bilinear response: linear elastic response at small depth and linear plastic response at large depth. At small penetrations, the material underneath the indenter deforms mainly elastically (inserted figure in Figure 3), consistent with Sneddon's solution on elastic indentation by a flat-ended cylindrical indenter, i.e. $L = \dfrac{2Ea}{1-v^2}h$ [19]. It is seen that the results from the FEM simulation correlate well with the Sneddon's solution at small indentation depth, while it deviates from the elastic solution at large depths. This is likely due to the presence of local plastic deformation in the material near the indenter circumference.

The stress field in an elastic medium under a flat-ended indenter has been solved analytically by Sneddon [21]. In particular, the normal compressive stress $\sigma_z$ at specimen surface (z=0) under a flat indenter is given by

$$(\sigma_z)_{z=0} = -\frac{1}{2}aP(a^2 - r^2)^{-1/2} \qquad (8)$$

The compressive stress $\sigma_z$ is plotted with respect to r/a and z/a for the aluminum material (v=0.3) (Figure 4). It is observed that the compressive stress increases

progressively from $\frac{1}{2}P$ at the center of the indenter (r/a=0) towards the edge. Right

at the indenter edge (r/a=1), this compressive stress approaches infinity. It indicates

that even for a small load, a local plastic deformation may occur near the corners of

the indenter. The initial yielding can be identified by examining the distribution of

the van Mises stress in the medium under the indenter (Figure 5). It is seen that the

maximum value of van Mises stress is approximately $\sigma_{Mises} \approx 0.78P$, right beneath

the indenter edge. So, the initial yielding occurs at the indentation pressure of

$\frac{P}{\sigma_y} \approx 1.28$, where $\sigma_y$ is the tensile yield stress of the indented material. This initial

yielding corresponds to the early stages of indentation, before the gross yield point

(at the "knee" of the indentation load-depth curve shown in Figure 3).

As the indentation depth increases, more material deforms plastically. A fully

developed plastic zone is formed underneath the indenter, corresponding to the

indentation depth at which the indentation load-depth curve reaches the beginning

of the second (lower) slope linear region. The bilinear load-depth responses from

the FEM simulation are consistent with experimental observations reported by

Wright, Huang and Fleck [8] and by Lu and Shinozaki [9]. Wright, Huang and

Fleck [8] conducted macroscopic cylindrical indentation tests on polycarbonate

(PC) that exhibits exponential work-hardening. The linear load responses were

observed at large indentation depths, up to a depth of 4-5 time of the indenter

diameter. Lu and Shinozaki [9] performed the microindentaion tests on various

polymeric materials including high density polyethylene (HDPE), polystyrene (PS), polymethyl methacrylate (PMMA) and high impact polystyrene (HIPS - the material used in the present FEM simulation). In all cases, the indentation load-depth curves were linear at large indentation depths.

According to Eq. (5), the load response at large indentation depth can be affected by the frictional load ($L_f$) on the side wall of the moving cylindrical indenter, the area of which increases linearly with depth. The effect of friction between indenter and specimen was examined by introducing a frictional component and recalculating the indentation test curve. A contact pair was defined between indenter sidewall and specimen upper surface and the coefficient of friction at the interface was varied from 0.0 to 0.6. Figures 6 and 7 show the resultant load-depth curves for HIPS and Al, respectively. It is observed that with the increase of interfacial friction at indenter-sample interface, the slope of the load-depth curves at large indentation depth increases. The friction is seen to have a greater effect on indentation response of relatively soft material (HIPS), whose modulus ($E/\sigma_y$) is approximately $1/10^{th}$ of the modulus of the aluminum.

The HIPS has been tested previously by using a cylindrical indenter of radius a=38.1 mm [9]. The experimental result is compared to the current simulations with various frictional coefficients. It is seen that the simulation without friction is more resemble to the experimental measurement (Figure 7), indicating that the frictional

stress for current HIPS is effectively zero. The aluminum has shown little dependence on friction (Figure 6). Thus, the frictionless condition is mostly used in subsequent analyses.

**4.2 Indentation deformation**

The deformation behavior of materials underneath indentation can be examined by computing the equivalent plastic strain ($\varepsilon^{eq}$) contours. The equivalent plastic strain $\varepsilon^{eq}$ is defined as $\varepsilon^{eq} = \sqrt{\frac{2}{3}[(\varepsilon_1^{pl})^2 + (\varepsilon_2^{pl})^2 + (\varepsilon_3^{pl})^2]}$, and $\varepsilon_1^{pl}$, $\varepsilon_2^{pl}$ and $\varepsilon_3^{pl}$, are the principal strains [14]. For $\varepsilon^{eq} > 0$, the plastic deformation occurs.

The plastic deformation under a spherical indenter has been studied recently by a number of researchers [1, 7, 22, 23]. Overall, the size of plastic zone underneath the spherical indenter increases with indentation depth since the contact between indenter and specimen keeps increasing. The plastic deformation generally initiates beneath the specimen surface and then moves towards the contact surface.

The plastic deformation for the indentation by a cylindrical indenter is significantly different from that by a spherical indenter. Figures 8 and 9 show the equivalent plastic strain ($\varepsilon^{eq}$) under a cylindrical indenter for HIPS and Al, respectively. It is

seen that the plastic deformation beneath the cylindrical indenter initiates around the circumference of the indenter. As the indentation depth increases, the plastic flow reaches a steady state. The size (diameter) of the plastic zone remains relatively constant, being approximately twice of the indenter diameter. For material with higher elastic modulus (aluminum), more pile-up is observed around the indenter (Figure 9), consistent with the recent investigation by Taljat and Pharr [22]. It is also noticed that the material directly ahead of the indenter shows little or no plastic deformation and remains constant, conical shape during the indentation.

## 4.3 Determinations of yield strength

The use of the spherical indentation for determining plastic properties of a material of small volume requires the use of multi-step loading-unloading indentation test. The responses of such tests from the FEM simulation are shown in Figures 10a, 10b, for HIPS and Al, respectively. From the loading-unloading curves, the indentation parameters, $L_a$, $S$, $h_c$, at each step are determined. The indentation pressures (P) are then calculated using Eq. (4). The indentation pressure is plotted against the normalized indentation strain (a/R), as shown in Figures 11a and 11b. It is observed that the indentation pressure obtained from the spherical indentation varies nonlinearly with the indentation strain. This is partially due to the fact that the deformation underneath the spherical indenter is at the elastic-plastic state.

To determine the yield strength of materials from the spherical indentation, the occurrence of initial plastic yielding is needed [1]. Mesarovic and Fleck [7] recently conducted a comprehensive finite element analysis of the spherical indentation of elastic-plastic materials and found that the occurrence of initial yielding was correlated to a critical indentation strain $a_c/R$. The magnitude of this critical indentation strain depends upon the normalized modulus of materials ($E/\sigma_y$). A detailed deformation map has been constructed for determining the critical indentation strain ($a_c/R$) as a function of $E/\sigma_y$. For materials with $\sigma_y/E$ exceeding approximately $2 \times 10^{-4}$, the initial yielding has been found to occur at a critical indentation strain of $a_c/R \approx 0.16$ [7]. Once $a_c/R$ is known, the corresponding mean indentation pressure $P_m$ can be determined. Using the critical indentation strain of $a_c/R = 0.16$, the mean indentation pressure $P_m$ is estimated as shown in Figures 11a and 11b, for HIPS and Al, respectively.

For cylindrical indentations, only one monotonic loading test is required for each material, as illustrated by Figures 3a and 3b. The indentation deformation consists of two distinct regions: linear elastic at small indentation and linear plastic at large indentation.

The linear plastic response at large indentation is a result of constant material flow under the indenter. The total indentation load is a sum of the axial load acting on the indenter end ($L_a$) and the frictional load acting on the indenter sidewall ($L_f$)

(Equation 5). The mean axial load ($L_a$) can be determined simply by extrapolating the load at large indentation, as shown in Figure 3, back to zero depth [$L_f$ becomes zero in Eq. (5)]. The mean indentation pressure is then calculated from the mean axial load using Eq. (6). The mean indentation pressure for HIPS obtained from the current 50 μm diameter indenter is approximately 36 MPa. Indenters of various sizes have been used in the simulation; and the resultant mean indentation pressures are approximately the same independent of the indenter size, as shown in Fig. 11, consistent with the experimental result [9].

The calculated mean indentation pressure ($P_m$) for HIPS and Al are summarized in Table 2 for both type of indenters. The yield strength corresponding to the plastic strain of 0.2% is determined for each material by using the appropriate constraint factors: C=3 for aluminum [6, 7] and C=2.6 for HIPS [9]. The overall predictions of the yield strength from both methods are identical, with the results from the cylindrical indentation being slightly closer to the yield strengths used for analysis. However, compared to the spherical indentation, the technique of the cylindrical indentation is more effective. It requires only one monotonic loading test, in contrast to the multi-step loading-unloading tests required by the method of spherical indentation. The analysis of the cylindrical indentation is much simpler, and it requires fewer parameters for computing the mean indentation pressure. This thus reduces the uncertainties in estimating the yield strength of materials.

## 5. Conclusions

The cylindrical indentation test has been analyzed by finite element simulation for determining plastic properties of two linear elastic, power law materials (HIPS and Al). The results have been compared to those obtained from spherical indentation tests. The computed deformation zones in material ahead of the two types of indenters are different. The deformation under a spherical indenter is mostly elastic-plastic and the resultant load in nonlinear. To obtain the mean indentation pressure, the existing spherical indentation technique requires the use of multi-step loading-unloading curves and then the estimates of several parameters, thus has greater uncertainties. In contrast, the deformation under a cylindrical indenter can quickly reach a steady state, fully plastic flow. As a result, the reaction load at that region is linear. The mean axial load can be readily obtained by extrapolating the load response at large indentation back to zero depth. The cylindrical indentation method requires only one monotonic loading test. The overall methodology is much simpler compared to the commonly used spherical indentation.

The cylindrical indentation technique can be useful in estimating the yield strength of the materials in small volumes such as thing films, coatings, interfaces, micro-electromechanical system (MEMS) and functionally graded materials, with which the conventional mechanical tests become ineffective or inaccessible.

**Acknowledgments**

**References**

[1] Park, Y.J. and Pharr, G.M., 2004, Nanoindentation with spherical indenters: finite element studies of deformation in the elastic-plastic transition regime, Thin Solid Films, 447-448, 246-250.

[2] Herbert, E.G., Pharr, G.M., Oliver, W.C., Lucas, B.N. and Hay, J.L., 2001, On the measurement of stress-strain curves by spherical indentation, Thin Solid Films, 398-399, 331-335.

[3] Feng, G.., Qu, S., Huang, Y. and Nix, W.D., 2007, An analytical expression for the stress field around an elastoplastic indentation/contact, Acta Materialia, 55, 2929-2938.

[4] Beghini, M., Bertini, L. and Fontanari, V. 2006, Evaluation of the stress-strain curve of metallic materials by spherical indentation, International Journal of Solids and Structures, 43, 2441-2459.

[5] Kang, B.S.-J, Yao, Z. and Barbero, E.J., 2006, Post-yield stress-strain determination using spherical indentation, Mechanics of Advanced Materials and Structures, 13, 129-138.

[6] Mesarovic, S. D. and Fleck, 1999, N.A., Spherical indentation of elastic-plastic solids, Proceedings of Royal Society of London, 455, 2707-2728.

[7] Tabor, D. 1951, The Hardness of Metals, Clarendon Press, Oxford, United Kingdom.

[8] Wright, S.C., Huang, Y. and Fleck, N.A., 1992, Deep penetration of polycarbonate by a cylindrical punch, Mechanics of Materials, 13, 277.

[9] Lu, Y. C. and Shinozaki, D.M., 2008, Characterization and modeling of large displacement micro-/nano-indnetation of polymeric solids, ASME Journal of Engineering Materials and Technology, Vol. 130, Oct. 1-7 (2008).

[10] Yu HY, Imam MA, Rath BB, 1985, Study of the deformation-behavior of homogeneous materials by impression tests, Journal of Materials Science, 20: 636.

[11] Dali, G., Argon, A. S. and Cohen, R. E. 1995, Particle-size effect in craze plasticity of high-impact polystyrene, Polymer, 36, 2173-2180.

[12] Bucknall, C. B. and Smith, R. R., 1965, Stress-whitening in high-impact polystyrenes, Polymer, 6, 437-446.

[13] Socrate, S., Boyce, M. C. and Lazzeri, A. 2001, A micromechanical model for multiple crazing in high impact polystyrene, Mechanics of Materials, 33, 155-175.

[14] Yang, F., Peng L. and Okazaki, K. 2006, Effect of the indenter size on the indentation of aluminum, Materials Characterization, 57, 321-325.

[15] Chollacoop, N., Dao, M. and Suresh, S. 2003, Depth-sensing instrumented indentation with dual sharp indenters, Acta Materialia, 51, 3713-3729.

[16] Oliver, W.C. and Pharr, G.M., 1992, An improved technique for determining hardness and elastic modulus using load and displacement sensing indentation experiments, Journal of Materials Research, 7, 1564.

[17] Oliver, W.C. and Pharr, G.M., 2004, Measurement of hardness and elastic modulus by instrumented indentation: advances in understanding and refinements to methodology, J ournl of Materials Research, 19, 3–20.

[18] Hertz, H, 1863 Miscellaneous papers, Ed. Hartz, H., Jones and Schott, Macmillon, London.

[19] Sneddon, I.N., 1965, The relation between load and penetration in the axisymmetric Boussinesq problem for a punch of arbitrary profile, International Journal of Engineering Science, 47-57.

[20] ABAQUS, 2007, ABAQUS Users' Manual, Hibbit, Karlson and Sorenson Inc., Pawtucket, RI.

[21] Sneddon, I.N., 1946, Boussinesq's problem for flat-ended cylinder, Proceeding of Cambridge Philosophy Society, 42, 29-39.

[22] Taljat, B and Pharr, G.M., 2004, Development of pile-up during spherical indentation of elastic-plastic solids, International Journal of Solids and Structures, 41, 3891-3904.

[23] Biwa, S and Storakers, B., 1995, An analysis of fully plastic Brinell indentation, Journal of Mechanics and Physics of Solids, 43, 1303-1333.
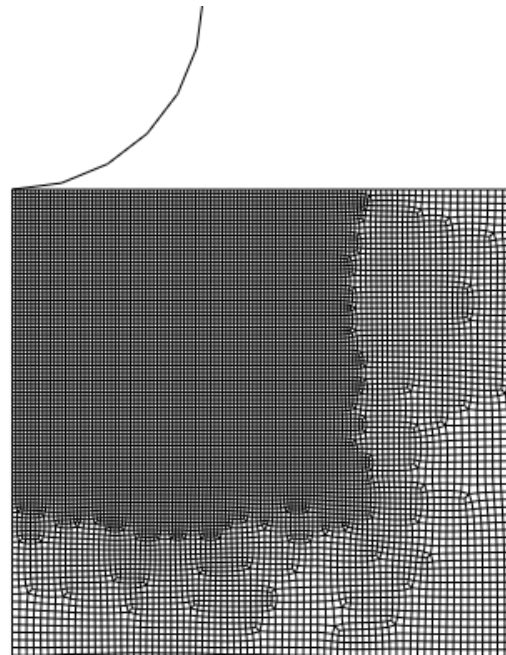
(a)
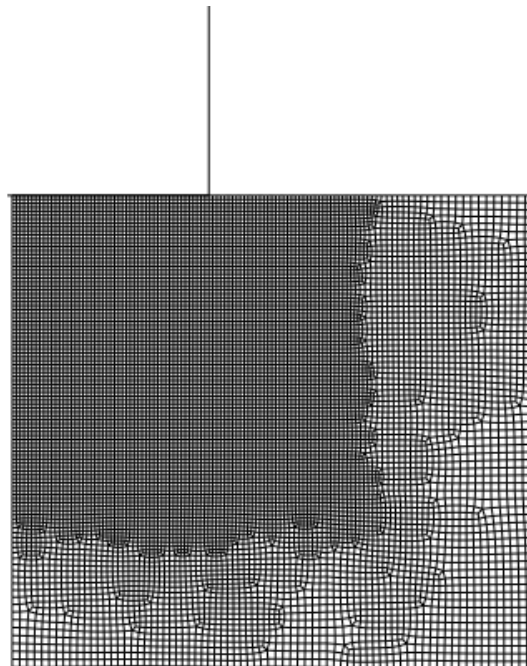
(b)

Figure 1 – The finite element models used for (a) spherical indentation (b) cylindrical indentation.
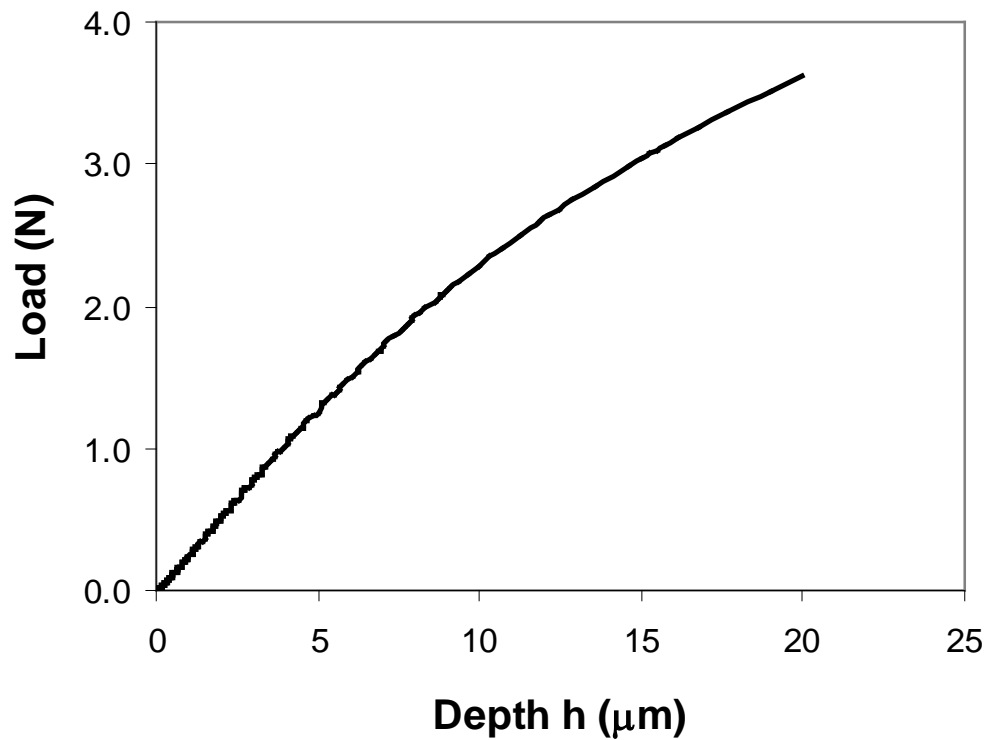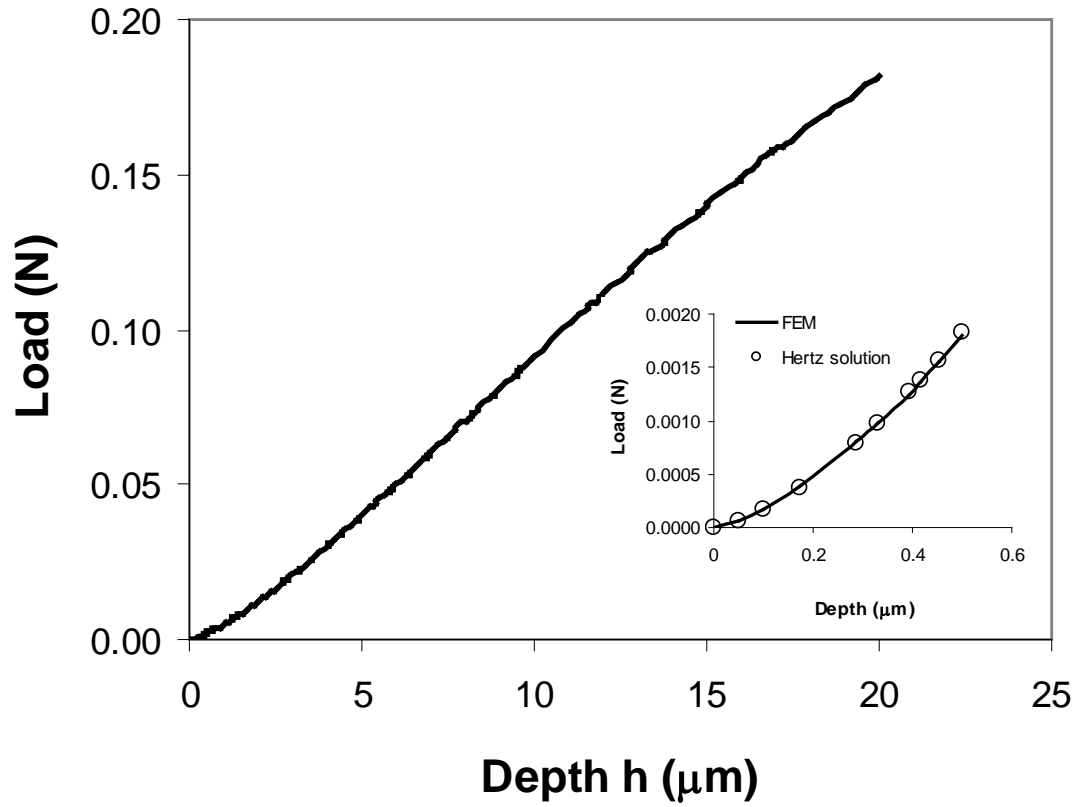
Figure 2 - Indentation load-depth curves of (a) high-impact polystyrene and (b) aluminum from spherical indentation.
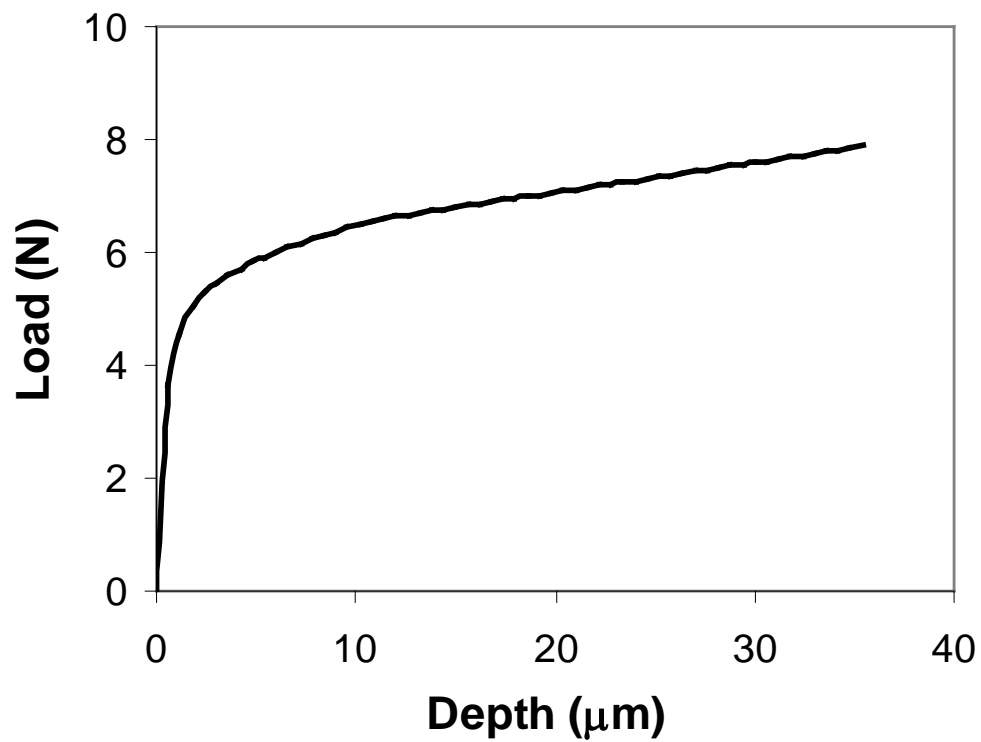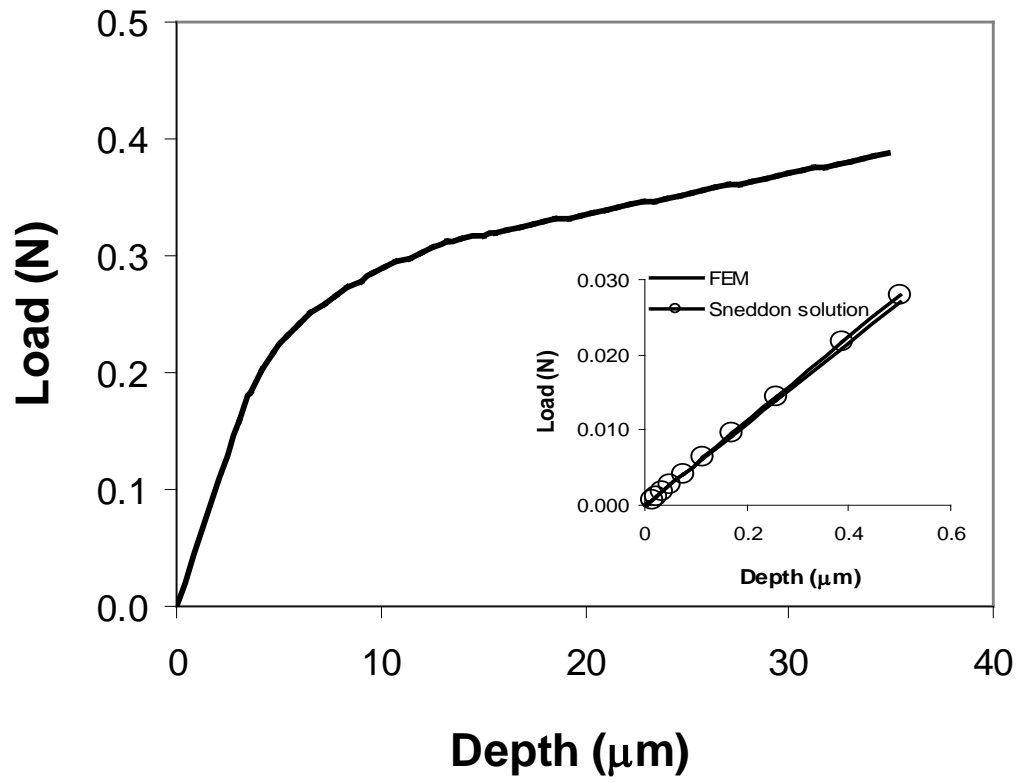
Figure 3 - Indentation load-depth curves of (a) high-impact polystyrene and (b) aluminum from cylindrical indentation.
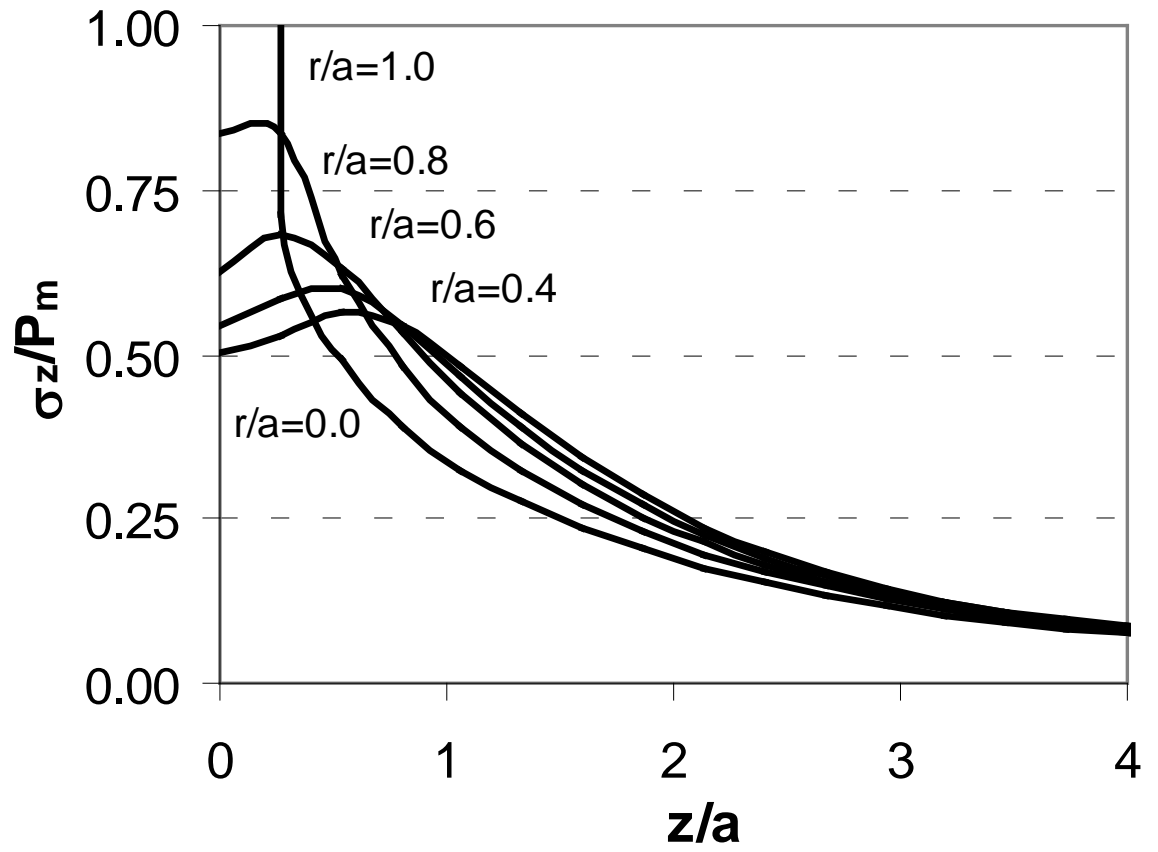
Figure 4 – Variation of indentation compressive stress ($\sigma_z$) with z/a and r/a in a material ($\upsilon=0.3$) under cylindrical indenter.
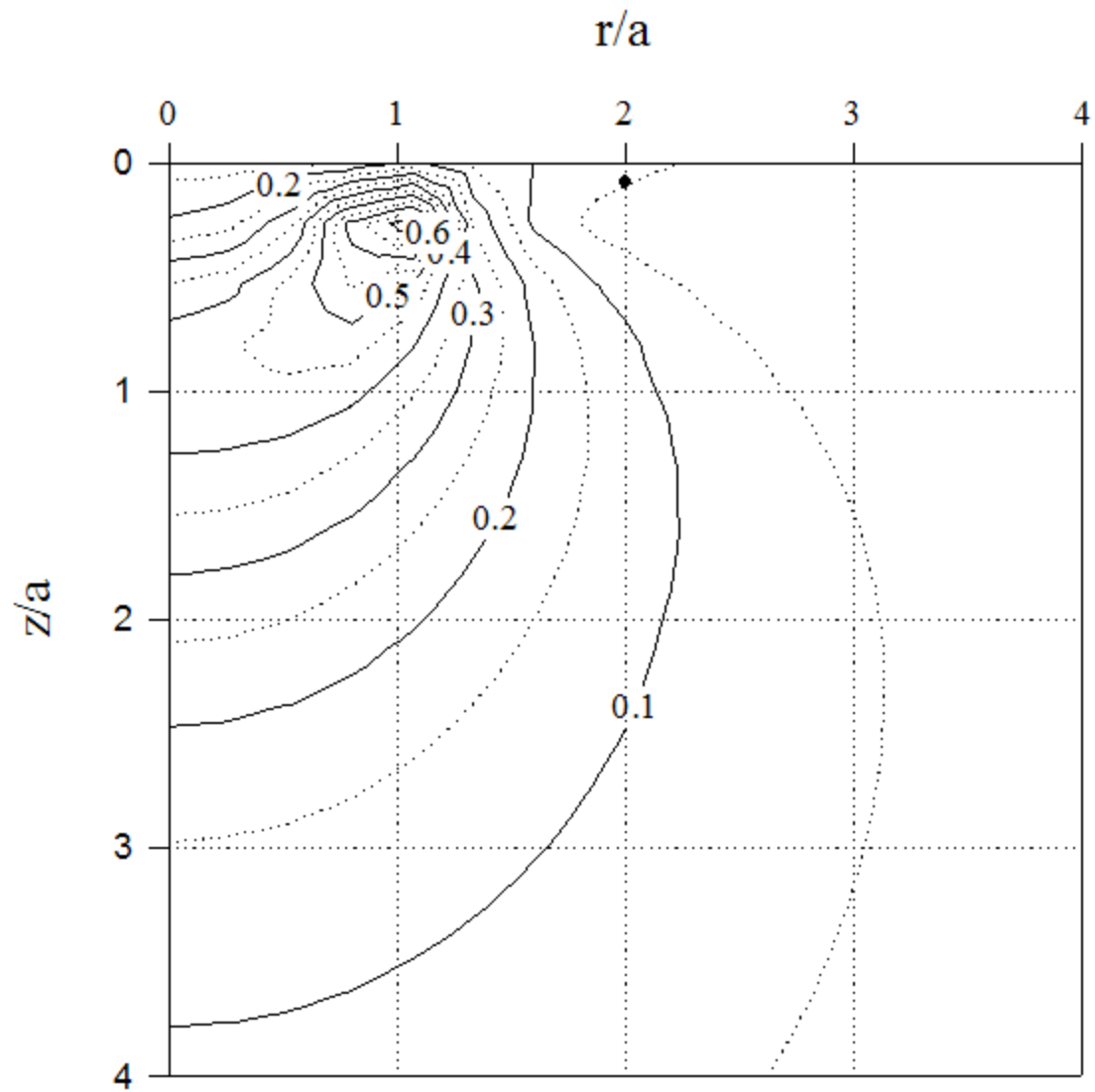
Figure 5 – Distribution of van Mises stress in aluminum under a flat indenter.
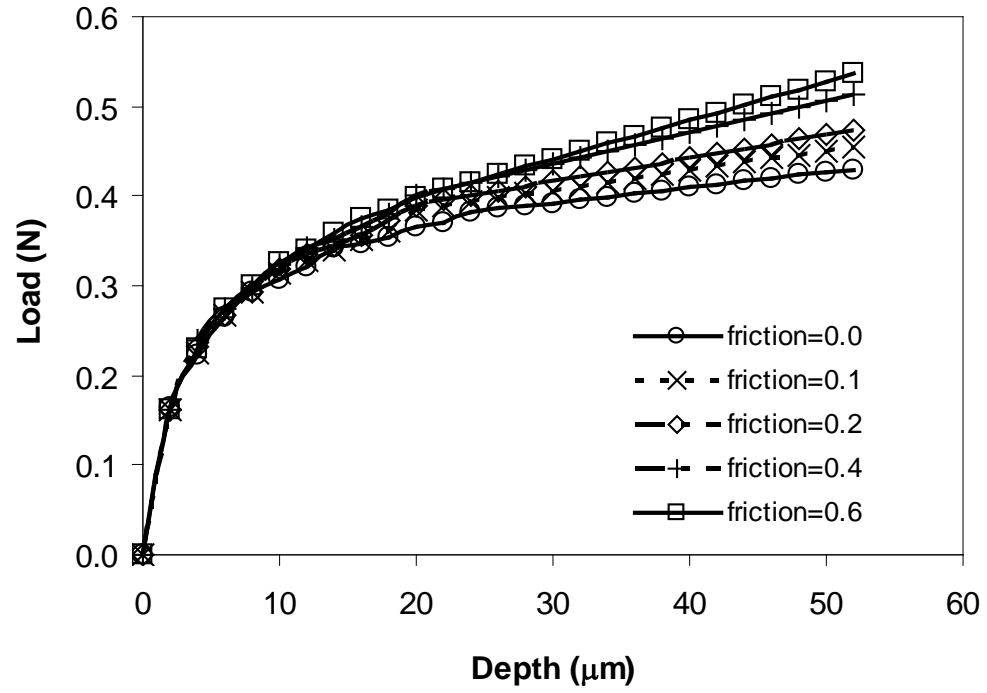
(a)
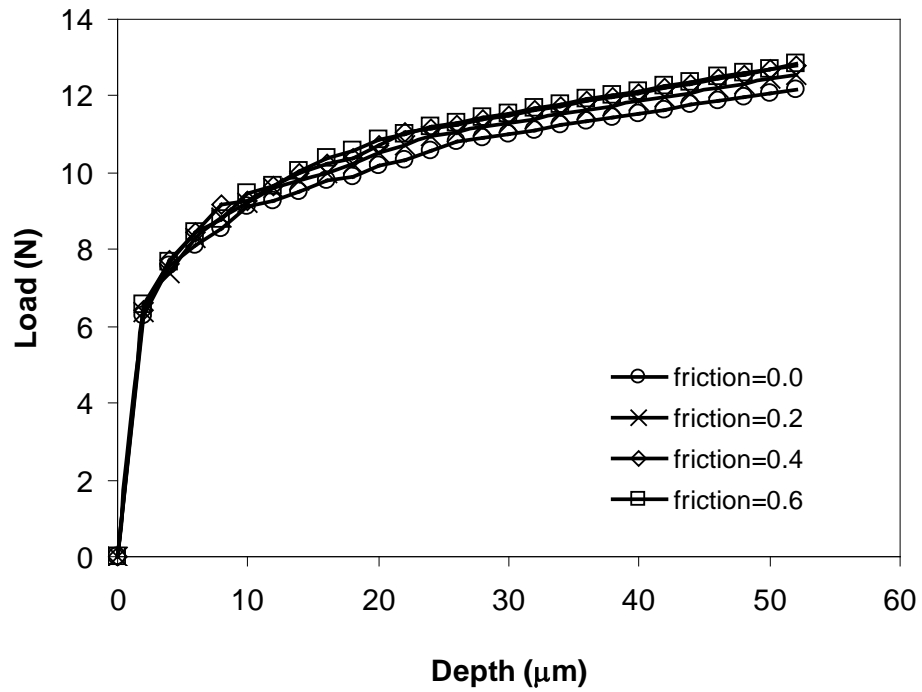


(b)

Figure 6 – Effect of interfacial friction on indentation load-depth responses of (a) high-impact polystyrene and (b) aluminum from cylindrical indentation.
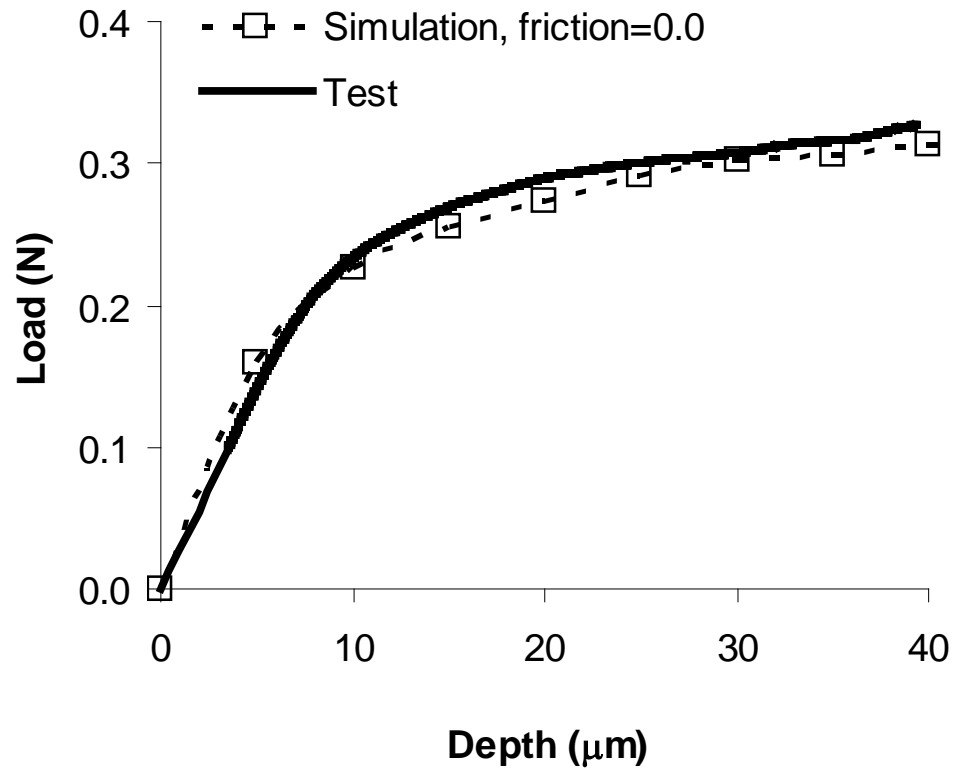
Figure 7 – Comparison of indentation load-depth responses of high-impact polystyrene between experiment and simulation. The indenter radius is 38.1 μm.
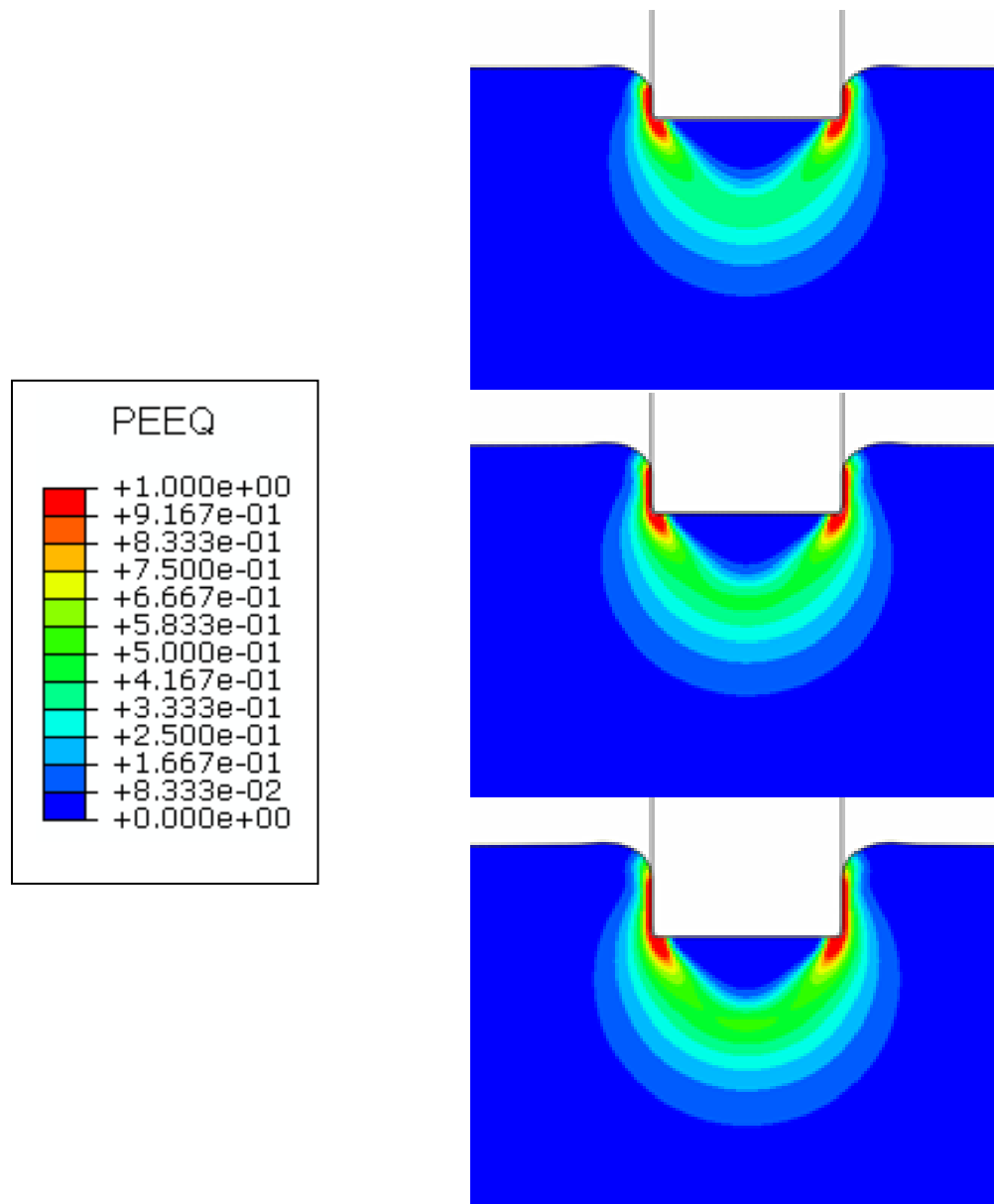
Figure 8 - Contours of equivalent plastic strain of high-impact polystyrene showing the development of the plastic zone under a cylindrical indenter.
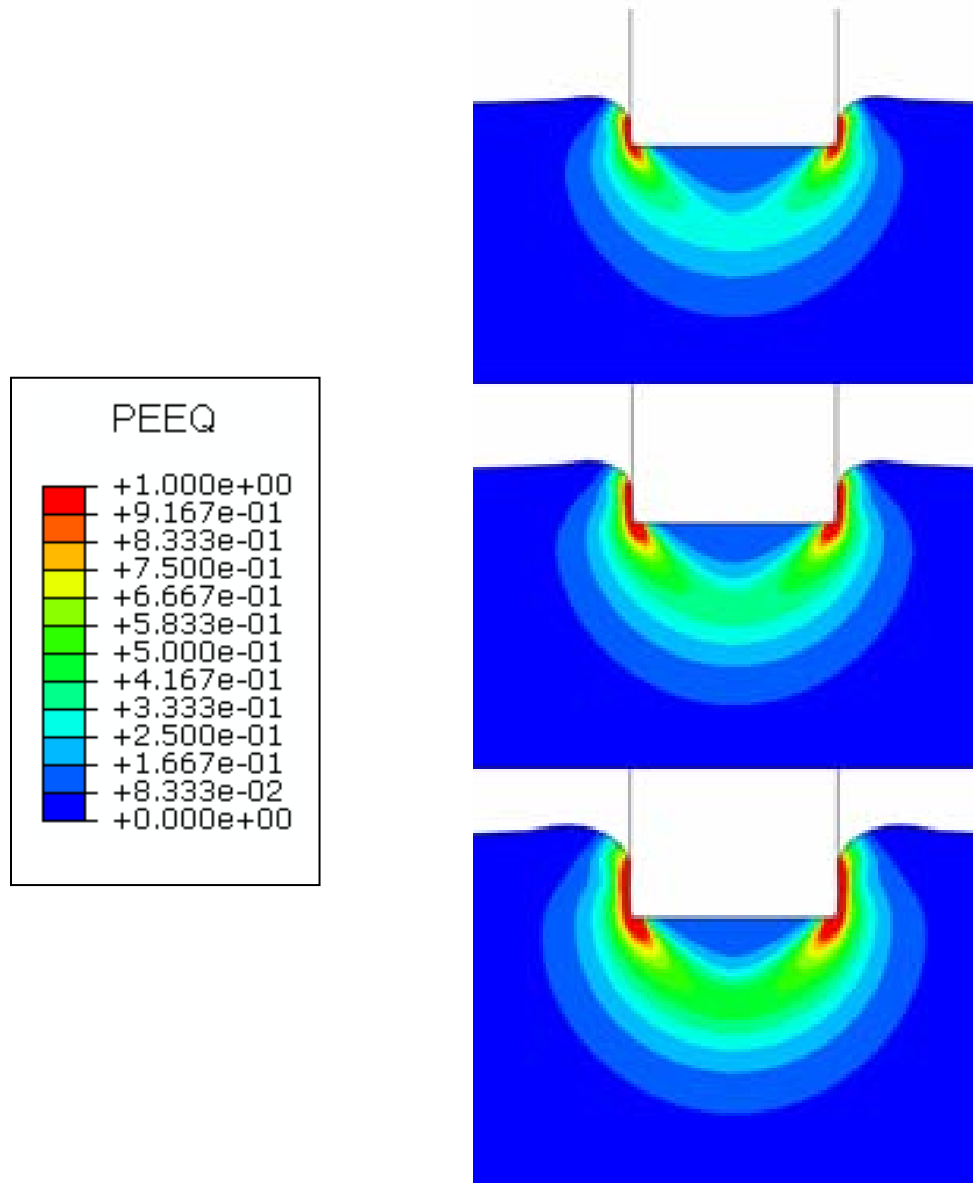
Figure 9 - Contours of equivalent plastic strain of aluminum showing the development of the plastic zone under a cylindrical indenter.

(a)

(b)
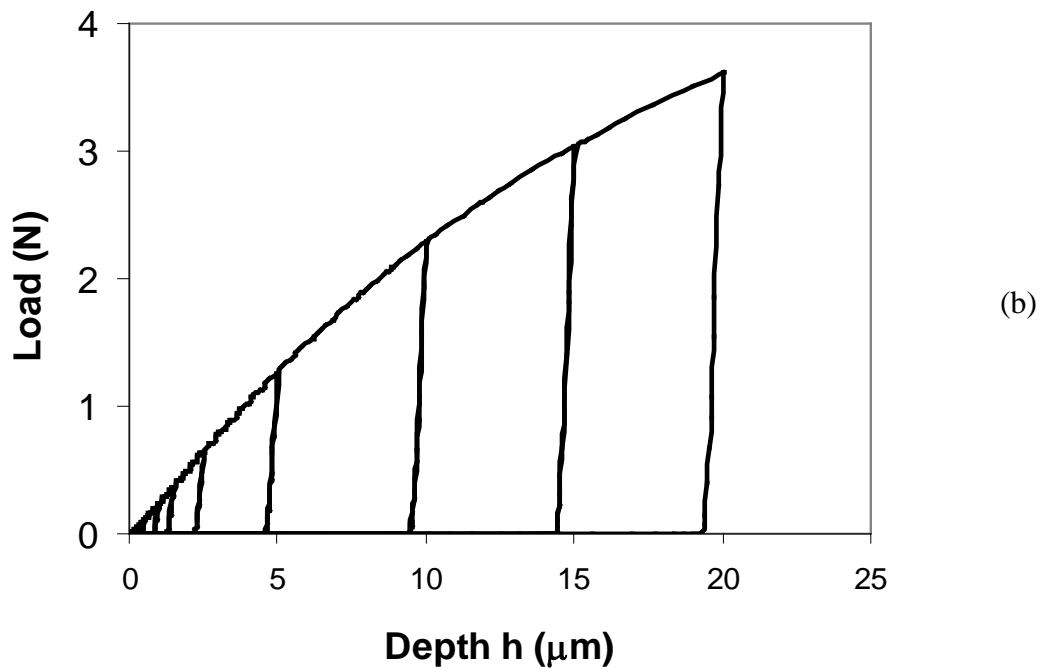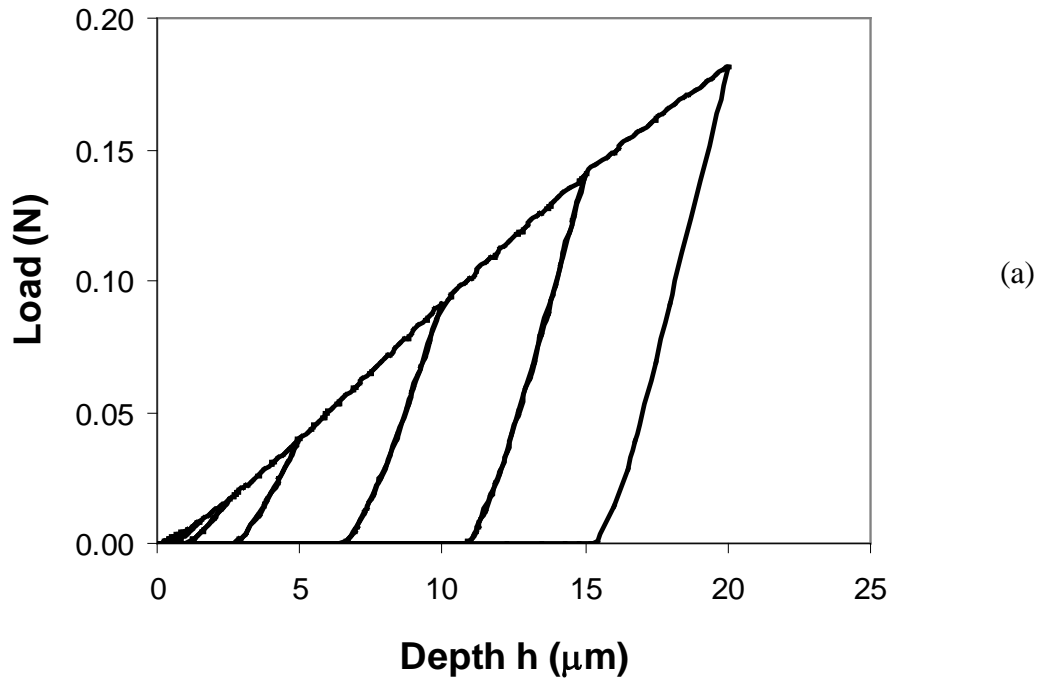
Figure 10 Figure 10 – The multi-step loading-unloading curves of (a) high-impact polystyrene and (b) aluminum from spherical indentation.
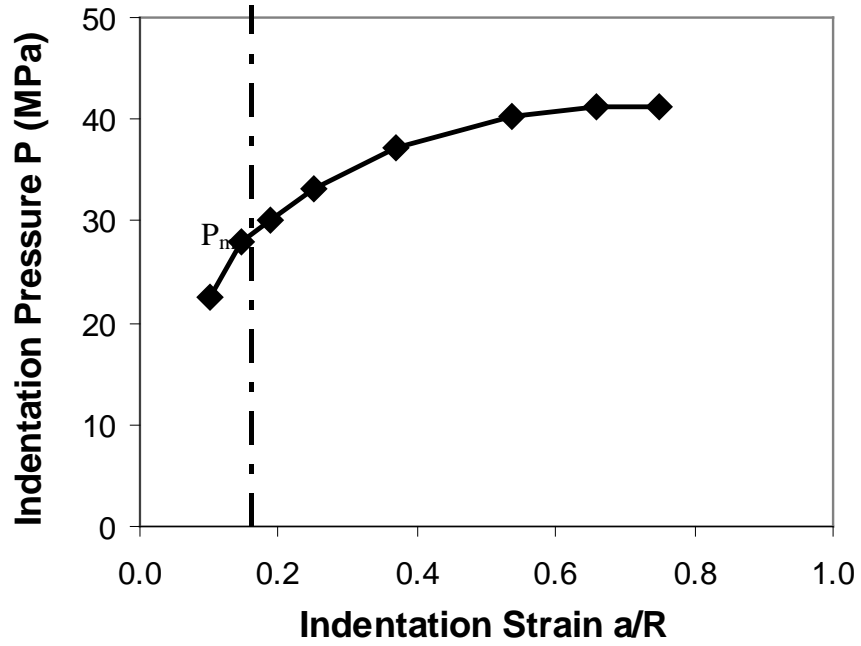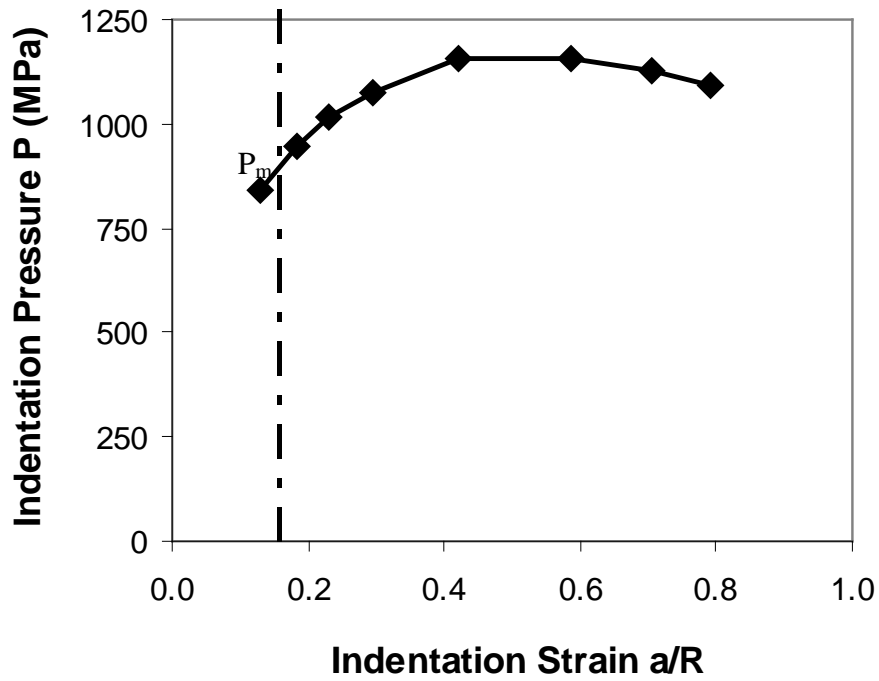
Figure 11 – The indentation pressure-strain responses of (a) high-impact polystyrene and (b) aluminum from spherical indentation. The mean indentation pressures are determined by using the critical indentation strain $a_c/R \approx 0.16$, shown as dashed lines.
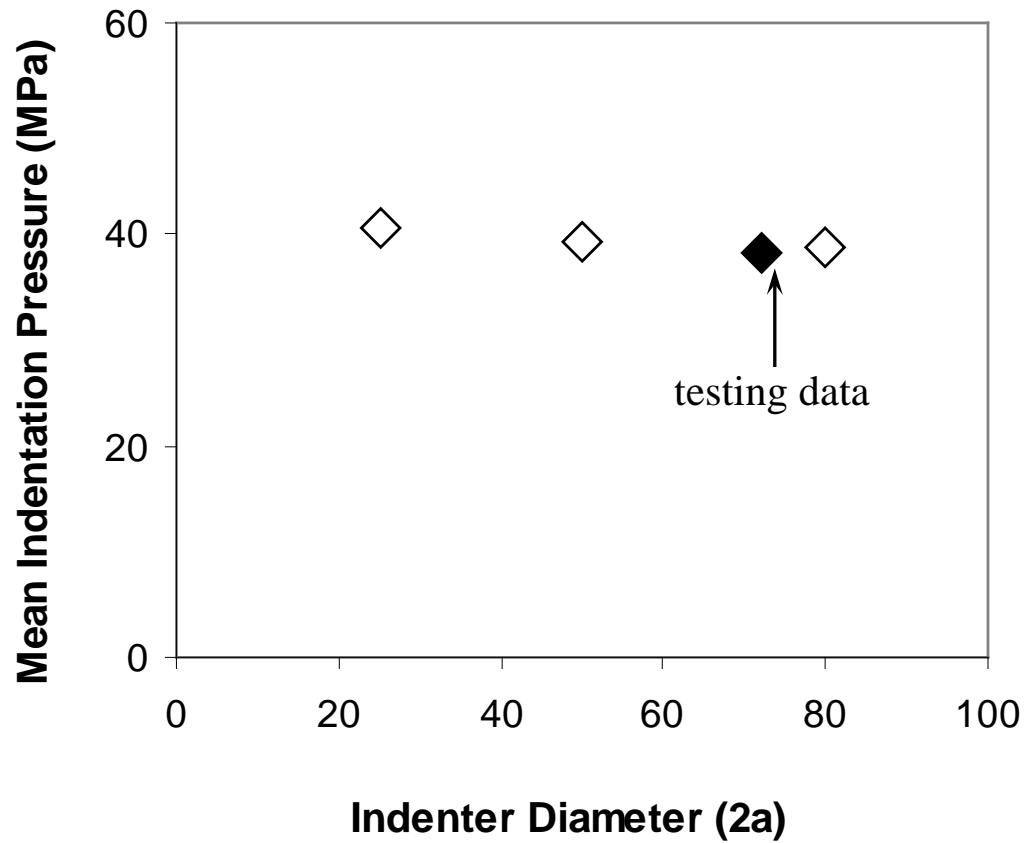
Figure 12 – The mean indentation pressures of high-impact polystyrene obtained from cylindrical indenters of various sizes (diameters). The experimental result is obtained with a cylindrical indenter of 72 μm diameter.

Table 1 - The material coefficients used in finite element analysis.

| | Modulus E (MPa) | Poisson's ratio v | Proportionality limit stress $\sigma_0$ (MPa) | Strain hardening index n |
|---|---|---|---|---|
| HIPS | 480 | 0.3 | 16 | 0.06 |
| Aluminum | 69000 | 0.33 | 255 | 0.1 |

Table 2 - Comparisons of plastic properties obtained from spherical indentation and cylindrical indentation.

| | Mean indentation stress $P_m$ (MPa) | | Yield strength $\sigma_y$ (MPa) | | *Theoretical yield strength $\sigma_y$ (MPa) |
|---|---|---|---|---|---|
| | spherical | cylindrical | spherical | cylindrical | |
| HIPS | 32 | 36 | 12 | 14 | 15 |
| Al | 920 | 789 | 306 | 263 | 264 |

* The theoretical yield strength is referred to the stress at 0.2% plastic strain, obtained form the stress-strain curves used in finite element analysis.

## References

1.      Hertz, H. "On the Contact of Elastic Solids", *J. Reine. Angew. Math. 92 156-171(1882).*

2.      Love, A.E.H. "Boussinesq's Problem for a Rigid Cone", *Quart. J. Math. 10161-175(1939).*

3.      Love, A.E.H. "A Treatise on the Mathematical Theory of Elasticity", *4th ed., Dover, New York (1944)*

4.      Harding, J.W. and Sneddon, I.N. "The Elastic Stresses Produced by The Indentation of The Plane Surface of a Semi-Infinite Elastic Solid by a Rigid Punch", *Proc. Camb. Phil. Soc. 41,16-26, (1945).*

5.      Hill, R. 'The Mathematical Theory of Plasticity', *Clarendon Press, Oxford, (1950).*

6.      Tabor, D. "The Hardness of Metals", *Clarendon Press, Oxford, United Kindom, (1951).*

7.      Mindlin, R.D. and Deresiewicz, H. "Elastic Spheres In Contact Under Varying Oblique Forces", *J. Appl. Mech. Trans. ASME 20 327-344(1953).*

8.      Sneddon, I.N. "The Relation Between Load and Penetration In The Axisymmetric Boussinesq Problem For a Punch of Arbitrary Profile", *Int.J.Engng sci. vol.3,pp.47-57,(1965).*

9.      O'Neill, H.  "Hardness Measurement of Metals and Alloys", *Chapman and Hall Ltd, London, (1967).*

10.     Johnson, K.L. "The Correlation of Indentation Experiments", *Journal of the Mechanics and Physics of Solids, Volume 18, 115-126, (1970).*

11.     Oliver, W.C., Hutchings, R. and Pethica, J.B. "Hardness Measurement at Penetration Depth As Small As 20 nm", *Phil. Mag. A,48, 593-606(1983).*

12.     Jonsson, B., Hogmark, S. "Hardness Measurements of Thin Films", *Thin Solid Films;114p257(1984).*

13.     Doerner, M.F. and Nix, W.D. "A Method For Interpreting The Data From Depth-Sensing Indentation Instruments", *Journal of Materials Research, Volume 1, 601, (1986).*

14.     Doerner, M.F., Gardner, D.S and Nix, W.D. "Plastic Properties of Thin Films on Substrates as Measured by Submicron Indentation Hardness and Substrate Curvature Techniques", *J. Mater. Res. 1 (6), Nov/Dec (1986).*

15.     Pollock, H.M., Maugis, D. and Barquins, M. "Characterisation of Submicrometer Surface Layers by Indentation", *in P. J. Blau and B.R. Lawn (eds.), Microindentation Techniques in Materials Science and Engineering, ASTM STP 889, American Society forTesting and Materials, Philadelphia, pp. 47771, (1986).*

16.     King, R.B. "Elastic Analysis of Some Punch Problems For a Layered Medium", *Int J Solids Struct;23p1657 (1987).*

17.     Burnett, P.J. and Rickerby, D.S. "The Mechanical Properties of Wear-Resistant Coatings Ii: Experimental Studies and Interpretation of Hardness", *Thin Solid Films;148p51(1987).*

18.     Burnett, P.J. and Rickerby, D.S. "The Mechanical Properties of Wear-Resistant Coatings I: Modelling of Hardness Behaviour", *Thin Solid Films;148p41(1987).*

19.     Bhattacharya, A.K. and Nix, W.D. "Analysis of Elastic and Plastic Deformation Associated With Indentation Testing of Thin Films on Substrates", *Int. J. Sol. & Structures, vol.24, no.12,pp.1287(1988).*

20.     Bhattacharya, A.K. and Nix, W.D. "Finite Element Simulation of Indentation Experiments, International Journal of Solids and Structures", *Vol. 24, 881-891, (1988).*

21.     O'Hem, M.E., Parrish, R.H. and Oliver, W.C. "Evaluation of Mechanical Properties of Tin Films by Ultralow Load Indentation", *Thin Solid Films, 181,357-363(1989).*

22.     Yu, H.Y., Sanday, S.C., Rath, B.B. "The Effect of Substrate on The Elastic Properties of Films Determined by the Indentation Test axisymmetric Boussinesq Problem", *J Mech Phys Solids;38 p745, (1990).*

23.     Bhattacharya, A.K. and Nix, W.D. "Finite Element Analysis of Cone Indentation, International Journal of Solids and Structures", *Vol. 27, 1047-1058, (1990).*

24.     Joslin, D.L. and Oliver, W.C. "A New Method For Analyzing Data From Continuous Depth-Sensing Micro-Indentation Tests", *J Mater Res;5p 123–6(1990).*

25.     Shih, C.W., Yang, M. and Li, J.C.M. "Effect of Tip Radius on Nano-indentation", *J. Mater. Res. 6, 2623-2628, (1991).*

26.     Gao, H., Cheng-Hsin, C. and Jin, L. "Elastic Contact Versus Indentation Modeling of Multi-Layered Materials", *Int J Solids Struct;29:2471 (1992).*

27.     Savvides, N. and Bell, T.J. "Microhardness and Young's Modulus of Diamond and Diamond like Carbon Films", *J. Appl. Phys., 7-1 2791-2796(1992).*

28.     Fabes, B.D., Oliver, W.C., McKee, R.A. and Walker, F.J. "The Determination of Film Hardness From the Composite Response of Film and Substrate To Nanometer Scale Indentations",  *J Mater Res;7,p3056(1992).*

29.     Whitehead, A.J.  and Page, T.F. "Nano-Indentation Studies of Thin Coated Systems", *Thin Solid Films, 220, 2777283(1992).*

 30.     Oliver, W.C.  and Pharr, G.M. "An Improved Technique For Determining Hardness and Elasticmodulus Using Load and Displacement Sensing Indentation Experiments", *Journal of Materials Research, Volume 7, 1564-1683, (1992).*

31.     Djabella, H. and Arnell, R.D. "Finite Element Analysis of The Contact Stresses In An Elastic Coating on and Elastic Substrate", *Thin solid films, 213, 205-219(1992).*

32.     Wright, S.C., Huang, Y. and Fleck, N.A. "Deep Penetration of Polycarbonate by a Cylindrical Punch", *Mechanics of Materials, 13, 277, (1992).*

33.     Xun, Cai. "Effect of Friction in Indentation Hardness Testing: a Finite Element Study", *Journal of material science letters. 12 (1993).*

34.     Montmitonnet, P., Edlinger, M.L. and Felder, E. "Finite-Element Analysis of Elastoplastic Indentation", *1. Homogeneous media, J. Tribology Trans. ASME, 115, 10-14, (1993).*

35.      Olaf, J.M. and Scheer,C. "Finite Element Analysis of Indentation Experiments In Surfaces and Surface Coated Materials", *Computational Materials Science 1 , 276-282(1993).*

36.      Page, T.F. and Hainsworth, S.V. "Using Nanoindentation Techniques For The Characterization of Coated Systems: A Critique", *Surf Coat Technol;61p201(1993).*

37.      Hainsworth, S.V., Bartlett, T. and Page, T.F. "The Nanoindentation Response of Systems With Thin Hard Carbon Coatings", *Thin Solid Films;236,p214(1993).*

38.      Sadeghipour, K., Chen, W. and Baran G. "Spherical Micro-Indentation Process of Polymer-Based Materials - A Finite-Element Study", *J. Phys. D: Appl. Phys. 27, 1300-1310, (1994).*

39.      Man, K.W. "Contact Mechanics Using Boundary Elements". *Computational mechanics publication, Southhampto, Hants.,(1994).*

40.      Yang, F.Q. and Li, J.C.M. "Computer Simulation of Impression Creep Using the Hyperbolic Sine Stress Law", *Mater. Sci. Eng. A 201, 50-57, (1995).*

41.      Hendrix, B.C. "The Use of Shape Correction Factors For Elasticindentation Measurements", *J. Mat. Research. 10,255,(1995).*

42.      Chechenin, N.G., Bottiger, J. and Krog, J.P. "Nano Indentation of Amorphous Aluminum Oxide Films I. The Influence of The Substrate on the Plastic Properties", *Thin Solid Films,261, p219 (1995).*

43.     Sun, Y., Bell, T. and Zheng, S. "Finite Element Analysis of the Critical Ratio of Coating Thickness to Indentation Depth For Coating Property Nanoindentation Measurements", *Thin Solid Films 258, 198-204(1995).*

44.     Larsson, L., Giannkopoulos,  A.E., Soderlund, E., Rowcliffe, D.J. and Vestergaard, R. "Analysis of Berkovich Indentation", *International Journal of Solids and Structures, Volume 33, 221, (1996).*

45.     Gan, L., Ben-Nissan, B. and Ben-David, A. "Modelling and Finite Element Analysis of Ultra-Microhardness Indentation of Thin Films",  *Thin Solid Films 290-291,362-366, (1996).*

46.     Giannkopoulos, A.E. and Larsson, P.L. "Analysis of Pyramid Indentation of Pressure-Sensitive Hard Metals and Ceramics" *Mechanics of Materials, Volume 25, 1-35, (1997).*

47.     Mencik, J., Munz, D., Quandt, E., Weppelmann, E.R. and Swain, M.V. "Determination of Elastic Modulus of thin Layers Using Nano-indentation",  *J Mater Res;12p2475(1997).*

48.     Shu, J.Y. and Fleck, N.A. "The Prediction of a Size Effect in Micro-Indentation", *Int. J. Solids Struct. 35, 1363-1383(1998).*

49.     Taljat, B.,  Zacharia, T. and Kosel, F. "New Analytical Procedure To Determine Stress-Strain Curve from Spherical Indentation Data", *INT. J. Solids Struct. 35, 4411-4426, (1998).*

50.     Yang, F.Q. "Indentation of an Incompressible Elastic Film", *Mech. Mater. 30, 275-286(1998).*

51.     Bolshakov, A. and Pharr, G.M. "Influences of Pileup on The Measurement of Mechanical Properties by Load and Depth Sensing Indentation Techniques", *J Mater Res;13p1049, (1998).*

52.     Korsunsky, A.M., McGurk, M.R., Bull, S.J. and Page, T.F. "On The Hardness of Coated Systems", *Surf Coat Technol;99:171, (1998).*

53.     Lichinchi, M., Lenardi, C., Haupt, J. and Vitali, R. "Simulation of Berkovich Nanoindentation Experiments on Thin Films Using Finite Element Method", *Thin Solid Films 312 , 240-248, (1998).*

54.     Cheng, Y.T. and Cheng, C.M. "Further Analysis of Indentation Loading Curves: Effects of Tip Imperfection on Mechanical Property Measurements", *Journal of Materials Research, 13, 1059 (1998).*

55.     Tang, K.C. and Arnell, R.D. "Determination of Coating Mechanical Properties Using Spherical Indenters", *Thin Solid Films;356:263, (1999).*

56.     Hay, J.C., Bolshakov, A. and Pharr, G.M. "A Critical Examination of The Fundamental Relations Used In the Analysis of Nanoindentation Data", *Journal of Materials Research,Vol. 14, pp. 2296-2305, (1999).*

57.     Tsui, T.Y. and Pharr, G.M. "Substrate Effects on Nano-Indentation Mechanical Property Measurement of Soft Films on Hard Substrates", *J Mater Res;14 p292, (1999).*

58.     Tsui, T.Y., Vlassak, J. and Nix, W.D. "Indentation Plastic Displacement Field:Part II. The Case Of Hard Films On Soft Substrates", *J Mater Res;14p2204, (1999).*

59.     Tsui, T.Y., Vlassak, J. and Nix, W.D. "Indentation Plastic Displacement Field:Part I. The Case of Soft Films on Hard Substrates", *J Mater Res;14:p2196, (1999).*

60.     Takeshi, S., Yasushi, A., Atsushi S. and Kohichi T. "Nanoindentation of a 10 Nm Thick Thin Film", *J. Mater. Res., Vol. 14, No. 6, Jun (1999).*

61.     Lim, Y.Y., Chaudhri, M.M. and Enomoto, Y. "Accurate Determination of the Mechanical Properties of Thin Aluminum Films Deposited on Sapphire Flats Using Nanoindentation", *J. Mater. Res., Vol. 14, No. 6, Jun (1999).*

62.     Mesarovic, S.D. and Fleck, N.A. "Spherical Indentation of Elastic-Plastic Solids", *Proceedings of Royal Society of London, 455,2707-2728, (1999).*

63.     Malzbender, J. and Den Toonder, J.M.J. "Elastic Modulus, Indentation Pressure and Fracture Toughness of Hybrid Coatings on Glass",  *Thin Solid Films, Volume 366, 139-149, (2000).*

64.     Chen, X. and Vlassak, J.J. " Numerical Study on The Measurement of Thin Film Mechanical Properties by Means of Nano-indentation", *J.Mater.Res., 16,2974-2982 (2001).*

65.     Strange, D.J. and Varshneya, A.K. "Finite Element Simulation of Micro Indentation on Aluminum", *J.Mat.Sci.36 (2001).*

66.     Hay, J.L. and Wolff, P.J. "Small Correction Required When Applying The Hertzian Contact Model to Instrumented Indentation Data", *Journal of Materials Research, Vol. 16, pp. 1280-1286, (2001).*

67.     Aditad, V. and Beuth, J.L. "Measurement of Interfacial Toughness in Thermal Barrier Coating Systems by Indentation", *Engineering Fracture Mechanics, 68, 843-860 (2001).*

68.     Herbert, E.G., Pharr, G.M., Oliver, W.C., Lucas, B.N. and Hay, J.L. "On The Measurement of Stress-Strain Curves by Spherical Indentation", *Thin Solid Films, 398-399,331-335,(2001).*

69.     Saha, R. and Nix, W.D. "Effects of the Substrate on the Determination of Thin Film Mechanical Properties by Nano-Indentation", *Acta Materialia 50 ,23–38, (2002).*

70.     Pharr, G.M. and Bolshakov, A. "Understanding Nano-Indentation Unloading Curves", *J.Material Res. 1, 2660, (2002).*

71.     Cheng, Y.T., Li, Z.Y. and Cheng, C.M. "Scaling, Relationships for Indentation Measurements", *Phil. Mag. A 82, 1821-1829, (2002).*

72.     Yang, F.Q. "Thickness Effect on the Indentation of an Elastic Layer", *Mater. Sci. Eng. A 358, 226-232, (2003).*

73.     Chollacoop, N., Dao, M. and Suresh, S. "Depth-Sensing Instrumented Indentation with Dual Sharp Indenters", *Acta Materialia, 51, 3713-3729, (2003).*

74.     He, J.L. and Veprek, S. "Finite Element Modeling of Indentation into Superhard Coatings", *Surface and Coatings Technology 163 –164, 374–379, (2003).*

75.     Park, Y.J. and Pharr, G.M. "Nano-Indentation with Spherical Indenters: Finite Element Studies of Deformation in the Elastic-Plastic Transition Regime", *Thin Solid Films, 447-448,246-250, (2004).*

76.     Cheng, Y.T., Page, T., Pharr, G.M., Swain, M. and Wahl, K.J. "Fundamentals and Applications of Instrumented Indentation in Multidisciplinary Research", *J. Mater. Res. 19 (2004).*

77.     Cheng, Y.T. and Cheng, C.M. "Scaling, Dimensional Analysis, and Indentation Measurements", *Material science and Engineering, R44, 91-149(2004).*

78.     Shaohua, C., Lei, L. and Tzuchiang, W. "Size Dependent Nanoindentation of a Soft Film on a Hard Substrate", *Acta Materialia 52, 1089–1095, (2004).*

79.     Taljat, B. and Pharr, G.M. "Developments of Pile-Up During Spherical Indentation of Elastic-Plastic Solids", *International Journal of Solids and Structures, Vol. 41, 3891-3904 (2004).*

80.     Panich, N. and Sun, Y. "Effect of Penetration Depth on Indentation Response of Soft Coatings on Hard Substrates: A Finite Element Analysis", *Surface and Coatings Technology 182,342–350, (2004).*

81.     "Theory & Practice of Instrumented Indentation Testing" *(IIT), MTS Systems Corporation, Oak Ridge, TN. (2004)*

82.     Oliver, W.C. and Pharr, G.M. "Measurement of Hardness and Elastic Modulus by Instrumented Indentation: Advances In Understanding and Refinements To Methodology", *J Mater Res 19, pp. 3–20. (2004).*

83.     Pal, J.W. and Jen, F.L. "A New Method Developed to Evaluate Both The Hardness And Elastic Modulus of A Coating–Substrate System", *Surface & Coatings Technology 200, 2489– 2496, (2005).*

84.     Bressan, J.D., Tramontin, A. and Rosa, C. "Modeling of Nanoindentation of Bulk and Thin Film by Finite Element Method", *Wear 258 (2005) 115–122*

85.     Shaohua, C., Lei L., and Tzuchiang, W. "Investigation of The Mechanical Properties of Thin Films by Nanoindentation, Considering the Effects of Thickness And Different Coating–Substrate Combinations", *Surface & Coatings Technology 191, 25– 32 (2005).*

86.     Yang, F., Peng, L. and Okazaki, K. "Effect of the Indenter Size on the Indentation of Aluminum", *Materials Characterization, 57, 321-325, (2006).*

87.     Yang, F.Q. and Saran, A. "Cyclic Indentation of An Elastic-Perfectly Plastic Material", *J. Mater. Sci. Lett. 41, 6077-6080, (2006).*

88.     Beghini, M., Bertini, L. and Fontanari, V. "Evaluation of the Stress-Strain Curve of Metallic Materials by Spherical Indentation", *International Journal of Solids and Structures, 43, 2441-2459, (2006).*

89.     Kang, B.S.J., Yao, Z. and Barbero, E.J. "Post-Yield Stress-Strain Determination Using Spherical Indentation", *Mechanics of Advanced Materials and Structures, 13, 129-138, (2006).*

90.     Feng, G., Qu, S., Huang, Y. and Nix, W.D.  "An Analytical Expression for The Stress Field Around An Elastoplastic Indentation/Contact", *Acta Materialia, 55,2929-2938, (2007).*

91.     Shuangbio, L.Q. and Jane W. "Determination of Young's Modulus And Poisson's Ratio for Coatings", *Surface & Coatings Technology 20 , 6470–6477, (2007).*

92.     ABAQUS, 2007, ABAQUS Users' Manual, Hibbit, Karlson and Sorenson Inc., Pawtucket, RI.

93.     Amaya Roncancio, S. and Restrepo-Parra, E. "Finite Elements Modeling of Multilayers of Cr/CrN", *Microelectronics Journal (2008).*

94.     Manhong, Z., Yong, X., Jessica, X., Nagahisa, O., Norimasa, C. and Xi, C. "Determining Mechanical Properties of Thin Films from the Loading Curve of Nano-Indentation Testing", *Thin Solid Films, 516, 7571-7580 (2008).*

95.     Lu, Y.C. and Shinozaki, D.M. "Characterization and Modeling of Large Displacement Micro-/Nano-Indentation of Polymeric Solids", *ASME Journal of Engineering Materials and Technology, Vol. 130, Oct. 1-7 (2008).*

## VITA

*Date and Place of Birth*

June 21, 1979 at Vijayawada-AP, INDIA

*Education*

Bachelor's Degree in Mechanical Engineering (B.E.), College of Engineering, Andhra

University, Visakhapatnam, AP, INDIA (2003)

*Work Experience*

- Worked as a Structural Assembly Engineer, Hindustan Aeronautics Limited, Bangalore, INDIA,(October 2003- June 2004).

- Worked as a Mechanical Design Engineer, Indian Space Research Organization, Trivandrum, INIDA, (June 2004-June 2007).

- Worked as a Research Assistant at the University of Kentucky, Department of Mechanical Engineering, (August 2007 – August 2008).

- Worked as a Teaching Assistant at the University of Kentucky, Department of Mechanical Engineering, (August 2008 – December 2008).

*Technical Publications*

- Lu, Y.C., Kurapati, S.N.V.R.K. and Yang, F.Q. *"Finite Element Analysis of Cylindrical Indentation for determining Plastic Properties of Material in Small Volumes"., J. Phys. D: Appl. Phys. -D/275807/PAP/170582.*

- Lu, Y.C., Kurapati, S.N.V.R.K. and Yang, F.Q. *"Finite element analysis of deep indentation by a spherical indenter"., J Mater Sci DOI 10.1007/s10853-008-2922-5*